UNCLASSIFIED

SECURITY CLASSIFICATION OF THIS PAGE (When Data Entered)

REPORT DOCUMENTATION PAGE		READ INSTRUCTIONS BEFORE COMPLETING FORM
1. REPORT NUMBER	2. GOVT ACCESSION NO.	3. RECIPIENT'S CATALOG NUMBER
4. TITLE (and Subtitle) Dynamic Response of an Ice-Breaker Hull to Ice Breaking		5. TYPE OF REPORT & PERIOD COVERED Final, Aug. 1982 - Feb. 1984 6. PERFORMING ORG. REPORT NUMBER IIHR Report No. 273
7. AUTHOR(s) A. Mueller and R. Ettema		8. CONTRACT OR GRANT NUMBER(s) ONR: 683:ysh NR062-638 N00014-79-C-0411
9. PERFORMING ORGANIZATION NAME AND ADDRESS Institute of Hydraulic Research The University of Iowa Iowa City, Iowa 52242		10. PROGRAM ELEMENT, PROJECT, TASK AREA & WORK UNIT NUMBERS
11. CONTROLLING OFFICE NAME AND ADDRESS Administrative Contracting Office Office of Naval Research 536 South Clark Street, Chicago, ILL 60605		12. REPORT DATE February 1984 13. NUMBER OF PAGES 114
14. MONITORING AGENCY NAME & ADDRESS(if different from Controlling Office)		15. SECURITY CLASS. (of this report) UNCLASSIFIED 15a. DECLASSIFICATION/DOWNGRADING SCHEDULE

16. DISTRIBUTION STATEMENT (of this Report)

Approved for Public Release; Distribution Unlimited

17. DISTRIBUTION STATEMENT (of the abstract entered in Block 20, if different from Report)

18. SUPPLEMENTARY NOTES

19. KEY WORDS (Continue on reverse side if necessary and identify by block number)

Ice-Breaker Ship, Ship Hull Motion, Ice, Ice Breaking, Hull-Ice Interaction

20. ABSTRACT (Continue on reverse side if necessary and identify by block number)

Experiments were conducted with the objective of studying the dynamic behavior of an ice-breaker hull moving continuously through an ice sheet. Of particular interest was the interaction of ice forces exerted against the hull and the hull's pitching motion. A 1:48-scale model hull of the USCGC "Polar Star" (WAGB10) was used in the study. The model hull was towed by a towing carriage.

cont.

DD FORM 1 JAN 73 1473 EDITION OF 1 NOV 65 IS OBSOLETE
S/N 0102-014-6601

UNCLASSIFIED

SECURITY CLASSIFICATION OF THIS PAGE (When Data Entered)

The dynamic response of the model hull to ice breaking was used to infer the vertical component of the ice forces exerted against the hull; to evaluate the temporal variation of the hull's buoyancy and pitching moment; and, to evaluate the inertia force components of the hull's motion. Examination of the dynamic response of the model hull required computer-based acquisition of temporal records of its pitch and draft as well as its vertical and angular accelerations. Time series analyses of the temporal records were performed.

It was found that, as a simplified but reasonable approximation, the dynamic response of an ice-breaker hull moving at constant velocity can be considered as a forced oscillation. It is characterized by the ratio of the frequency V_o/l_c to the hull's natural frequencies of pitching and heaving, which for the scale model were found to be about the same value, f_o. The frequency V_o/l_c is associated with the cycle of ice forces that is experienced by a hull moving with a velocity V_o through a sheet of ice with a characteristic length l_c. The mean spacing between the consecutive cracks developed in the ice sheet by the hull is proportional to l_c; consequently the parameter V_o/l_c is a measure of the dominant frequency of ice forces.

For relatively low velocities, $V_o/f_o l_c << 1$, the force terms related to a hull's buoyancy are largely in equilibrium with ice forces against a hull, and the inertia forces are negligible. If $V_o/f_o l_c = 1$, the hull is in a state of resonance. As the buoyancy-force components are 180-degrees out of phase with the inertia force components and the two sets of forces partly compensate for each other. At relatively high velocities of hull motion, $V_o/f_o l_c >> 1$, a superposition of two conditions occurs; the inertia forces compensate the high-frequency components of the ice forces against the hull, and buoyancy forces are negligible; and transient motions of the hull are stimulated at the frequency f_o.

The bow of a hull moving at low velocities through an ice sheet depresses the ice sheet, which then becomes locally flooded. However, for a hull travelling at relatively high velocity, there may not be sufficient time for the ice sheet to become flooded. Consequently, the hull experienced reduction in buoyancy in the region of its bow, and an increase in the ice forces. The reduction in buoyancy and increase of vertical ice-forces were estimated from the temporal mean values of forces and moments acting on the hull. For the model hull, it was estimated that the depression of the water level was of the order of 0.01 m, which accounted for about one half of the total reduction in the hull's displacement. The reduction in buoyancy force is associated with both increased vertical ice forces against the hull and increased ice-hull friction.

DYNAMIC RESPONSE OF AN ICE-BREAKER HULL TO ICE BREAKING

by

A. Mueller and R. Ettema

Sponsored by

Office of Naval Research
Contract No. N00014-79-C-0411

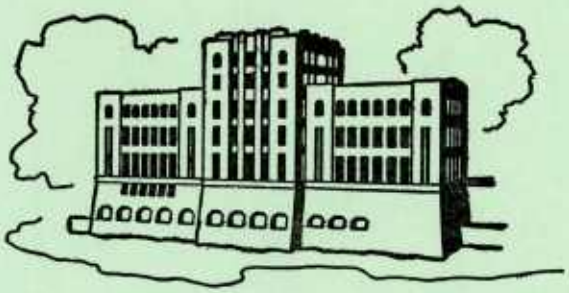

IIHR ~~Report No.~~ 273

Iowa Institute of Hydraulic Research, University of Iowa,
The University of Iowa
Iowa City, Iowa 52242

February 1984

DYNAMIC RESPONSE OF AN ICE-BREAKER HULL TO ICE BREAKING

by

A. Mueller and R. Ettema

Sponsored by

Office of Naval Research
Contract No. N00014-79-C-0411

IIHR Report No. 273

Iowa Institute of Hydraulic Research
The University of Iowa
Iowa City, Iowa 52242

February 1984

ACKNOWLEDGEMENTS

This study was conducted while the first author was on leave from the Swiss Federal Institute of Technology at the invitation of Dr. John F. Kennedy, Director of the Iowa Institute of Hydraulic Research (IIHR).

Funding was provided by the Office of Naval Research under Contract No. N00014-79-C-0411.

The authors would like to thank LCDR. D. Humphreys of the U.S. Coast Guard, Icebreaker Technology Section, for the loan of a 1:48-scale model of the USCGC "Polar Star".

IIHR's experimental facilities for scale-model testing of ice-breaker hulls were designed by Dr. J.C. Tatinclaux and Dr. J.F. Kennedy. Their effort initiated this study. Support provided by IIHR's mechanical and electronic shops, especially by D. Harris, R. Hamer, and J. Cramer, was essential and very much appreciated. Special thanks go to Dr. J.C. Tatinclaux, Dr. L. Landweber, Dr. V.C. Patel, Dr. K. Mori (Hiroshima University, Japan) and Dr. T. Kitazawa (Hitachi Zosen Corp., Japan) for helpful advice given during this study.

TABLE OF CONTENTS

LIST OF FIGURES

LIST OF TABLES

LIST OF SYMBOLS

A	amplitude
A_w	area of the hull's waterplane
$d\tilde{A}$	normal to surface element
A_1	representative area of depression of water level at the hull's bow
b	beam of hull
b_c	width of cantilever beam
$\tilde{B}, \Delta\tilde{B}, \Delta B_x, \Delta B_z$	buoyancy force, and increments thereof
$\Delta B'$	reduction of buoyancy force due to depression of water level at bow
c_1, c_2	damping coefficients for heave and pitch
C_{IB}	coefficient of resistance due to breaking of ice
C_{IS}	coefficient of resistance due to submergence of ice
C_v	coefficient of resistance due to velocity
C_w	coefficient of open-water resistance
Co	co-spectrum
E_f	elastic modulus for flexure of ice sheet
E	voltage output of velocity meter
ΔE	change in voltage
f	frequency
$Fr = \frac{V_o}{\sqrt{gL_s}}$	Froude number of the ship
$F, \overline{F}, \overline{F}_m, F_x, F_z$	ice forces
F_{zo}	amplitude of forcing function
f_h, f_p	natural frequencies of heave and pitch
$f_o \simeq f_h \simeq f_p$	natural frequency for heaving and pitching of the model hull

f_d	sampling frequency
$\Delta f = 1/T_s$	resolution band width of spectra
g	acceleration due to gravity
GM	Metacentric height
$G_x(n\Delta f)$	one-sided power spectrum
$G_{xy}(n\Delta f)$	one-sided cross spectrum
H	draft of hull
h	ice thickness
$H_R(x)$	height of rails of carriage
I	mass moment of inertia
I_v	virtual mass moment of inertia
I_{yy}	area moment of inertia of the waterline for pitching
k	radius of gyration
L, L_I	moment arm of forces
L_s	length of ship
l_c	characteristic length of ice sheet
l_o	length of pendulum
l_1, Δl	moment arms to determine length of pendulum
m	mass of ship
m_v	virtual mass for vertical motion
m_a	mass in accelerometer
Δm	mass increment to calibrate accelerometer
M_y	y component of moment of ice forces about hull's center of gravity
$\overline{M}_{ym}$	mean measured value of M_y
ΔM_{yB}	moment due to buoyancy forces

$\Delta M'_y$	moment due to depression of water level at bow
N	number of segments
n	index
P	fracture load of cantilever beam
p_H	hydrostatic pressure
p_I	ice pressure
Quad	Quad-spectrum
$\tilde{R}$	resultant force on ice-breaker hull
R_I	resistance due to breaking of ice
S	wetted area of hull
s	index
t	time
$\tilde{T}$, T_x	thrust of propeller
T_e	equilibrium temperature of urea ice
T_S = 3.84 sec	length of time segments for calculation of spectra
T	record length of time series
V_o	hull velocity
$\tilde{V}$	velocity vector of ice on ship hull
V(t)	carriage velocity
$\tilde{W}$	weight of ship
$x_s(t)$	time series
$X_s(t)$	Fourier transform of $x_s(t)$
x(t)	position of hull
x	coordinate axis from stern to bow of the hull
y	transverse coordinate

z	vertical coordinate
Δz	average depth of the depression of water level at bow
z_o	peak-to-peak value of fluctuations of draft
$\ddot{z}_o$	peak-to-peak value of fluctuations of vertical acceleration
α	phase shift
$\alpha_1\ \alpha_2\ \alpha_3$	coefficients
γ^2	coherence function
δ	displacement of ice sheet
θ	pitch angle (positive bow up)
θ_o	peak-to-peak value of fluctuation of pitch
$\ddot{\theta}_o$	peak-to-peak value of fluctuations of angular acceleration
ν	Poisson's ratio for ice
ν_k	kinematic viscosity of water
ρ_w	density of water
ρ_I	density of ice
γ_{xy}	correlation coefficient
σ_f	flexural strength of ice sheet
$\tilde{\tau}_v\ dA$	differential viscous friction
$\tilde{\tau}_I\ dA$	differential ice friction
ϕ	roll angle
ω	radial frequency
$\overline{\quad}$	time mean
$\sim$	vector
$\cdot$	derivative with respect to time
m	as a subscript, measured value

I. INTRODUCTION

The use of physical modelling to obtain reliable predictions for the mean resistance forces that are encountered by an ice-breaker hull moving through ice is an open field for research. An improved understanding of the complex dependence of the ice-related resistance force R_I on the parameters of the ice sheet, on the dimensions of the hull and on its motion requires better knowledge of ice-breaking mechanics. This report presents the results of an experimental study in which more parameters were measured than is customary in testing practice. One of the study's objectives was to explore whether new insights could be derived from such additional information. In particular, vertical forces due to ice breaking, buoyancy and inertia as well as the moments involved in pitching motion of the hull were all included in the analysis of its dynamic response to ice breaking.

Scaling laws provide the relations with which to scale up results of model tests to prototype values. Dimensional analysis is the standard approach used to relate the resistance force R_I to key parameters involved in the motion of an ice-breaker hull through ice. The parameters are marshalled as groups of dimensionless variables which can then be associated with contributing ice-resistance forces. This approach was taken by Kashteljan (1968), Lewis and Edwards (1970), Edwards et al. (1972), Enkvist (1972), Vance (1975) and others. Edwards et al. (1972), for example, equated the resistance force R_I to three, ice-related, resistance forces, which they determined from the results of model and full-scale tests of the USCGC "Mackinaw";

$$R_I = C_{IB}\sigma_f bh + C_V \rho_w bhV_o\sqrt{gh} + C_{IS}\rho_w gbh^2 \quad (1)$$

resistance due to flexural failing of ice sheet	resistance due to passage of the hull through broken ice (velocity-dependent resistance)	resistance due to interaction with broken ice floes (gravity resistance)

By dividing R_I by $\rho_w gbh^2$, (1) can be rewritten in the following nondimensional form:

$$\frac{R_I}{\rho_w gbh^2} = C_{IB}\frac{\sigma_f}{\rho_w gh} + C_V\frac{V_o}{\sqrt{gh}} + C_{IS} \quad (2)$$

where ρ_w = density of water; σ_f = flexural strength of ice; b = beam of the hull; g = acceleration due to gravity; h = ice sheet thickness; V_o = velocity of ship; and, C_{IB}, C_{IS} and C_V are coefficients.

A regression analysis can be used to provide the values of the three coefficients C_{IB}, C_{IS} and C_V and to obtain a set of prototype-scale data from model-scale tests. The three coefficients are assumed to be independent of the dimensionless variables in (2). For a more detailed discussion of the application of dimensional analysis to the study of the resistance to motion of an ice-breaker hull moving continuously through an ice sheet, the reader is referred to the aforementioned studies and also to the studies by Schwarz (1974), Poznyak (1981) and Enkvist (1972, 1983). The latter studies also contain descriptions of experiments that were conducted to determine the contributions to R_I that are made by the ice-related resistance components.

Resistance to hull motion through level ice sheets can be examined more directly by analyzing the physics involved in ice breaking. White (1969) analyzed vertical and horizontal forces and the moments involved in the ice-hull interaction. Enkvist (1972) gave individual estimates of the contributions of the different components to the total horizontal resistance force, R_I. Milano (1973, 1975) tried to model all phases of the ice-force cycle for a hull moving through a level ice sheet and proposed a numerical model for predicting R_I. The present study follows essentially the same lines of analysis that were initiated by these authors.

An ice-breaker hull moving through a level ice sheet breaks ice by applying a vertical force to the ice sheet. This force builds up to the fracture point associated with the flexural strength of ice, subsequently relaxes, then increases until the ice sheet fails once again. This cyclic, or time-dependent, force interacts with the pitch oscillation of the hull. In order to properly understand the dynamic behavior of an ice-breaker hull, it is necessary to consider vertical forces and the pitch moments of the hull as well as horizontal forces. In the present study, a scale model of an ice-breaker hull was instrumented so that its vertical, horizontal and pitching motions could be monitored. This was accomplished by recording the horizontal force imparted to the hull; the draft and pitch angle of the hull; and the vertical and angular accelerations of the hull. From these data, the behavior of the vertical forces imparted to ice sheets by a model ice-breaker hull were estimated as a function of hull velocity. Experiments were conducted using a 1:48-scale model hull of the United States Coast Guard ice-breaker ship USCGC "Polar Star" (WAGB10).

II. ANALYSIS OF FORCES AND MOMENTS ON AN ICE-BREAKER HULL

The following simplified analysis of forces and moments on an ice-breaker hull outlines the ideas of experimental design and data interpretation that were adopted for the study. The analysis is applied to a hull moving at constant velocity through a level ice sheet.

Here it is noted that differences exist between the dynamic response of hulls which are towed at constant velocity and self-propelled hulls. For the latter, velocity may not be constant during a cycle of ice forces. Also, the pitching amplitude experienced by a self-propelled hull may be less than for a hull moving with constant velocity through a level ice sheet.

Further, because the ice-breaking pattern of a hull may be influenced by hull shape, so the ice-force cycle experienced by a hull may be affected by hull shape. Rolling oscillation of a hull may also affect the ice-breaking pattern, or cycle of ice forces, especially when the natural frequency of roll is close to the frequency of the ice-force cycle.

An additional consideration is the influence of the material behavior of ice on the cycle of ice forces. As was pointed out by Milano (1982), the cycle of ice forces may vary for changing hull velocity because the deformation behavior of ice may change.

A. General Considerations

The resistance to motion of an ice-breaker hull is the horizontal component of the total force $\tilde{R}$ due to hydromechanical, viscous and ice forces acting on the hull. The total force is the integral of the normal and tangential stresses acting on the surface areas of the hull, and can be written in vector notation as

$$\tilde{R} = \iint_S (p_H + p_I)\, d\tilde{A} + \iint_S (\tilde{\tau}_V + \tilde{\tau}_I)\, dA \qquad (2.1)$$

where p_H = hydrostatic and hydrodynamic pressure; p_I = ice pressure; and, $d\tilde{A}$ = elemental area. The term $\tilde{\tau}_V\, dA$ is the viscous stress which is negligibly small compared to the shear stress $\tilde{\tau}_I\, dA$ attributable to friction between ice and the hull. The shear stress $\tilde{\tau}_I$ can be expressed as

$$\tilde{\tau}_I = F_{ID}\, \tilde{V}\, p_I\, \frac{\tilde{V}}{|\tilde{V}|} \qquad (2.2)$$

where $\tilde{V}/|\tilde{V}|$ is the unit vector in the direction of the ice movement on the surface element of the hull and F_{ID} is the coefficient of dynamic friction which may be dependent on the relative velocity, $\tilde{V}$, of the hull and ice.

The total resistance force $\tilde{R}$ is in equilibrium with the thrust $\tilde{T}$ of the propeller as well as with the weight $\tilde{W}$ and the inertia forces of the hull (Figure 1a). The equation of motion of the hull can be written, in vector notation, as

$$m_V \ddot{\tilde{X}}_{cg} = \tilde{R} + \tilde{W} + \tilde{T} \qquad (2.3)$$

where m_V = virtual mass of the moving hull; and $\ddot{X}_{cg}$ = acceleration of the hull's center of gravity. The corresponding moments of the forces $\tilde{R}$, $\tilde{W}$, and $\tilde{T}$ have also to be in equilibrium with the net moment of the inertia force acting on the hull.

If the hull is floating in open water at a vertical position z = 0 (see Figure 1a), the hydrostatic forces $\tilde{B}(z=0)$ are in equilibrium with the weight $\tilde{W}$ of the hull,

$$\tilde{W} + \tilde{B}(z=0) = 0 \tag{2.4}$$

If the bow of the hull rides up onto the ice sheet (Figure 1b), it places part of the hull's weight on the ice sheet and the hydrostatic force is changed by $\Delta\tilde{B}$;

$$\tilde{B}(z) = \tilde{B}(z=0) + \Delta\tilde{B} \tag{2.5}$$

The ice force $\tilde{F}_I$ can then be separated from the total resistance force $\tilde{R}$ and written as

$$\begin{aligned} \tilde{F}_I &= \tilde{R} - \tilde{B} = \iint_S p_I \, d\tilde{A} + \iint_S F_{ID} \, p_I \frac{\tilde{V}}{|\tilde{V}|} \, dA \\ &= \tilde{R} + \tilde{W} - \Delta\tilde{B} \end{aligned} \tag{2.6}$$

so that the vector sum of total force $\tilde{R}$ and weight $\tilde{W}$ becomes

$$\tilde{R} + \tilde{W} = \tilde{F}_I + \Delta\tilde{B} \tag{2.7}$$

Note that (2.6) and (2.7) neglect all hydrodynamic forces associated with viscous drag and wave resistance to hull motion.

The complex spatial and temporal distributions of p_I, F_{ID} and $\tilde{V}$ are not known and cannot be measured by way of a simple experiment. As an alternative approach, considering only the ice forces and hull motion in the two-dimensional x-z plane (see Figure 1b), the ice forces, F_x, F_z and their corresponding moment about the y-axis, M_y, can be estimated from the dynamic response of the hull if the buoyancy force increment $\Delta\tilde{B}$ and its corresponding moment increment ΔM_{yB}, associated with pitching and heaving of the hull, can be estimated from the hull's position in the x-z plane.

B. Estimation of Buoyancy Forces

The equation of motion, (2.3), of a hull moving with constant horizontal velocity along the x-axis can be written as

$$m_v \ddot{x}_{cg} = 0 = F_x + \Delta B_x + T_x \tag{2.8}$$

and

$$m_v \ddot{z}_{cg} = F_z + \Delta B_z \tag{2.9}$$

The equation for the pitching motion of the hull is

$$I_v \ddot{\theta} = M_y + \Delta M_{yB} \tag{2.10}$$

where I_v = virtual mass moment of inertia; and $\ddot{\theta}$ = angular acceleration. The temporal mean values of $\ddot{z}_{cg}$ and $\ddot{\theta}$ are zero, since heave and pitch motions are limited. The acceleration $\ddot{x}_{cg}$ is also zero because the model hull is towed at constant velocity.

The hydrostatic pressure distribution acting against the hull is not disturbed at low velocities of hull motion provided the depressed portion of the ice sheet at the hull's bow is flooded with water. At higher hull velocities this may no longer be true because there may not be sufficient time for water to flood the depressed portion of the ice sheet. In addition, it has been observed in field and model tests (e.g., Enkvist 1972) that a ventilated area may form between a high velocity bow and the depressed portion of an ice sheet. The disturbance to the distribution of hydrostatic pressure and the depression of the water surface level at the hull's bow may lead to a reduction of the buoyancy force ΔB_z and give rise to a positive value for the buoyancy force component ΔB_x. Consequently, only for relatively low hull velocities (see Figure 1) can the buoyancy force increments ΔB_z and ΔB_x, and their resulting moment increment ΔM_{yB}, be estimated* using the following relationships:

$$\Delta B_z = - A_w \rho_w g \bar{z} \tag{2.11}$$

$$\Delta B_x = 0 \tag{2.12}$$

and

$$\Delta M_{yB} = - I_{yy} \rho_w g \theta \tag{2.13}$$

---

*The proportionality constant $I_{yy} \rho_w$ in (2.13) can be obtained experimentally by measuring trim angle of the model hull due to a known weight at its bow or stern. Similarly, one can determine the proportionality constant $A_w \rho_w g$ in (2.11).

where A_w = area of the waterplane of the hull; $\bar{z}$ = average position of the hull above the equilibrium level z = 0; I_{yy} = area moment of inertia of the waterline for pitching; and θ = pitch angle. The additional terms for higher hull velocities can only be crudely estimated since no measurements are available. The additional change in the buoyancy force $\Delta B'_z$ must be of the order of the reduction of the weight of the displaced fluid; that is

$$\Delta B'_z \simeq - A_1 \rho_w g \overline{\Delta z} \tag{2.14}$$

where A_1 and $\overline{\Delta z}$ are the characteristic area and average depth, respectively, of the depressed portion of the ice sheet. The moment increment $\Delta M'_y$ can be estimated (Figure 1c) as

$$\Delta M'_y = \Delta B'_z L \tag{2.15}$$

where L = the moment arm of $\Delta B'_z$. The buoyancy force increment $\Delta B'_x$ is of the order of the vertically-integrated hydrostatic pressure; that is

$$\Delta B'_x \simeq b \rho_w g \frac{\overline{\Delta z}^2}{2} \tag{2.16}$$

where b = width of the beam at the relevant station of the hull. The ratio $\Delta B'_z / \Delta B'_x$ is large compared with unity because the area of the depressed portion of the ice sheet, A_1, is large compared with the area $b\overline{\Delta z}$;

$$\frac{\Delta B'_z}{\Delta B'_x} = \frac{A_1 \overline{\Delta z}}{b\overline{\Delta z}^2/2} = \frac{2A_1}{b\overline{\Delta z}} >> 1 \qquad (2.17)$$

It follows from the preceeding analysis, (2.11) through (2.17), that the temporal mean values of F_x, F_z and M_y can be estimated using the following equations:

$$\overline{F}_x = \overline{T}_x + \overline{\Delta B'_x} \qquad (2.18)$$

$$\overline{F}_z = A_w \rho_w g \overline{z} + A_1 \rho_w g \overline{\Delta z} \qquad (2.19)$$

and

$$\overline{M}_y = I_{yy} \rho_w g \theta + \Delta B'_z L \qquad (2.20)$$

The force $\overline{F}_x$ is approximately equal to the towing force $\overline{T}_x$ because the contribution of the buoyancy term, $\Delta B'_x$, is small. The force $\overline{F}_z$ is increased by the depressed water level at the bow. The vertical force due to the mean change in the hull's draft, $\overline{z}$, by itself is an underestimate of $\overline{F}_z$. Part of the buoyancy which had compensated for the hull's weight is replaced by an ice force. Since an increase in ice forces against the hull causes a larger friction force to be exerted against the hull, $\overline{F}_x$ and $\overline{T}_x$ are, therefore, also increased by the depression of the water level. The moment $\overline{M}_y$ is underestimated when it is equated solely to the term containing the pitch angle θ, if the water level of the bow is depressed at higher velocities. For the purpose of the interpretation of the experimental results, it is assumed that the distribution of hydrostatic pressure around the hull is undisturbed by the deflection of the ice sheet. The validity of this assumption is to be

checked from the results of experimentation and estimates of $\Delta B'_z$ $\Delta B'_x$ and $\Delta M'_y$ are attempted by making use of relations discussed in the following section.

C. Estimation of Ice Forces

The components F_x and F_z of the resultant ice force F_I are components of the same distribution of the ice pressure against the hull. Because integration of (2.6) for each force component involves the same surface area of the hull, the two force components have the same scale and their ratio can be assumed to be approximately constant for each hull velocity,

$$\frac{F_z}{F_x} = \alpha_1 \tag{2.21}$$

This assumption is valid so long as both the distribution of ice pressure and the directions of ice-rubble movement around the hull are similar from test to test.

The line of action of the ice force usually acts through the hull's bow. If the contribution of the horizontal ice force, F_x, to the pitching moment, M_y, is small compared with the contribution of the vertical ice force F_z, the length of the moment arm L_I is equal to the distance of the line of action of F_z, where it crosses the waterline, to the hull's center of gravity;

$$L_I = \frac{M_y}{F_z} \tag{2.22}$$

The moment arm L_I has to stay within one half of the ship length.

The vertical ice force, F_z, is produced by the buoyancy of the depressed and submerged ice and the bending force needed to break the ice sheet;

$$F_z = \alpha_2 A_w(\rho_w - \rho_I) g h + \alpha_3 \sigma h^2 \tag{2.23}$$

where α_2 and α_3 are constants of the order of unity. The first term in (2.23) can be assumed to be constant with time, while the second term is time-dependent as it represents the increase and relaxation of the bending forces in the ice sheet. Inertial forces of the ice floes and the water moving around the hull, which may be important at high velocities of hull motion, are not included in this estimate.

D. Interaction of Ice Forces with Heaving and Pitching Motions of a Hull

The equation of heaving motion for a hull can be written as

$$\underset{\text{(i)}}{m_v \ddot{z}} + \underset{\text{(ii)}}{c_1 \dot{z}} + \underset{\text{(iii)}}{\rho_w g A_w z} = \underset{\text{(iv)}}{F_z(t)} \tag{2.24}$$

where m_v = virtual mass for vertical motion; A_w = area of the waterplane of the ship; and, c_1 = damping coefficient. The linearized equation for pitching of a hull can be written as

$$\underset{\text{(i)}}{I_v \ddot{\theta}} + \underset{\text{(ii)}}{c_2 \dot{\theta}} + \underset{\text{(iii)}}{\rho_w g I_{yy} \theta} = \underset{\text{(iv)}}{M_y(t)} \tag{2.25}$$

where θ = pitch angle; I_v = virtual mass moment of inertia; I_{yy} = area moment of inertia of the waterplane about the y-axis; c_2 = damping coefficient;

and, $M_y(t)$ = moment of the ice forces relative to center of gravity of the hull.

Both heaving and pitching motions of a hull can be analyzed as forced oscillations. The inertia terms, (i), the damping terms, (ii), and the buoyancy terms, (iii), are in equilibrium with forcing functions, (iv). The natural frequencies of heaving and pitching of a hull are f_h and f_p, respectively, where

$$f_h = \frac{1}{2\pi} \left(\frac{\rho_w g A_w}{m_v}\right)^{0.5} \tag{2.26}$$

and

$$f_p = \frac{1}{2\pi} \left(\frac{\rho_w g I_{yy}}{I_v}\right)^{0.5} \tag{2.27}$$

For the model hull of the USCGC Polar Star, it was determined that f_h and f_p are approximately 1Hz and are both hereinafter referred to as f_o. The parameters m_v, I_v, A_w, and I_{yy} are properties of the hull and were estimated in accordance with their open-water values. The damping coefficients, c_1 and c_2, for ice are as yet unknown. However, it is of interest to examine the form of a solution of (2.24) and (2.25), both of which include damping terms.

With a forcing function in the form of $F_z(t) = F_{zo} \exp(i2\pi ft)$, (2.24) has the following steady-state solution:

$$z(t) = \frac{1}{4\pi^2} \frac{F_{zo}}{(m_v^2(f_o^2-f^2)^2 + c_1^2 f^2)^{0.5}} \exp(i(2\pi ft - \alpha)) \tag{2.28}$$

where

$$\alpha = \text{arc tg} \frac{2\pi f_c}{4\pi^2 m_v (f_o^2 - f^2)} \tag{2.29}$$

The second derivation of z(t) with respect to time is

$$\begin{aligned} \ddot{z}(t) &= -4\pi^2 f^2 z(t) \\ &= -\frac{F_{zo} f^2}{(m_v^2 (f_o^2 - f^2)^2 + c_1^2 f^2)^{0.5}} \exp(i(2\pi ft - \alpha)) \end{aligned} \tag{2.30}$$

The ratio of the inertia term $m_v \ddot{z}(t)$ and the buoyancy term $\rho_w g A_w z(t)$ is

$$\frac{m_v \ddot{z}(t)}{\rho_w g A_w z(t)} = -4\pi^2 f^2 \frac{m_v}{\rho_w g A_w} = -\frac{f^2}{f_o^2} \tag{2.31}$$

The inertia and the buoyancy terms are 180 degrees out of phase for all frequencies of pitching and heaving of the hull. At resonance, f equals f_o, so that both terms have the same amplitude. At low frequencies, when f tends to zero, the buoyancy term $\rho_w g A_w z$ is in equilibrium with F(t) and the inertia term is negligible. At high frequencies, when f tends to infinity, $m_v \ddot{z}$ tends to F(t) and the buoyancy term is negligible. The phase angle, α, of z(t) relative to the forcing function, F(t), is 90 degrees at resonance. It tends to zero at low frequencies and to 180 degrees at high frequencies, for which $\ddot{z}(t)$ is in phase with the forcing function.

In addition to the above steady-state solution, the transient solution which is the response to an impact in z, or $\ddot{z}$, has the form

$$z(t) = A \frac{c_1}{m_v} \exp\left(i2\pi \left(f_o^2 - \frac{c_1^2}{16\pi^2 m_v^2}\right)^{0.5} t\right) \qquad (2.32)$$

where the amplitude, A, depends on the initial conditions of z or $\ddot{z}$. Physically, (2.32) relates to a damped oscillation at a fixed frequency which is determined by the resonant frequency f_o together with the ratio of the damping coefficient and the mass m_v. The ratio of the inertia and the buoyancy terms is close to unity if damping is small;

$$\frac{m_v \ddot{z}(t)}{\rho_w g A_w z(t)} = \frac{1}{f_o^2}\left(f_o^2 - \frac{c_1^2}{16\pi^2 m_v^2}\right) \leq 1 \qquad (2.33)$$

Analogous relations can be formulated for $I_v \ddot{\theta}$ and $\rho_w g I_{yy} \ddot{\theta}$.

If the draft z(t), the pitch angle $\theta(t)$, as well as their derivatives with respect to time, $\ddot{z}(t)$ and $\ddot{\theta}(t)$, are measured as functions of time, information on the ice forces for the entire of frequency band can be gained by Fourier analysis. A direct evaluation of the sum of the damping term and the ice forces (terms (ii) and (iv) in (2.24) and (2.25)) is, however, difficult because the phases of z(t) and $\ddot{z}(t)$ with respect to $\theta(t)$ and $\ddot{\theta}(t)$ must be measured with high accuracy.

The temporal behaviors of $I_z(t)$ and $M_y(t)$ are governed by the breaking pattern of the ice sheet. During impact with the ice sheet, the hull rides onto the ice sheet until the sheet fails. When this occurs, the vertical ice force acting through the hull relaxes. The radius of the resulting approximately circular crack, through the ice sheet in the vicinity of the hull's bow, scales with the ice sheet's characteristic length, l_c, where

$$l_c = \left[\frac{E_f h^3}{12\,\rho g(1-\nu^2)}\right]^{0.25} \tag{2.34}$$

and E_f = elastic modulus for flexure of the ice sheet; ν = Poisson's ratio for ice. The term l_c/V_o is the period of travel between consecutive circular cracks. Consequently, the time-dependent part of the forcing functions $F_z(t)$ and $M_y(t)$ can be considered as a series of impacts of different intensities at the preferred frequency of V_o/l_c. The dynamic response of the hull to ice breaking is thus a superposition of a quasi-steady-state solution oscillating at a frequency of V_o/l_c and transient solutions starting at strong impacts and oscillating at a frequency of $((f_o^2 - c_1^2)/16\pi^2 m_v^2)^{0.5}$.

If $V_o/f_o l_c$ equals unity, the pitching of the hull is in resonance with the frequency of ice breaking and the inertia term is approximately equal to the buoyancy term with a 180-degree phase shift. If $V_o/f_o l_c$ is significantly less than unity--i.e., for low velocities--buoyancy forces are in equilibrium with ice forces and inertia terms can be neglected. If $V_o/f_o l_c$ is much greater than unity--i.e. for high velocities--inertia forces become dominant and are chiefly responsible for ice breaking. Draft and pitch of the hull will adjust to the mean forces only, provided that there are no strong impacts which induce a superimposed transient solution at the resonant frequency.

The foregoing analysis of the dynamic response of an ice-breaker hull to ice breaking does not account for a likely feed-back of hull motion on ice forces; i.e., in the foregoing analysis, the z-axis component of the ice force and the pitching moment, $F_z(t)$ and $M_y(t)$, are both assumed to be independent of $z(t)$ and $\theta(t)$, respectively.

III. EXPERIMENTATION

A. Experimental Facilities

1. The IIHR Ice Towing Tank

The experiments were conducted in the 20m x 5m x 1.3-meter deep model ice towing tank of the IIHR. Figure 2 is an overview of the towing tank, the cold room in which it is housed, and its cooling system. The cooling system is composed of two compressors which provide coolant to the two cooler units situated at each end of the cold room. The compressors are in turn cooled by water pumped from a 200 m^3 sump. If the sump temperature exceeds a certain limit, a cooling tower situated outside of the building is operated to cool the sump water.

Fans inside the four cooler units draw air from the cold room and, after the heat exchange has occurred discharge it into eight ducts which extend the whole length of the cold room. The chilled air is forced through an array of half-inch diameter holes along the base of each duct, thereby producing a flow of chilled air over the towing tank. The four ducts of each side alternate to provide an even distribution of the cold air. Every two hours, one pair of cooler units is defrosted by electrical heating. Depending on the ambient air temperature outside the cold room, the total cooling capacity of the system varies between 15 and 20 kW, and enables an ice sheet to grow at a rate of 1.5 to 2 mm per hour.

The 5-meter wide x 2.4-meter long motorized carriage, depicted in Figure 3, was used to tow the model ice-breaker hull. The carriage runs along rails on the concrete walls of the towing tank. The vertical level of each rail was

adjusted to a tolerance of ± 1.5mm along its length. An angle beam on one side of the basin gives the lateral guidance and carries the rack of the rack-and-pinion drive mechanism. The D.C. motor on the carriage has a maximum torque of 31 Nm and a speed range of 58 to 1750 RPM. A 1:15 gear box increases the torque to 413 Nm and gives a reduced speed range of 3.9 to 117 RPM. The effective radius of the pinion is 0.06m; consequently the carriage has a maximum driving force of 6800 N and a velocity range of 0.024 m/sec to 0.74 m/sec. Higher velocities, up to 2.2 m/sec, can be achieved if a 1:5 gear box is coupled to the D.C. motor.

In order to measure the velocity of the carriage, a wheel carrying a circular array of holes is mounted on the drive shaft of the D.C. motor. The passage of each hole, as the shaft rotates, is sensed by a photo detector which emits a light through the hole. The number of pulses counted during a time interval is proportional to the velocity of the carriage. The length of the time interval is 0.371 seconds so that 1000 pulses correspond to a velocity of 0.333 m/sec. After each interval of 0.371 sec, the number of pulses is latched to a display and to a digital-analog converter which holds the voltage during the following interval until the next measurement is available. The mean velocity of the preceding interval is therefore, displayed and can be sampled.

2. The Model Ice-Breaker Hull

A 1:48-scale model of the USCGC "Polar Star" (WAGB10), loaned to the IIHR by the U.S. Coast Guard, was used to conduct the study. The abbreviated lines of the prototype, and model, hull of the Polar Star are depicted in Figure 4 and its principal model dimensions are given in Table 1.

Care was taken to accurately determine the relevant mechanical constants of the hull in order to accurately evaluate forces and moments due to inertia and buoyancy. The model hull was loaded with a mass of 102.6 kg so that its center of gravity was located, to within a tolerance of 0.014 m, at the longitudinal center of buoyancy. The area A_w of the model hull's water plane (the plan area of the hull at its water line) was determined to be 0.81 m^2. This value was controlled by loading the floating hull with a mass increment Δm and measuring the change in draft Δz. From the relation

$$\rho A_w \Delta z = \Delta m \tag{3.1}$$

the result $A_w = 0.82\ m^2 \pm 0.08\ m^2$, was obtained.

The hull was suspended as a pendulum so that its moment of inertia could be evaluated in accordance with the equation of motion

$$(m\ell_o^2 + I)\ddot{\theta} + Mg\ell_o\theta = 0 \tag{3.2}$$

which enables I to be determined from the length of the pendulum, ℓ_o, the mass of the hull, m, and the radial frequency of oscillation, ω, where

$$\omega^2 = \frac{mg\ell_o}{m\ell^2 + I} \tag{3.3}$$

The length ℓ_o was measured by loading the suspended hull with a mass m_1 at its bow (see Figure 5 for a definition of the terms in (3.3)). The equilibrium of moments,

$$m \Delta \ell = m_1 \ell_1 \tag{3.4}$$

together with the relation

$$\Delta \ell = \theta \ell_o \tag{3.5}$$

permits ℓ_o to be determined in terms of m, $m_1 \ell_1$ and the angle of rotation, θ. The resulting moment of inertia, I, was calculated to be 33.3 ± 0.5 kg m^2, corresponding to a radius of gyration k = 0.57 m; according to the relation

$$I = mk^2 \tag{3.6}$$

No prototype values were available for comparison with the measured values of I and k.

The area moment of inertia, I_{yy}, for pitching of the hull about the y axis (Figure 1) was determined by loading the floating hull with a mass at its stern and measuring the resulting pitch angle of the hull. A value of I_{yy} = 0.25 ± 0.02 m^4 was calculated. This value corresponds to a metacentric height GM = 2.4 m. The vertical distances of the water-line to the center of gravity and the center of buoyancy were assumed to be small compared to the metacentric height GM;

$$GM \simeq \frac{\rho I_{yy}}{m} \tag{3.7}$$

The added mass for vertical motions of the hull was estimated using the method formulated by Landweber and Macagno (1957). They describe the hull for each section as a Lewis form which is based on two parameters; the ratio of beam, b, to the draft, H; and the ratio of the sectional area to the area defined by the product bH. In this manner, an added-mass coefficient, a = 1.38, was calculated for the model hull. The added-mass moment of inertia, I_V, (or the virtual moment of inertia) was estimated by measuring the pitch frequency of the hull. An eccentric driven by a small D.C. motor with a variable speed control was mounted at the stern of the ship hull and operated so that it produced an oscillating vertical force with an amplitude of about 1N. From the equation of motion for hull oscillation, (2.25), the resonant frequency was determined to occur when

$$4\pi^2 f_p^2 = \frac{mg\ GM}{I_V} = \frac{mg\ GM}{I(1+A)} \tag{3.8}$$

The resonant frequency, f_p, was determined to be 1.09 Hz, which is associated with an added-mass moment of inertia, I_V = 51.5 kg m^2, or an added-mass moment of inertia coefficient, A = 0.55. The two coefficients, a and A, were estimated for hull motion in open water. They are at best a lower limit for the coefficients of the hull when it is breaking an ice sheet.

The open-water resistance force F_{XO} was measured as a function of hull velocity. The resistance force F_{XO} and the resistance coefficient C are listed in Table 2 together with Froude number, $V_O/\sqrt{gL}$, and Reynolds number, $V_O L/\nu$, for each test run. The resistance coefficient C was estimated as

$$C = \frac{F_{xo}}{0.5\,\rho_w V_o^2 S} \tag{3.9}$$

where S is the wetted area of the hull. As was assumed for the analysis of forces on an ice-breaker (Chapter II), it is evident in Table 2 that the open-water resistance to the hull's motion is small compared with the ice-breaking resistance. Furthermore, the Froude numbers of the hull are too small for the wave resistance to be of significance (Lackenby 1965).

The coefficient of friction for evaluating the friction force acting between ice and hull was measured for saline ice during tests conducted by Arctec Inc. (Lecourt and Deslaurian 1976). For the surface finish of the model hull used at IIHR, the Arctec Inc. study gave $F_{ID} = 0.478$. No additional measurement of F_{ID} was made during the present study.

3. Instrumentation

The model hull was connected by a 25-millimeter diameter shaft to a dynamometer supported from the carriage, as is shown in Figure 6. The shaft was connected to a vertical plate of the dynamometer by way of two ball bushings which enabled the shaft, and the hull, to move vertically. To ensure an almost moment-free connection of the hull, the shaft was fixed by a ball bearing to the base of the hull. Friction in the ball bushings affected the vertical motion of the model hull. A measurement of the hysteresis of the vertical position of the hull under zero load resulted in an uncertainty $\Delta z = \pm 0.65$ mm in its vertical displacement. This value corresponded to a vertical resistance force $\Delta F_z = \rho_w g A_w \Delta z \simeq 5$N. Once static friction in the ball bushing

was overcome, the vertical resistance is reduced because friction is reduced to a lower value commensurate with dynamic friction.

The dynamometer, which was used to measure the translational inertia force of the hull, or the towing force, consisted of two 0.15-millimeter thick plates which allowed a horizontal motion that was restricted by a 50 lb Statham UL4-50 load cell instrumented with a Statham UC-3 force transducer. The load cell limited the full-scale displacement of the dynamometer to 0.12 mm. The dynamometer and its supports had a resonant frequency of 6 Hz which was detected in the signal produced by the force transducer. Yawing of the hull was restricted by the location of a vertical rod at its stern. The rod was constrained to slide in a 36-millimeter diameter ring which was connected by a frame (which can be seen in Figure 10).

Angular and vertical accelerations of the hull were measured using accelerometers mounted at its bow and stern. Each accelerometer was formed of a 5 lb UL4-5 Statham load cell loaded with a mass of 2.23 kg in order to sensitize it to vertical acceleration. The range of the force transducers correspond to accelerations of about 1g, or 9.81 m/sec^2. The resolution of each accelerometer was of the order of 0.01 m/sec^2. This precision could not be further improved since measured acceleration amplitudes were small compared to the maximum load range of 1g. Resonant frequencies of the accelerometers were well beyond the bandwidth of the data acquisition system that was used for the experiments. The accelerometers were sensitive to tilting because a roll of angle ϕ would reduce the vertical load against the hull by an amount

$$\Delta(gm) = gm(1-\cos\phi) \simeq gm\frac{\phi^2}{2} \qquad (3.10)$$

This reduction of the load is equivalent to a negative (downward) acceleration of

$$\ddot{z} = -\frac{\Delta(gm)}{m} = -\frac{g\phi^2}{2} \tag{3.11}$$

The accelerometer resolution of 0.01 m/sec^2 is equivalent to a roll angle of $\phi = 2.6°$. In some ice-breaking tests, a low frequency deviation of the vertical acceleration was observed and was attributed to rolling of the hull. Both accelerometers sensed the same roll angle. Therefore, the measured angular accelerations of the hull were not affected by rolling of the hull. Pitch angles were too small to be sensed by the accelerometers.

The force transducer of the dynamometer and the two accelerometers were powered by a bridge amplifier, which was located outside of the ice room.

Heave and pitch motions of the hull were measured by recording, with linear displacement potentiometers, the vertical position of the hull at two positions. The potentiometers were excited with 12 volts, which corresponded to a full stroke movement range of 0.15 m. The outputs of the potentiometers were transmitted by means of two voltage followers.

The six voltages from the load cells, accelerometers, and potentiometers, together with the carriage velocity, were scanned using a digital voltmeter. The digitized data were serially transmitted through a telephone link to the IIHR's HP-1000 computer system and were there stored on disk. The bandwidth of the data acquisition link was 100 Hz so that each channel was sampled at a rate of 16.7 Hz. At this sampling rate, the 6 Hz resonance on the force

signal could be resolved and was filtered digitally at 3 Hz. The signals from the two accelerometers were filtered with a 48-dB/octave analog filter with the 3-dB point set at 6 Hz. The signals of both the linear potentiometers and the carriage velocity did not need filtering before sampling.

B. Experimental Procedures

1. Ice Sheet Growth

Ice sheets were grown from a 1.3-percent, by weight, urea solution according to the following procedure: With the cooler system operating at full capacity, the water in the towing tank was cooled down to a temperature of -0.2°C and the room was simultaneously cooled to about -12°C. An air-bubble system provided the necessary mixing of the solution to prevent supercooling of its surface layer. Before being wet-seeded, the surface of the urea solution was screened to remove floating ice crystals. Then, the air bubbles and the blowers of the cooling units were shut off and the cold room was fogged with a fine spray of water droplets. The spray was produced with the use of a pressurized air spray gun and a pressurized tank. The water droplets froze in the cold air and settled onto the surface of the water which had by then reached the freezing temperature of -0.4°C for the urea solution. The wet-seeding process prevented the formation of relatively large ice crystals and enabled a multitude of small crystals to grow simultaneously over the surface of the urea solution.

Each ice sheet was permitted to grow to about 80 percent of its thickness, h. The room temperature was then raised to about 2°C and the ice sheet allowed to warm and weaken. The bending strength, σ_f, and the flexural

elastic modulus, E_f, of the ice sheet were monitored until σ_f reached the values prescribed for the ice-breaker test. The load, f, to flexurally fail a cantilever beam of length ℓ and width d was used as to estimate the value of σ_f, where

$$\sigma_f = \frac{6f\ell}{dh^2} \tag{3.12}$$

Four to six cantilever beams were failed in order to get a representative mean value of σ_f. The flexural elastic modulus, E_f, was determined by measuring the increment, δ, of the vertical deflection of the ice sheet due to small increments of a point load, ΔP, at the center-point of the ice sheet. Thereby

$$E_f = \frac{3}{16} \frac{(1-\nu^2)}{\rho_w g h^3} \left(\frac{\Delta P}{\delta}\right)^2 \tag{3.13}$$

2. Calibration of the Transducers

For each of the six channels of data (force, accelerations at bow and stern of the hull, two linear potentiometers and the carriage velocity) the zero level and the sensitivity of the transducer were determined before every run. The sensitivities of the transducers proved to be constant for all the runs.

The sensitivity of the dynamometer was determined to be 33.5 N/Volt. It was measured by means of a horizontal load applied at the stern of the hull. The sensitivities of the accelerometers were determined by measuring the change in output voltage, ΔE, due to an applied load increment, ΔF, of 1.47 N. The corresponding sensitivity of - 0.42 m/sec^2/Volt equal to $\Delta F/m_a \Delta E$

where m_a is the suspended mass in the accelerometer. The sensitivity of the linear potentiometers, reckoned to be 13.0 mm/Volt, was measured as the ratio of a change in length to a change in signal output. The sensitivity of the circuit for the carriage velocity was determined by correlating its output voltage with the mean velocity of the carriage (determined by use of a stop watch and a length scale). Then, the analog setting of the carriage speed control was calibrated against the output voltage.

Using the linear displacement potentiometers to measure the position of the model hull relative to the carriage rails, it was found that, as is stated in Section III.A.1, the level of the carriage rails varied to within a tolerance of ±1.5 mm along the length. In order to improve the accuracy of the measurements of hull motion, the position of the rails relative to the water surface had to be determined as a function of the position of the carriage along the ice tank. This was accomplished by slowly towing the freely-floating model hull in open water and observing the change in hull position as was indicated by the potentiometers.

In order to calculate the position x(t) of the carriage during the ice-breaking tests, the velocity signal, V(t), was integrated with respect to time. As is mentioned in Section III.A.3, the voltage output, $E_V(t)$, lagged behind the velocity signal, V(t), because $E_V(t)$ was equal to the mean velocity of the preceeding interval. In order to improve the estimate of the mean actual velocity of the nth time interval, the step in the signal was detected and it was assumed that the change in velocity from interval n-1 to n was the same as the step intervals n-2 to n-1. An accuracy of x(t) of ± 50 mm was required for the tests. Therefore, the elevation of the rails, $H_R(x)$, (Figure

7) was smoothed by a moving-average integration technique applied to 50 mm lengths of rail, so as to be consistent with the resolution of hull position. Table 3 is a summary of the bandwiths, and the sensitivities of the various transducers comprising the instrumentation. The errors of the various measured quantities are listed in Table 4.

3. Conduct of the Experiments

In order to get the model hull prepared for each test, a rectangular slot was cut in the ice sheet while it was warming and weakening. With the hull in open water, zero levels for the six data channels were recorded and the sensitivities of the transducers were checked. For each ice sheet, data were taken for an initial run of about two hull lengths, with the hull moving at a low velocity of 0.03 m/sec. Subsequently, a second run was executed with the velocity set as is indicated in the list of parameters given in Table 5. In addition to recording the motion of the hull on video tape, photographs of the hull were taken during each test. At the completion of a test, the ice fragments in the channel behind the ship were also photographed.

4. Numerical Methods

Mean, $\bar{x}$, and standard deviation, σ_x, of a time series x(t) of record length T and sample rate f_d were calculated using the relationships

$$\bar{x} = \frac{1}{f_d T} \sum_{n=1}^{Tf_d} x(n/f_d) \tag{3.14}$$

and

$$\sigma_x = \left[\frac{1}{f_d T} \sum_{n=1}^{Tf_d} x^2(n/f_d) - \bar{x}^2\right]^{0.5} \tag{3.15}$$

The covariance, σ_{xy}, of two time series x(t) and y(t) was determined using

$$\sigma_{xy}^2 = \frac{1}{f_d T} \sum_{n=1}^{Tf_d} x(n/f_d)\, y(n/f_d) - \overline{xy} \tag{3.16}$$

The correlation coefficient for two time series x(t) and y(t) is

$$\rho_{xy} = \frac{\sigma_{xy}^2}{\sigma_x \sigma_y} \tag{3.17}$$

Power spectra, cross spectra and coherence functions were calculated by way of the following methods (e.g., see Bendat and Piersol 1971):

The time series were split into N segments each with M = 64 samples or segment period $T_s = M/f_d = 3.84$ seconds. For each segment, a Fourier series was calculated with a resolution bandwith $\Delta f = 1/T_s = 0.26$ sec. Frequency leakage was reduced by subtracting the time mean and by a cosine taper window.

Each tapered segment $x_s(t)$ of the signal was then represented by

$$x_s(t) = \sum_{n=-M/2}^{M/2} \frac{1}{T_s} X_s(n\Delta f)\, \exp\,(i2\pi n\Delta f t) \tag{3.18}$$

where $X_s(n\Delta f)$ is the Fourier transform at $n\Delta f$ and

$$X_s(n\Delta f) = \int_0^{T_s} x_s(t)\, \exp\,(-i2\pi n\Delta f t)\,dt \tag{3.19}$$

The summation over the range [-M/2, + M/2] is sufficient as $x_s(t)$ was filtered at $f_d/2$ before the analog to digital conversion of the data. The

complex number $(1/T_s)\ X_s\ (n\Delta f)$ describes the amplitude and the phase of the oscillator at the frequency $n\Delta f$.

The one-sided power spectrum $G_x(f)$ was estimated as

$$G_x(n\Delta f) = \frac{2}{NT_s} \sum_{s=1}^{N} X_s^*(n\Delta f)\ X_s(n\Delta f) \tag{3.20}$$

where $n = 1, 2, \ldots M/2$

and $G_x(n\Delta f)$ is the density of the power in the frequency space; it indicates the contribution of the frequency interval $[(n-1/2)\Delta f, (n + 1/2)\ \Delta F]$ to the mean square value

$$\overline{(x(t) - \bar{x})^2} = \sum_{n=1}^{M/2} G_x(n\Delta f)\ \Delta f \tag{3.21}$$

The one-sided cross spectrum $G_{xy}\ (n\Delta f)$ of a pair of functions $x(t)$ and $y(t)$ was estimated by calculating the Fourier transform of segments $x_s(t)$ and $y_s(t)$ and using the relationship

$$G_{xy}\ (n\Delta f) = \frac{2}{NT_s} \sum_{s=1}^{N} X_s^*\ (n\Delta f)\ Y_s(n\Delta f) \tag{3.22}$$

The cross spectrum is a complex-valued function and is represented as

$$G_{xy}(n\Delta f) = Co(n\Delta f) - i\ Quad\ (n\Delta f)$$

where $Co(n\Delta f)$ is the cospectrum and $Quad\ (n\Delta f)$ is the quadspectrum of the functions. The magnitude, $G_{xy}(n\Delta f)$ is equal to the average product of the magnitudes $|X_s(n\Delta f)|$ and $|Y_s(n\Delta f)|$ and the phase is equal to the average phase difference of the two oscillators at $(n\Delta f)$. The covariance is equal to the sum over the cospectrum, or

$$\overline{(x(t) - \bar{x})(y(t)-\bar{y})} = \sum_{n=1}^{M/2} Co_{xy}(n\Delta f)\Delta f \tag{3.23}$$

The coherence function γ^2_{xy} is defined as

$$\gamma^2_{xy}\ (n\Delta f) = \frac{Gxy(n\Delta f)^2}{G_x(n\Delta f)\ G_y(n\Delta f)} \tag{3.24}$$

and is equal to unity, if the phase difference of the two oscillators $X_s\ (n\Delta f)$ and $Y_s(n\Delta f)$ is constant for all segments.

IV. RESULTS

A. Test Parameters

In accordance with the exploratory nature of this study, only a limited set of data was taken. The hull velocity V_o, or the derived frequency scale V_o/l_c (l_c = characteristic length of the ice sheet), was the main parameter that was varied in order to study the interaction of the ice forces experienced by the hull with its pitching motion. Two runs, or tests, were performed for each ice sheet: The first run involved the movement of the model hull at the relatively low velocity of 0.03 m/sec; and a second run was conducted with the model hull moving at a velocity of either 0.22, 0.3 or 0.6 m/sec. The flexural strengths of the ice sheets were chosen so that, for each hull velocity, runs were conducted for two values of σ_f. Ice-sheet thickness, h, was kept constant at about 0.023 m, with the exception of sheet G for which h = 0.032 m. The physical parameters of the seven ice sheets used in the study are summarized in Table 5. The mean and standard deviations of draft, vertical acceleration, pitch and angular acceleration of the model hull are presented in Appendix 1. The buoyancy and inertia terms are additionally scaled according to (2.24) and (2.25) so that they are directly comparable. The scaling factors are listed in Table 6. Appendix 1 also gives the mutual covariance of the five quantities together with the correlation coefficients. The errors of measurement were discussed in the Section III.A.3. Table 4 is a summary of the error estimates.

In Appendix 2, examples of the time series of the measured quantities for every run, as scaled using (2.24) and (2.25), are presented. A scaling to prototype values was not the purpose of this study.

The resultant trends that were obtained for the temporal mean values of forces and moments experienced by the hull are discussed in Section B, while the time-dependent characteristics of the forces and moments are discussed in Section C.

B. Discussion of Mean Forces and Moments

1. Calculated Data

The measured* temporal mean values of the ice-related resistance forces, $\overline{F_{xm}}$ and $\overline{F_{zm}}$ as well as the temporal mean values of the moment $\overline{M_{ym}}$ are represented, in Figures 8a, b, c, as functions of hull velocity V_o. As was discussed earlier, it is assumed that $\overline{F}_{xm}$ is approximately equal to the towing force $\overline{T}_x$ (see (2.18)) ; that $\overline{F}_{zm}$ is approximated by the buoyancy term $\rho_w g A_w \overline{z}$ (see (2.19)); and that $\overline{M}_y$ is approximated by the buoyancy term $I_{yy} \rho_w g \overline{\theta}$ (equation 2.20).

The temporal mean horizontal ice force $\overline{F}_{xm}$ generally increases with increasing hull speed. The measured mean buoyancy force $\overline{F}_{zm}$ increases with hull speed up to V_o = 0.3 m/sec; and subsequently decreases toward V_o = 0.6 m/sec. For an ice-sheet thickness of 0.023 in, the moment $\overline{M}_{ym}$ is constant for hull speeds up to a value of 0.3 m/sec and thereafter increases for speeds upto a value, V_o = 0.6m/sec.

---

*Measured quantities have the subscript m.

2. Comparison with Data Obtained by Arctec Inc.

Extensive model tests of the USCGC "Polar Star" were conducted in 1976 by Arctec Inc. of Maryland USA (Lecourt and Deslauriers, 1976). For these tests, Arctec used saline ice (NaCl solution), instead of urea ice, with flexural strength ranging from 7 to 12 kPa.

Values of the resistance force, $\overline{F}_{xm}$ as were obtained in the present study are compared in Figure 9 with those obtained during the tests conducted by Arctec. The IIHR data are in good agreement with those Arctec data that are associated with a coefficient of friction, between ice and hull, of F_{ID} = 0.124. The Arctec data for F_{ID} = 0.478, which was associated with the initial surface finish of the model hull (prior to its use by the IIHR) are consistantly higher than the IIHR data. During the present study, no measurement of F_{ID} was made with urea ice.

3. Effects of the Depression of the Water Level in the Bow Region

The trends of $\overline{F}_{xm}$ $\overline{F}_{zm}$ and $\overline{M}_{ym}$, that are shown in Figure 8, can be interpreted by considering the effect that the depression of an ice sheet has on the distribution of hydrostatic pressure that is exerted against the hull (as discussed in Section II.B). Because little information is available on these trends, it is of interest to get at least approximate estimates.

At the relatively low value of hull velocity V_o = 0.03 m/sec, the loaded ice sheet was flexed down below the water level and became flooded with water. The photograph Figure 10a illustrates the flooding of such a semicircular area which had a diameter of about twice the beam of the hull. For moderate hull velocities, V_o = 0.22 m/sec, this area did not flood (Figure 10b), and at V_o = 0.6 m/sec, not only did flooding not occur but a small air

gap was visible between the deflected surface of ice sheet and the hull's bow (Figure 10c). It can be concluded from these observations that, at V_o = 0.03 m/sec, the distribution of the hydrostatic pressure against the hull is not affected by the depression of the ice sheet and that the analysis as is embodied in (2.7) through (2.12) can be used to estimate the actual ice forces exerted against the hull. The influence of water surface depression due to the downward flexing of the ice sheet becomes progressively significant at higher velocities of hull motion. This result is supported by the observation that at V_o = 0.03 m/sec, the measured vertical ice force $\overline{F}_{zm}$ correlates well with the range given by the two contributions in (2.23), $F_z = A_w (\rho_w - \rho_I) gh + \sigma_f h^2$ (Figure 11). The second term is time dependent and contributes only with its temporal mean to $\overline{F_z}$. The coefficients α_2 and α_3 in (2.23) were set equal to unity for this comparison.

In order to analyze the effect of ice sheet depression for higher velocities of hull motion, estimates of the ice force $\overline{F_z}$ and its moment $\overline{M_y}$ are required in order to evaluate $\Delta B_z'$ and $\Delta M_y'$ (see (2.18) and (2.19)); where

$$\overline{F}_z = \overline{F}_{zm} + \Delta B_z' \simeq \overline{F}_{zm} + A_1 \rho_w g \Delta z$$

and

$$\overline{M}_y = \overline{M}_{ym} + \Delta M_y' = \overline{M}_y + \Delta B_z' L$$

The estimates can be derived from the ratios $\alpha_1 = \overline{F}_{zm}/\overline{F}_{xm}$ and $L_I = \overline{M}_{ym}/\overline{F}_{zm}$ which are plotted in Figures 12a, b. For relatively low hull velocities, values of α_1 show little scatter and a mean value of α_1, for the ice sheets tested, can be evaluated as

$$\bar{\alpha}_1(V_o = 0.03 \text{ m/sec}) = 1.5 \pm 0.3 \qquad (4.1)$$

It is evident from Figure 12 that α_1 decreased with increasing hull velocity for all the ice sheets that were tested. However, α_1 is within the range of values given in (4.1), except when V = 0.6 m/sec, for which the value of α_1 dropped to about one half (sheet F) and one third (sheet E) of its value given in (4.1).

As stated in Section III.2.C, it can be assumed, as an approximation, that α_1 is constant provided that the distribution of the ice pressure and the motion of the broken ice is similar. If it is further assumed that $\alpha_1 = 1.5$ when $V_o = 0.6$ m/sec and that the characteristic area A_1 of the depressed water level is of the order of 10-percent of A_w, it follows from (2.14) and (2.19) that

$$\Delta B'_z \simeq 1.5\ \bar{F}_{xm} - \bar{F}_{zm} \qquad (4.2)$$

and

$$\Delta z = \frac{1.5\ \bar{F}_{xm} - \bar{F}_{zm}}{0.1\ A_w \rho_w g} \qquad (4.3)$$

Estimated values of $\Delta B'_z$ and Δz are listed in Table 7. For ice sheets E and F, the estimated value of Δz is 0.025 m. This value seems to be the right order of magnitude. It is, however, a quandary as to how the ice sheet can transmit the total vertical force F_z, which considerably exceeds its bearing capacity for a stationary load.

Calculation of the buoyancy force increment $\Delta B'_x$, using (2.16) with Δz = 0.25m, indicates it to be small compared to the measured resistance, or the towing force, T_x. The approximation $\overline{F}_x = \overline{T}_x$ is therefore a valid assumption for the given margin of experimental errors.

The ratio $\overline{M}_y/\overline{F}_z$ is an estimate of the moment arm L_I of the resultant ice force acting against the hull. When V_o = 0.03 m/sec, the mean value of L_I was

$$\overline{L}_I = 0.73 \pm 0.08 \text{ m} \tag{4.5}$$

For moderate hull velocities, L_I marginally decreased to 0.63 m with a root-mean square value of 0.13 m. When V_o = 0.6 m, L_I increased to 1.04m (sheet F) and 1.54 m (sheet E). This estimate for L_I is in contradiction to the requirement that the line of action of the ice forces must lie within the hull. In other words, this result supports the argument that $\overline{F}_{zm}$ must underestimate the true value of the vertical ice forces acting against the hull.

The moment increment $\Delta M'_y$ can be estimated using an argument similar to that used for estimating the force increment $\Delta B'_z$: If L_I = 0.73m is an adequate estimate of the moment arm for all hull velocities, then

$$\overline{M}_y \simeq L_I \, \overline{\alpha}_1 \overline{F}_x$$

and

$$\Delta M'_y = L_I \overline{\alpha}_1 \, \overline{F}_x - \overline{M}_{ym} \tag{4.6}$$

The moment arm, L, of the buoyancy force increment $\Delta B'_z$ is

$$L = \frac{L_I \overline{\alpha}_1 \overline{F}_x - \overline{M}_{ym}}{\Delta B'_z} \tag{4.7}$$

For ice sheets E and F, L = 0.35m and 0.41 m, respectively. However, these estimates are too approximate to place the depression of the ice sheet in the bow region.

The results summarized in Table 7 indicate that the depression of the water level at the bow region of the hull depressing an ice sheet plays an important role in the generation of ice forces. It leads to an increase in the resistance to motion that is experienced by the hull. There is a need for more detailed experiments to investigate the influence of water level depression, at the bow region, on the dynamic response of an ice-breaker hull to ice breaking.

C. Temporal Variation of Forces and Moments

In section II.D, the motion for the heaving and pitching motions of a hull were analyzed as forced oscillations and the following relationships were proposed:

$$m_v \ddot{z} + c_1 \dot{z} + \rho_w g A_w z = F_z(t) \qquad (2.24)$$

$$I_v \ddot{\theta} + c_2 \dot{\theta} + \rho_w g I_{yy} \theta = M_y(t) \qquad (2.25)$$

Inertia Damping Buoyancy Forcing function

The vertical ice force $F_z(t)$ and the moment $M_y(t)$ act as forcing functions which are in equilibrium with the inertia forces and the buoyancy forces. The inertia and buoyancy forces were measured during each of the

tests. However, the damping terms could not be isolated in the experiment. In particular, friction in the ball bushing support for the model hull caused a fluctuating vertical force of unknown size to act through the center of gravity of the hull and to damp fluctuations of F(t). Errors due to this damping effect have considerably influenced the vertical forces that were recorded during experimentation.

1. Amplitudes of Forces and Moments

It is useful to compare peak-to-peak values of the fluctuations of the inertia and the buoyancy forces with an estimate of the ice forces that were needed to flexurally fail the ice sheet. The load cycle associated with the increase and subsequent relaxation of the ice forces was considered to be the source of the temporal fluctuations of the forcing functions $F_z(t)$ and $M_y(t)$ acting on the hull. In Figures 13a and b, typical maxima and minima of peak-to-peak values of $\rho_w g A_w z(t)$ and $m_v \ddot{z}(t)$, respectively are scaled with $\sigma_f h^2$, and are plotted against the frequency parameter V_o/l_c. In Figures 13c and d, typical maxima and minima of peak-to-peak values of $\rho_w g I_{yy} \theta(t)$ and $I_v \ddot{\theta}(t)$, respectively, are scaled with $\rho_f h^2 L_I$ and are plotted versus V_o/ℓ_c. The moment L_I of the ice force acting against the hull is taken to be $L_I = 0.73$ m.

The bearing capacity of an infinite ice sheet sustaining a circular load of finite diameter is reported to be a factor of 1.5 to 2 times $\sigma_f h^2$. For a semiinfinite ice sheet, the factor is 0.4 to 0.6 (Michel 1978). The buoyancy and inertia forces that were measured in this study were 180 degrees out of phase with each other. Consequently these forces partly compensated one another, especially at the resonant frequency (2.32). The observed minimal peak-to-peak values appear to be good indicators for the fracture load and the

maximal peak-to-peak values indicate the presence of a strong resonance. From this point of view, the fracture load, as is shown in Figure 13, has a magnitude between 0.4 and 0.8 times $\sigma_f h^2$, for the model hull. This result is in agreement with the fracture load of a semiinfinite ice sheet. Strong resonance in the pitching motion of the hull was recorded for values of V_o/l_c between 1 and 2. At high velocities (V_o/l_c = 3.4 and 4.2) higher peak-to-peak values were observed. This result can possibly be attributed to the effects of the inertia forces of the ice floes and the water underneath the ice.

2. Spectral Distributions of Forces and Moments

In section II.D it was assumed that the period between the formation of consecutive cracks in the ice sheet has a maximum value of l_c/V_o, where l_c is the characteristic length of the ice sheet and V_o is the speed of the hull. If the rate of increase of the ice force is not too great, the spectrum of the forcing function has a peak value at the frequency v_o/l_c.

The response of the hull was determined by calculating the power spectra, the cross spectra and the coherence functions for the temporal records of the five measured variables of hull motion--i.e., draft, pitch, vertical and angular accelerations and towing force. The power spectra, cross spectra and coherence functions for the measured variables are summarized in Appendix C.

The bandwidth of the data channels are listed in Table 3. The upper frequency limit of F_x, given by the filter frequency of 3 Hz, appeared to be inadequate, especially at higher velocities (sheets E,F) and for sheets of thicker ice (sheet G). The draft and pitch motions of the hull were not filtered. The decline of their spectra is therefore given by the motion of the hull. The accelerations were filtered at a frequency of 6 Hz. The low

frequencies that were recorded for the vertical acceleration $\ddot{z}(t)$ are due to rolling motion of the hull.

Examples of the time histories of forces and moments are given in Appendix 2. From these examples, the relative size of the terms in (2.24) and (2.25) can be qualitatively estimated. The power spectra (Figure C1) give, in a more quantitative way, the average contribution of each frequency interval to the mean square of the fluctuation and enable a comparison to be made of the strength of the forces and moments in the frequency space. The cross-spectra and coherence functions of the pairs $z(t)$ and $\ddot{z}(t)$, $\theta(t)$ and $\ddot{\theta}(t)$ (see Figure C2), $F_x(t)$ and $z(t)$, $F_x(t)$ and $\ddot{z}(t)$, (see Figure C3), $F_x(t)$ and $\theta(t)$, and F_x and $\ddot{\theta}(t)$ (see Figure C4) provide information on the frequency range where both quantities have simultaneously strong spectral lines, and information on the average phase relation. The cross spectra and the coherence functions also facilitate the checking of the data for consistency. The theoretical coherence functions of z and $\ddot{z}$, as well as θ and $\ddot{\theta}$, are unity. Any deviation of the actual values from the theoretical values must be due either to unwanted filtering, to noise if the signals are small, to error of measurements or to a violation of the basic assumptions which lead to the formulation of (2.23) and (2.24). The coherance function of $\theta(t)$ and $\ddot{\theta}(t)$ (pitch with angular acceleration) is close to unity in a frequency band around the resonant frequency f_o = 1Hz. The coherance function decreases to zero for higher frequencies of pitching motion. The relationship between $z(t)$ and $\ddot{z}(t)$ (draft and vertical acceleration) are less coherent if the fluctuations of the forces are small. This may be due to friction in the ball bushings as was mentioned before. The cross spectra of $\theta(t)$ and $\ddot{\theta}(t)$ show the expected behavior. The cospectrum has normally a

negative peak at the resonance frequency and the quadspectrum is close to zero. This result agrees with the fact that $I_v\ddot{\theta}$ is 180 degrees out of phase with $\rho_w g I_{yy}\theta$.

In Appendix C, one set of power spectra and the three sets of cross spectra and coherence function are organized in the following way: Figure (a) of each set gives examples of three low velocity runs; Figure (b) collects the runs at medium velocity (V_o = 0.22 m/sec and V_o = 0.30 m/sec); Figure (c) shows the high velocity runs (V_o = 0.6 m/sec); and Figure (d) gives the results for the two runs of sheet G, which was distinguished by its greater ice thickness.

3. Classification of Tests According to Frequency Response of the Hull

The tests can be classified according to the frequency response of the hull to the forcing functions exerted against it during the process of ice breaking. As is described in Section II.D, the parameter $V_o/f_o l_c$ can be used as a measure of the dynamic, or frequency, response of the hull to ice forces. It was found for the model hull that the natural frequencies of heaving and pitching are sufficiently equivalent that the two resonances cannot be separated. Values of $V_o/f_o l_c$ for the tests are given in Table 5.

For the relatively low hull velocity of V_o = 0.03 m/sec, when $V_o/f_o l_c$ is significantly less than unity, the acceleration terms are small and the buoyancy terms are in equilibrium with the forcing function due to ice forces. The power spectra of the inertia terms are zero and the power spectra of pitch θ and F_x are nonzero only at the lowest frequencies (Figures C1a,d). These two quantities show there are also some positive values in the co-spectrum, which means that they are in phase (Figures C4a through d).

An average distance, Δx, between consecutive cracks in the ice sheets can be estimated from the fluctuations in the temporal records of pitch angle θ. Values of the measured frequency of the ice force cycle, $f = V_o/\Delta x$, are compared with V_o/l_c in Figure 14. In Figure 15 the same data is used to correlate the distance x directly with l_c.

At hull velocities for which $V_o/f_o l_c$ is in the range of 1 to 2, buoyancy and inertia terms are of equal magnitude and partly compensate one another, as is indicated in (2.33). The cross-spectra and power spectra, as shown in Figure C1-4b, depict the resonance effect, especially for the pitch and angular acceleration of the hull $\theta(t)$ and $\ddot{\theta}(t)$. For sheet G the resonance is also evident for the vertical motion of the hull, z and $\ddot{z}$. As can be seen from the positive resp. negative cospectrum given in Figures C4b through d (sheet G), F_x is in phase with $\theta(t)$ and $z(t)$ at the resonant frequency f_o and out of phase with $\ddot{\theta}(t)$.

For high hull velocities, with $V_o/f_o l_c$ approximately equal to 4, the power spectra of the buoyancy terms decrease toward higher frequencies. Ice sheets are broken predominantly by inertia forces, which show strong lines in the spectra at V_o/l_c (Figure C1c). For sheet F, when V_o = 0.6 m/sec, there is a peak in the cospectrum of z and $\ddot{z}$ as well as θ and $\ddot{\theta}$ at the frequency f = 1.3 Hz. This indicates the presence of transients (see(2.32) and (2.33)). There is also a dominant peak in the power spectra of F_x at the frequency f = 1.6 Hz (Figure C1c) which is also clearly visible in the time histories (Figure B). This peak is also apparent in the cross spectra of F_x and $\ddot{z}(t)$ and F_x and $\ddot{\theta}(t)$ (Figures C3c and C4c). The phase angle is not clearly defined by the ratio of the cospectrum and the quad-spectrum because at this frequency the phase error of the data acquisition is about 10 percent

of 2π. The distance travelled by the hull during the period T = 0.62 sec, corresponding to the dominant frequency of ice forces, f = 1.6 Hz, is equal 0.36 m. This length, which is 2 times l_c, is an indication that these fluctuation of F_x may be produced by an interaction effect of the pitch motion and the breaking of the ice sheet. As was stated in Section II.D, such an interaction effect is not included in the present analytical model of forced oscillation of an ice-breaker hull. The accuracy of the spectra is marginal-limited at high velocities of hull motion, because the observation time and data acquisition is restricted by the length of the towing tank.

The peaks in the power spectra can be used to estimate the recorded frequency f_m of the forcing function and to estimate the distance, Δx, between consecutive cracks formed in the ice sheet as the hull moved through it. For the high velocity runs, the peaks at the highest frequency were chosen. Figure 14 shows the correlation of f_m with the frequency scale V_o/l_c and Figure 15 shows the same information as a correlation of V_o/f_m with l_c. The good correlation that is evident in Figures 14 and 15 is a confirmation that the average value of the initial breaking length, Δx, is adequately estimated using the characteristic length of the ice sheet, l_c. This result, nonetheless, is somewhat contradicted by the observation that, at relatively high hull velocities, the mean size of the ice floes in the wake of the hull is significantly smaller than l_c. Figure 16 shows typical sizes of these ice rubble, after a run at a relatively low velocity, V_o = 0.03 m/sec (Figure 16a), and after a run at a relatively high velocity, V_o = 0.60 m/sec (Figure 16b). However subsequent fracture of the ice floes at high velocity during passage of the hull may explain this contradiction.

VI. CONCLUSIONS

Based on experimentation involving a 1:48-scale model of the USCGC ice-breaker ship "Polar Star" moving with constant velocity through level ice sheets, the following principal conclusions were drawn on the dynamic response of an ice-breaker hull to ice breaking:

1. The dynamic behavior of an ice-breaker hull breaking ice can be described in terms of a forced oscillation and classified according to the parameter $V_o/f_o l_c$, where V_o = the hull's velocity, f_o = the natural frequency of pitching (and heaving) motion of the hull. l_c = the characteristic length of the ice sheet, relates directly to the distance between consecutive cracks formed circumferentially around the bow of an ice-breaker hull.

   The flexural failure of an ice sheet by a hull causes a quasiperiodic forcing function of frequency V_o/l_c to be exerted against the hull. The amplitude of the forcing function was estimated to be in the range of 0.4 to 0.8 $\sigma_f h^2$.

   For relatively low hull velocities, $V_o/f_o l_c \ll 1$, the buoyancy terms in the equation of motion are approximately equivalent to the ice forces, or the forcing function, exerted on the hull during ice breaking. When an ice sheet is broken by a hull moving at relatively high velocity, $V_o/f_o l_c \gg 1$, the inertia forces of the hull are principally responsible for ice breaking. When a hull is moving at a velocity such that $V_o/f_o l_c = 1$, both buoyancy and inertia forces of the hull are large compared to ice forces. These forces partly compensate one another, because they are 180-degrees out of phase.

2. For relatively high cruise velocities, the hydrostatic pressure distribution acting against the hull may be reduced because the depressed portion of the ice sheet at the hull's bow may no longer be flooded with water.

The distance that the leading edge of the ice sheet was depressed and the effect on the hulls motion were estimated using the assumption that the ratio of vertical and horizontal ice forces is a constant value of about 1.5. The depression of the ice sheet, and the water level was estimated to be of the order of 0.01 m for a model hull moving at a velocity of 0.6 m/sec. This depression of water level was estimated to produce about one half of the reduction of the hulls buoyancy necessary to load the ice sheet.

LIST OF REFERENCES

Bendat, J.S. and Piersol, A.G., (1971), "Random Data: Analysis and Measurement Procedures", Wiley-Interscience, New York, USA.

Edwards, R.Y., Lewis, T.W., Wheaton, J.W., and Coburn, T. (1972), "Full-Scale and Model Test of a Great Lakes Icebreaker", Transactions of the Society of Naval Architects and Marine Engineers, Vol. 80.

Enkvist, E. (1972), "On the Ice Resistance Encountered by Ships Operating in the Continuous Mode of Icebreaking", Report No. 24, The Swedish Academy of Engineering Science in Finland.

Enkvist, E. (1983), "A Survey of Experimental Indications of the Relation Between the Submersion and Breaking Components of Level Ice Resistance to Ships", in Proceedings of the Seventh International Conference of Port and Ocean Engineering under Arctic Conditions, Helsinki, Finland.

Kashteljan, V.I., Poznyak, I.I., and Rivlin, A.J. (1968), "Ice Resistance to Motion of Ship", Sudostroenic, Leningrad, USSR.

Lackenby, H. (1965), "An Investigation Into the Nature and Interdependence of the Components of Ship Resistance", Royal Institution of Naval Architects, Britain.

Landweber, L. and Macagno, M.C. (1957), "Added Masses of Two Dimensional Form Oscillating in a Free Surface", Journal of Ship Research, November 1957.

Lecourt, E.Y., Deslauriers, P.C. (1976), "Icebreaking Model Tests of the USCGC Polar Star", Report No. 278C-2, Arctec Inc., Maryland, USA.

Michel, B., (1978), "Ice Mechanics", Les Presses de l'Universite Laval, Quebec, Canada.

Milano, V.R. (1973), "Ship Resistance to Continuous Motion on Ice", Transactions of the Society of Naval Architects and Marine Engineers, Vol. 81.

Milano, V.R., (1975), "Variation of Ship/Ice Parameters on Ship Resistance to Continuous Motion in Ice", in Proceedings Ice Tech 75, Paper No. B1, Montreal, Canada, SNAME-Eastern Canadian Section.

Poznyak, I.I. and Inou B.P. (1981), "The Division of Ice Breaker Resistance into Components", in Proceedings Sixth Ship Technology and Research (STAR) Symposium June 1981, SNAME, New York, USA.

Schwarz, J. (1974), "Present Status of Icebreaker Research", in Proceedings, 17th American Towing Tank Conference, Pasadena, California, USA.

Vance, G.P., (1975), "A Scaling System for Vessels Modeled in Ice", Proceedings, Paper No. H1, in Ice Tech 75, Montreal, Canada, SNAME-Eastern Canadian Section.

White, R.M. (1969), "Prediction of Ice Breaker Capability", Royal Institution of Naval Architects", Britain.

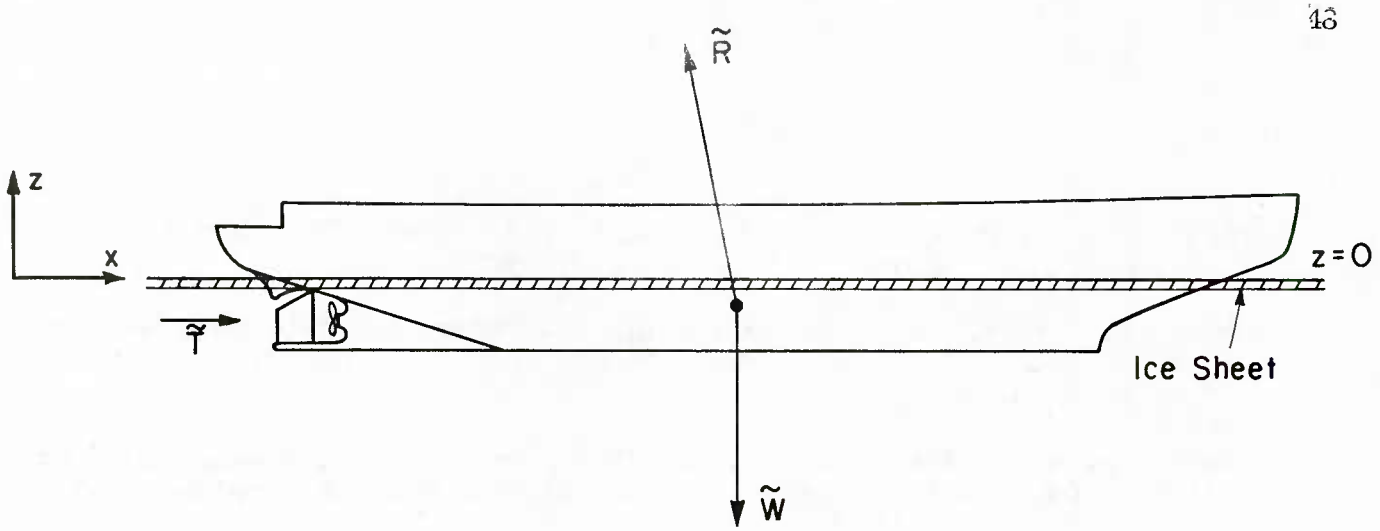

(a) Total forces

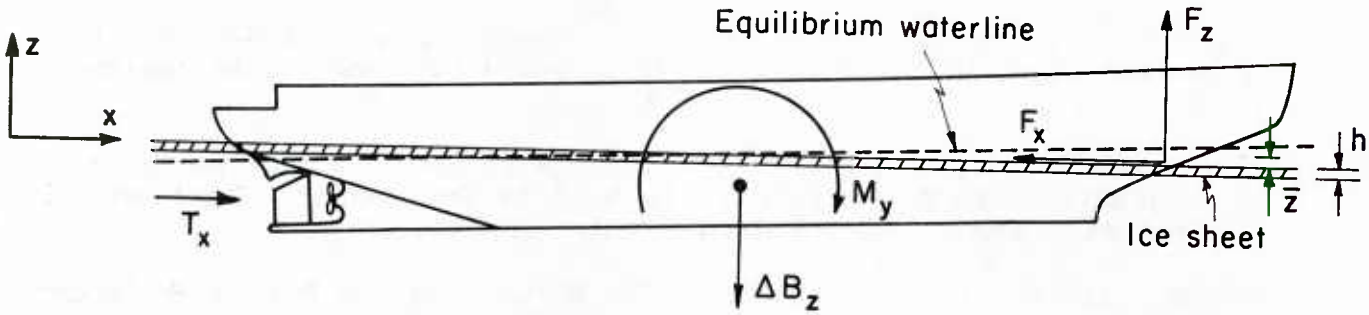

(b) Forces and moment due to ice breaking

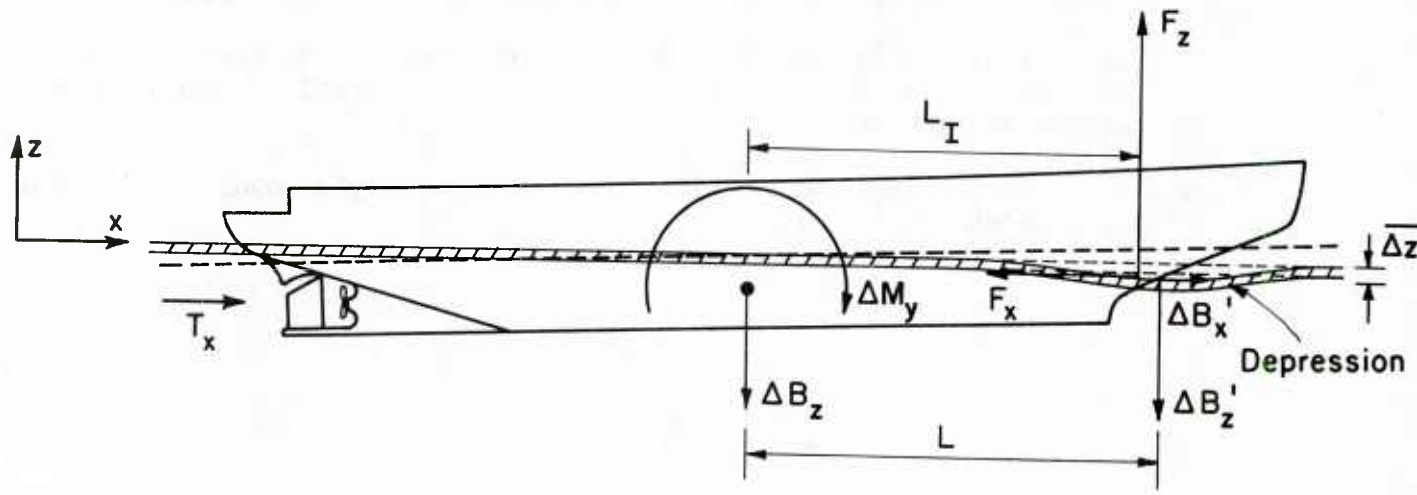

(c) Influence of ice-sheet and water level depression, at the bow, on the loading of a hull.

Figure 1. Definition sketch of forces acting on an ice-breaker hull.

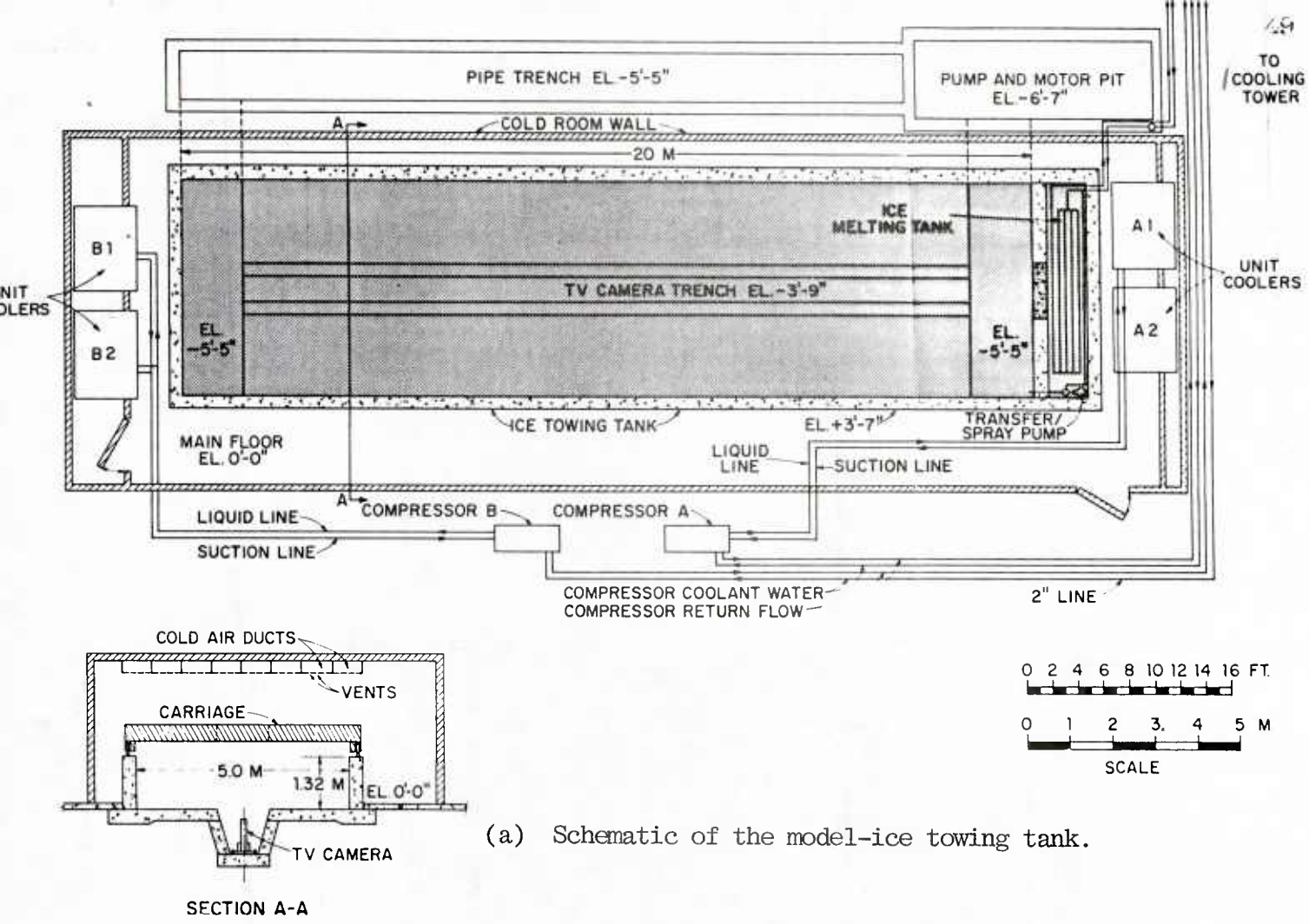

(a) Schematic of the model-ice towing tank.

(b) Towing tank and motorized carriage

Figure 2. The IIHR model-ice towing tank

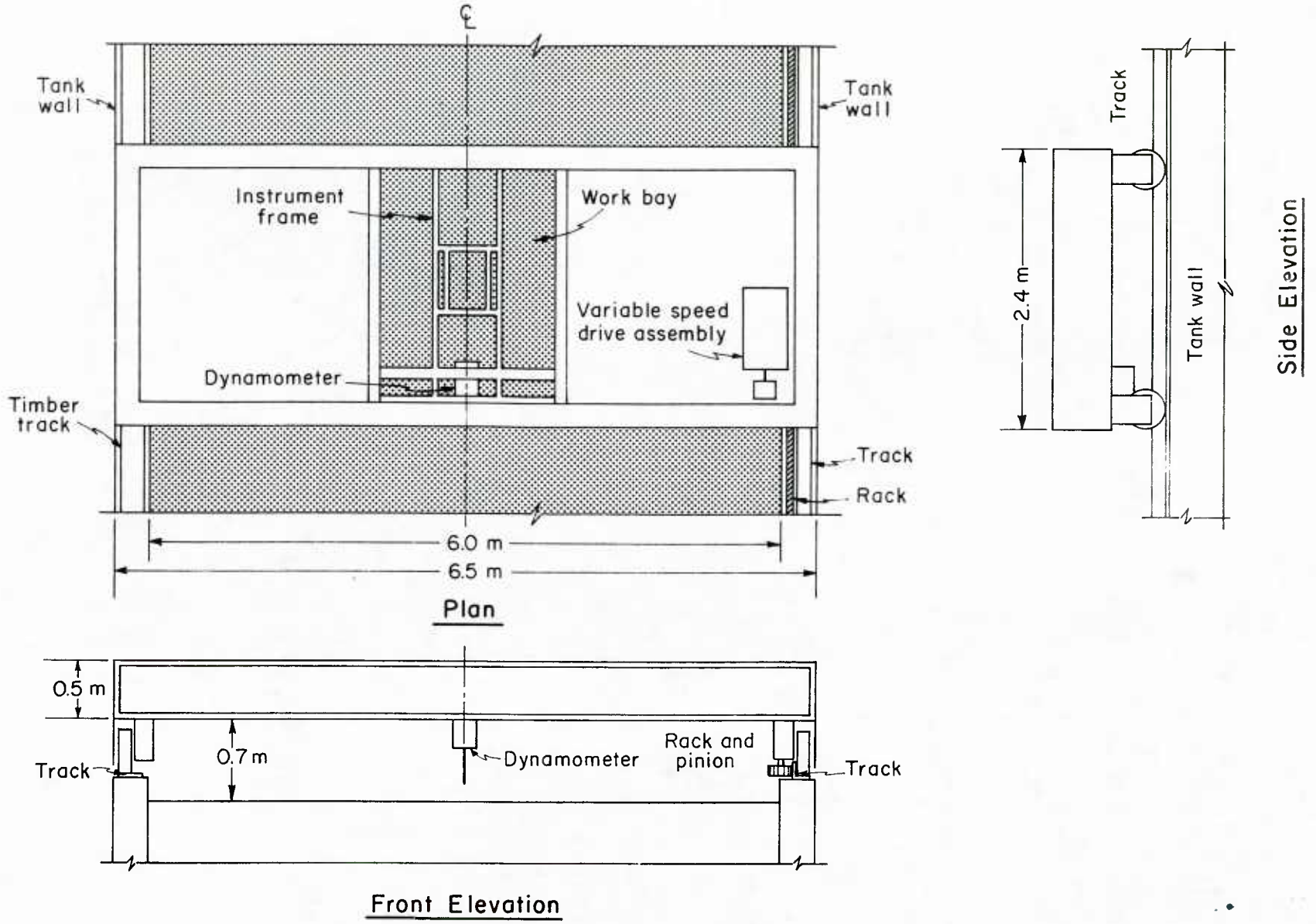

Figure 3. Sketch of the motorized carriage

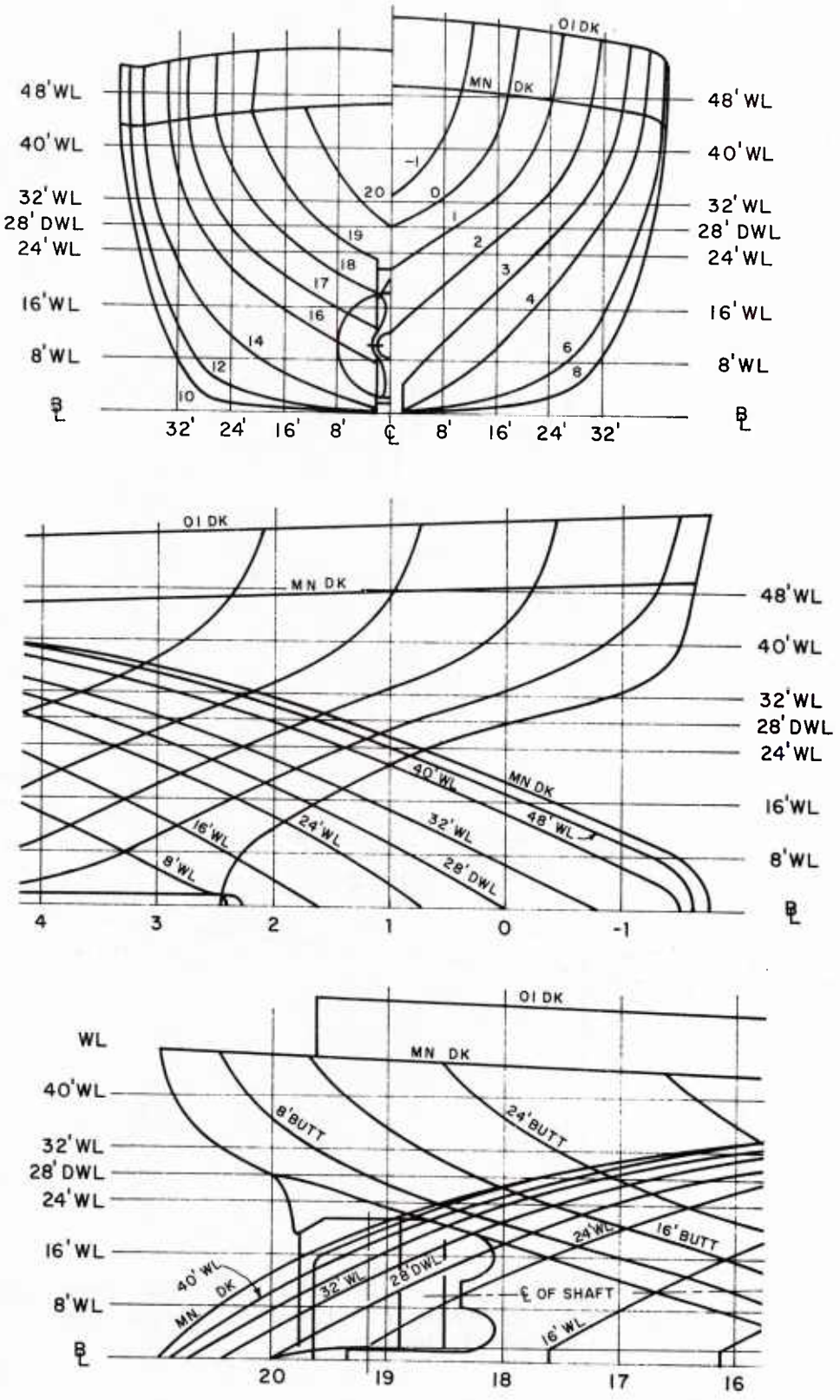

Figure 4. Abbreviated lines of the USGSC ice-breaker ship "Polar Star"

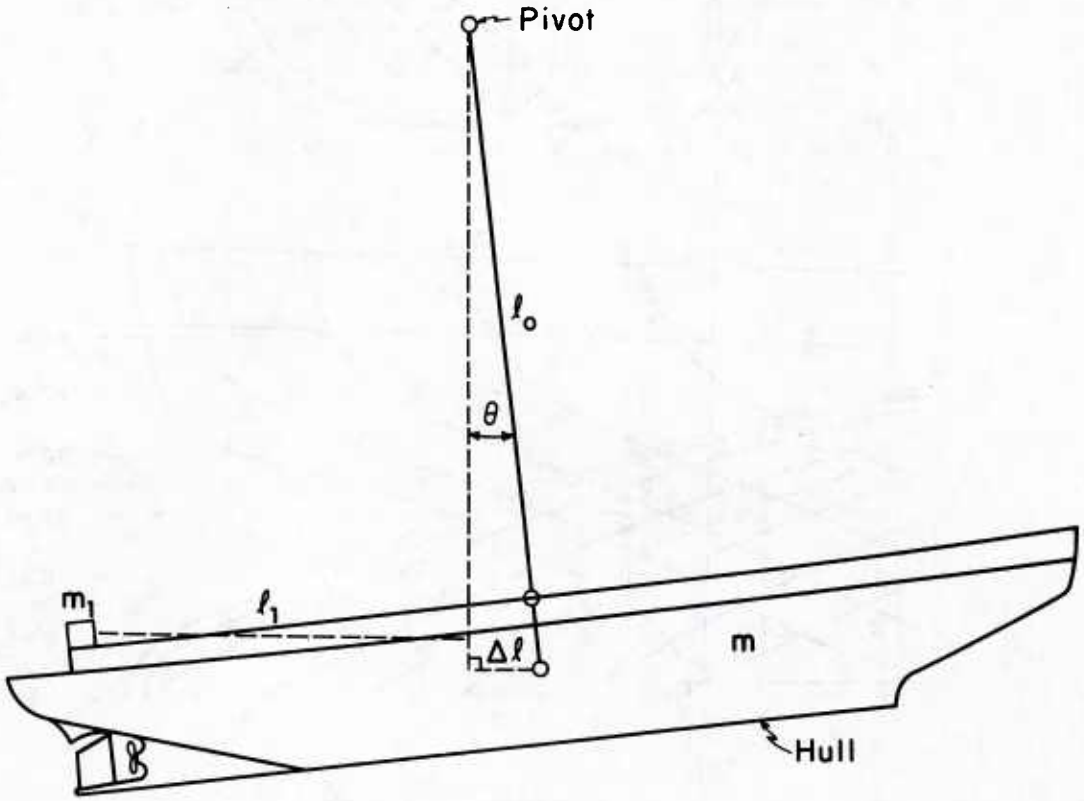

Figure 5. Definition sketch of the pendulum arrangement that was used to determine the mass moment of inertia of the model hull.

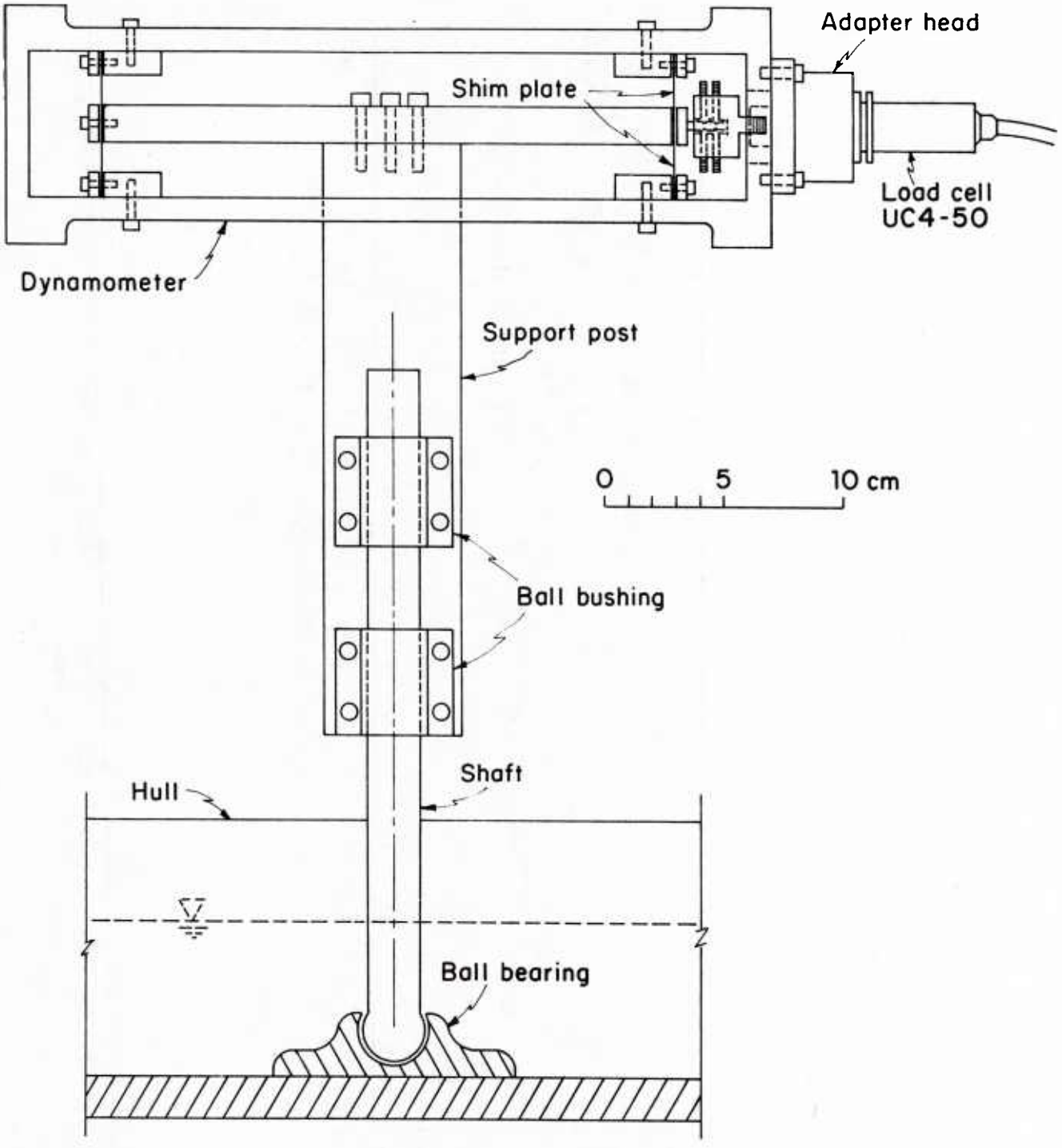

Figure 6. Details of the dynamometer that was used for measuring towing force.

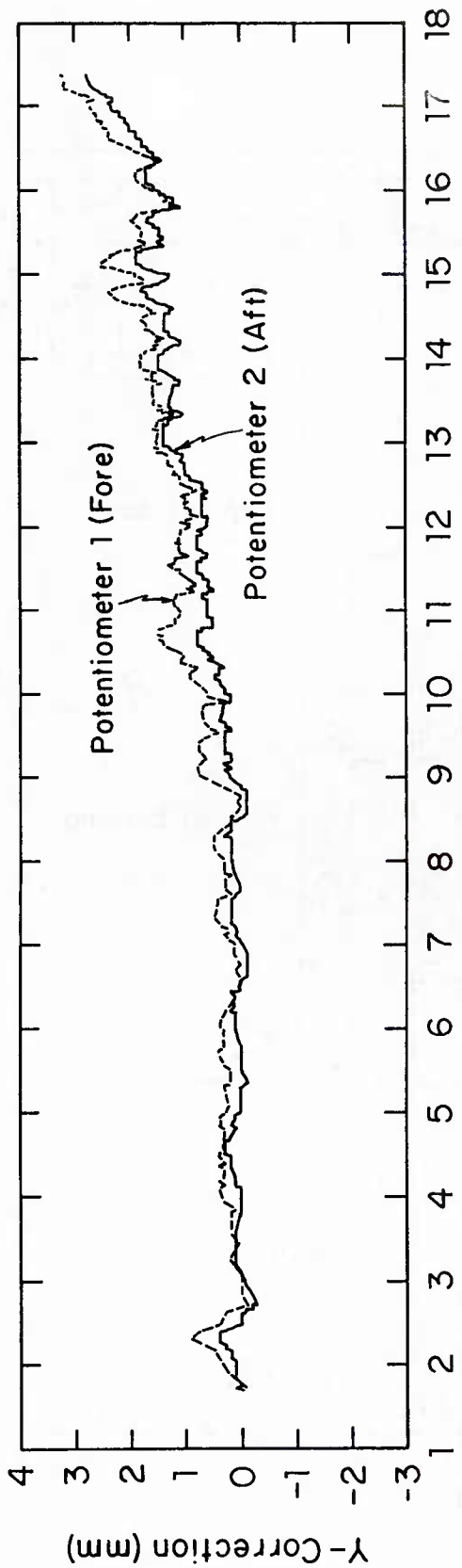

Figure 7. Relative height, $H_R(x)$, or vertical correction for position along the tracks of the motorized carriage.

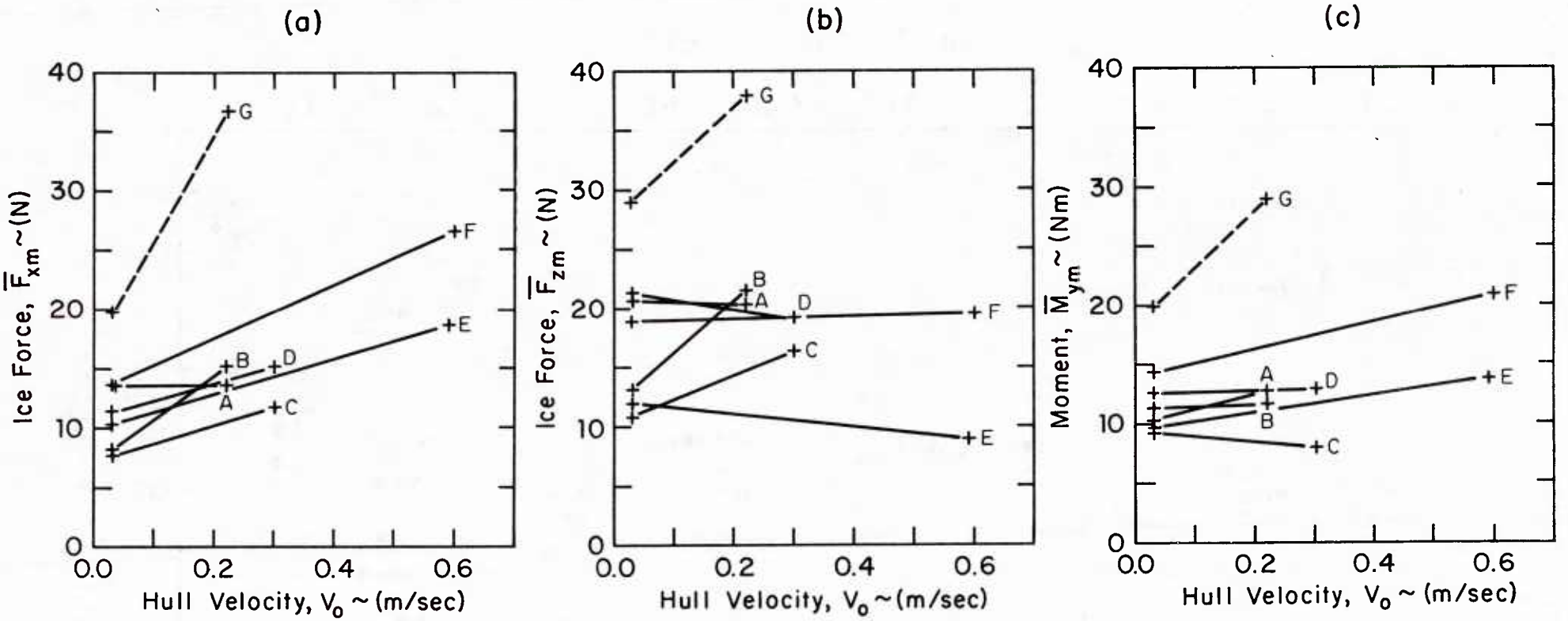

(a) Horizontal force $\overline{F}_{xm}$

(b) Vertical force, $\overline{F}_{zm}$, approximated by $\rho_w g A_w \overline{z}(t)$

(c) Moment, $\overline{M}_{ym}$, approximated by $\rho_w g A_w I_{yy} \overline{\theta}$

Figure 8. Temporal mean values of measured forces and moments acting against the hull.

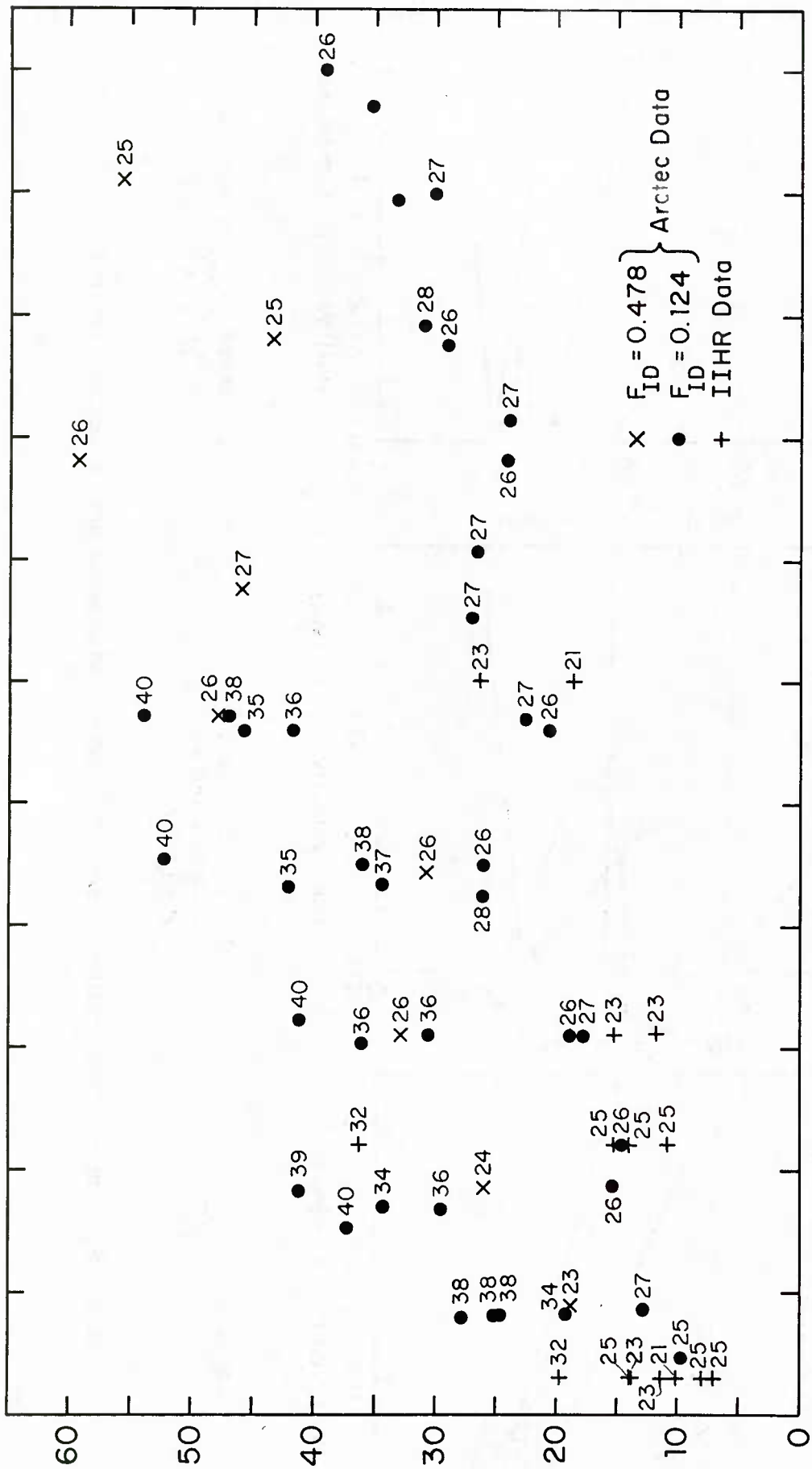

Figure 9. Comparison of $\overline{F}_{xm}$ with the results of the model tests conducted by Arctec Inc. The number on each plot point indicates ice sheet thickness in mm.

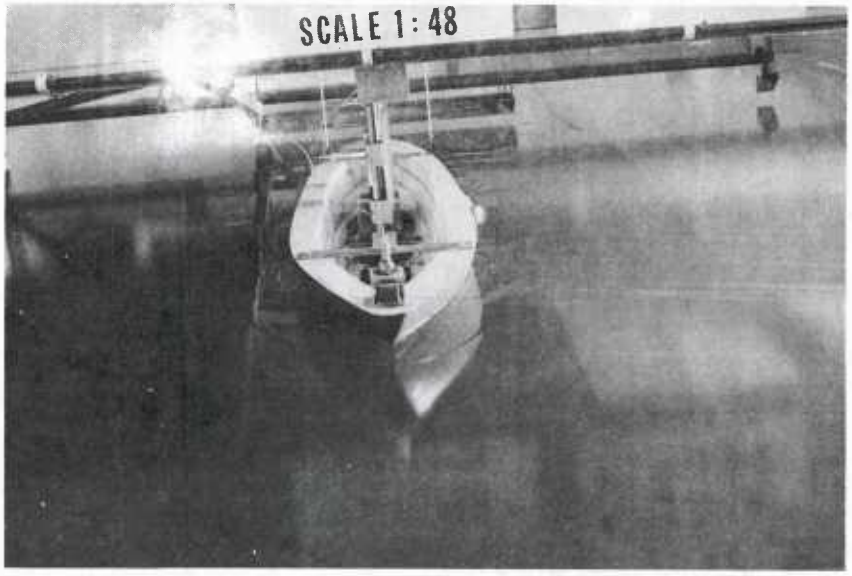

(a) For a low speed (V_o = 0.03 m/s), the depression is flooded

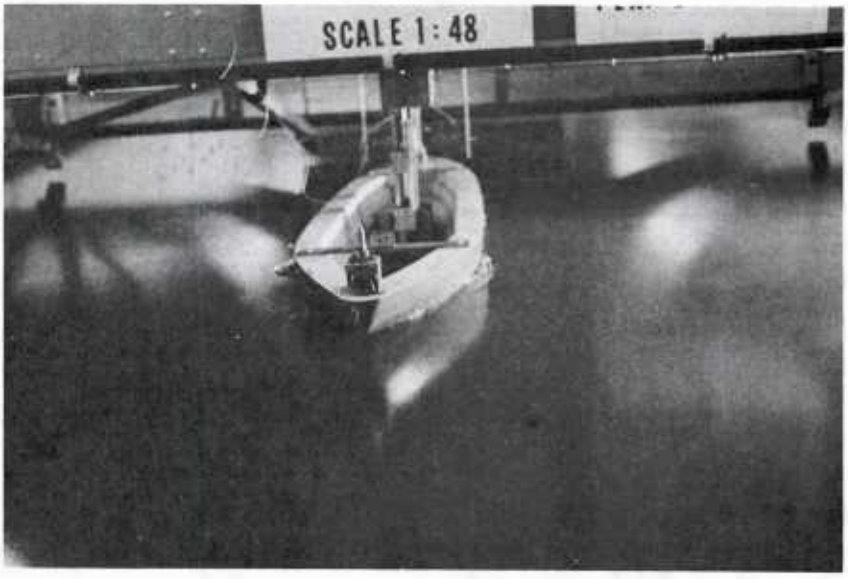

(b) For a medium speed (V_o = 0.22 m/s), the depressed area is dry

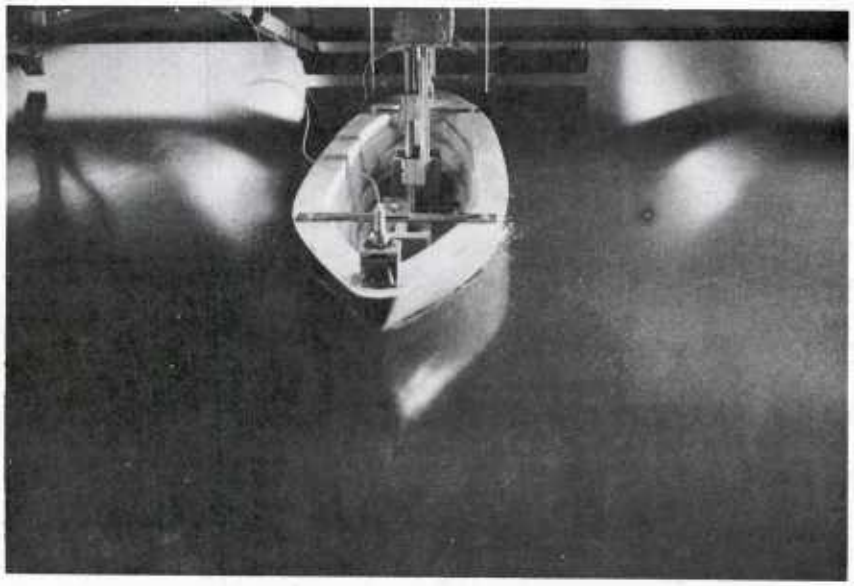

(c) For a high speed (V_o = 0.60 m/s), an air gap was visible at the bow

Figure 10. Depression of the ice sheet at the bow of the hull.

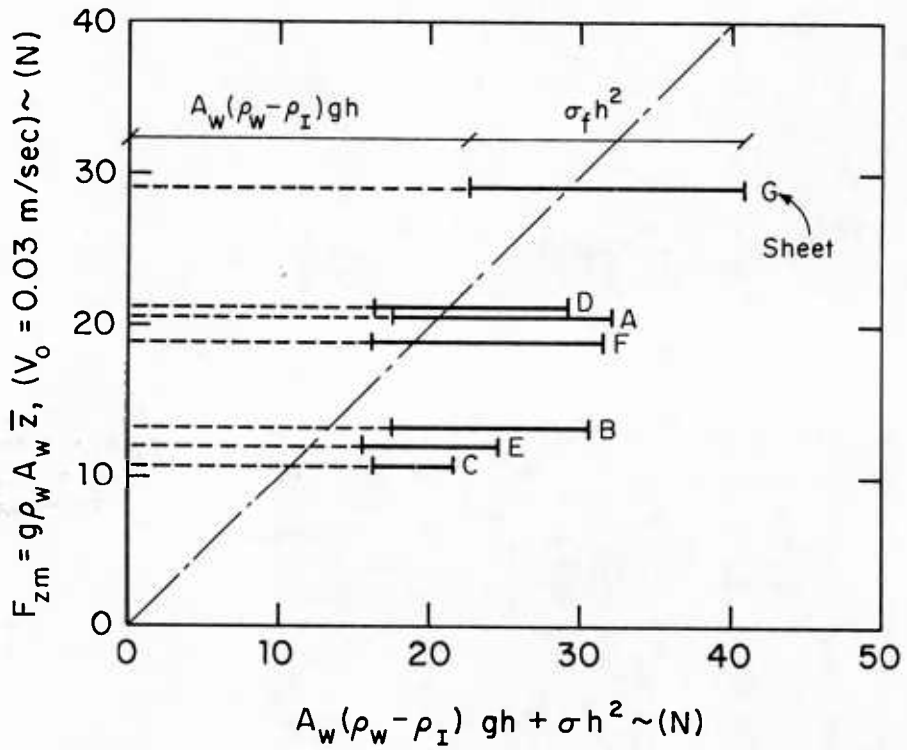

Figure 11. Comparison of $\overline{F}_{zm}$, at V_o = 0.03 m/s, with $A_w(\rho_w - \rho_I)\ gh + \sigma_f h^2$.

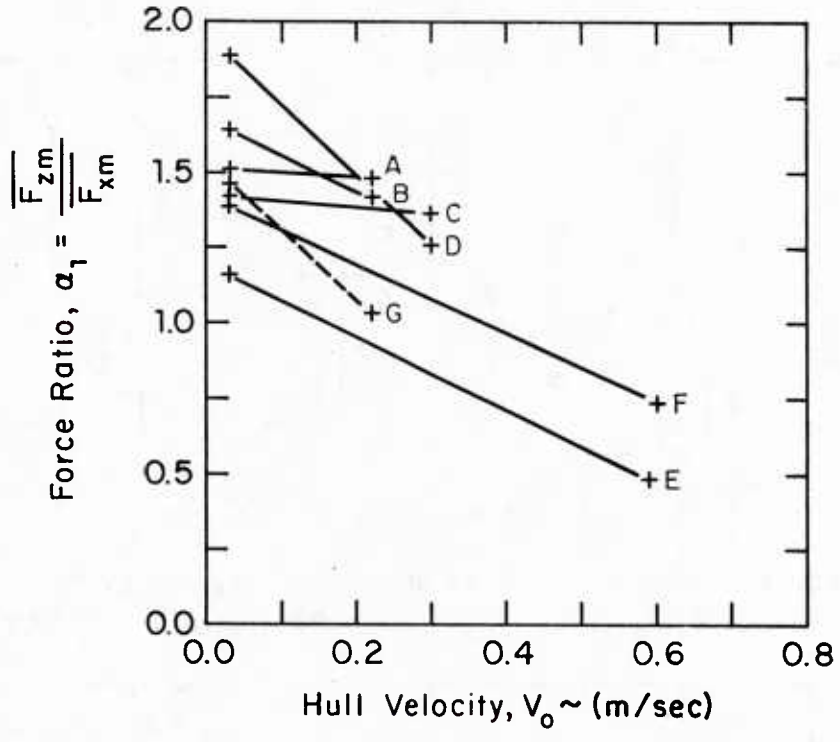

(a) Force ratio versus hull velocity

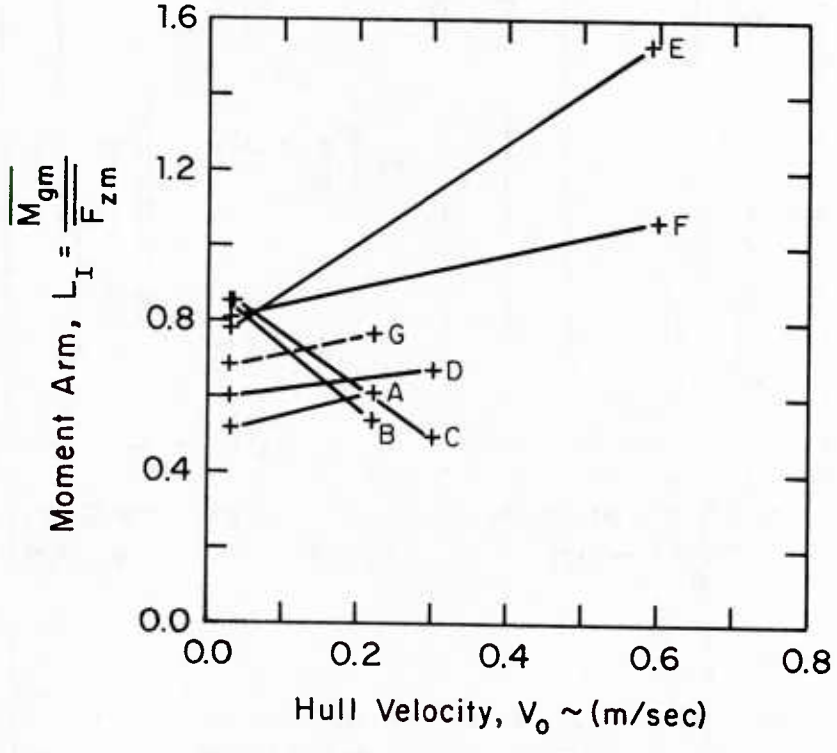

(b) Moment arm versus hull velocity

Figure 12. Variation of force ratio α_1 and moment arm L_I with hull velocity, V_o.

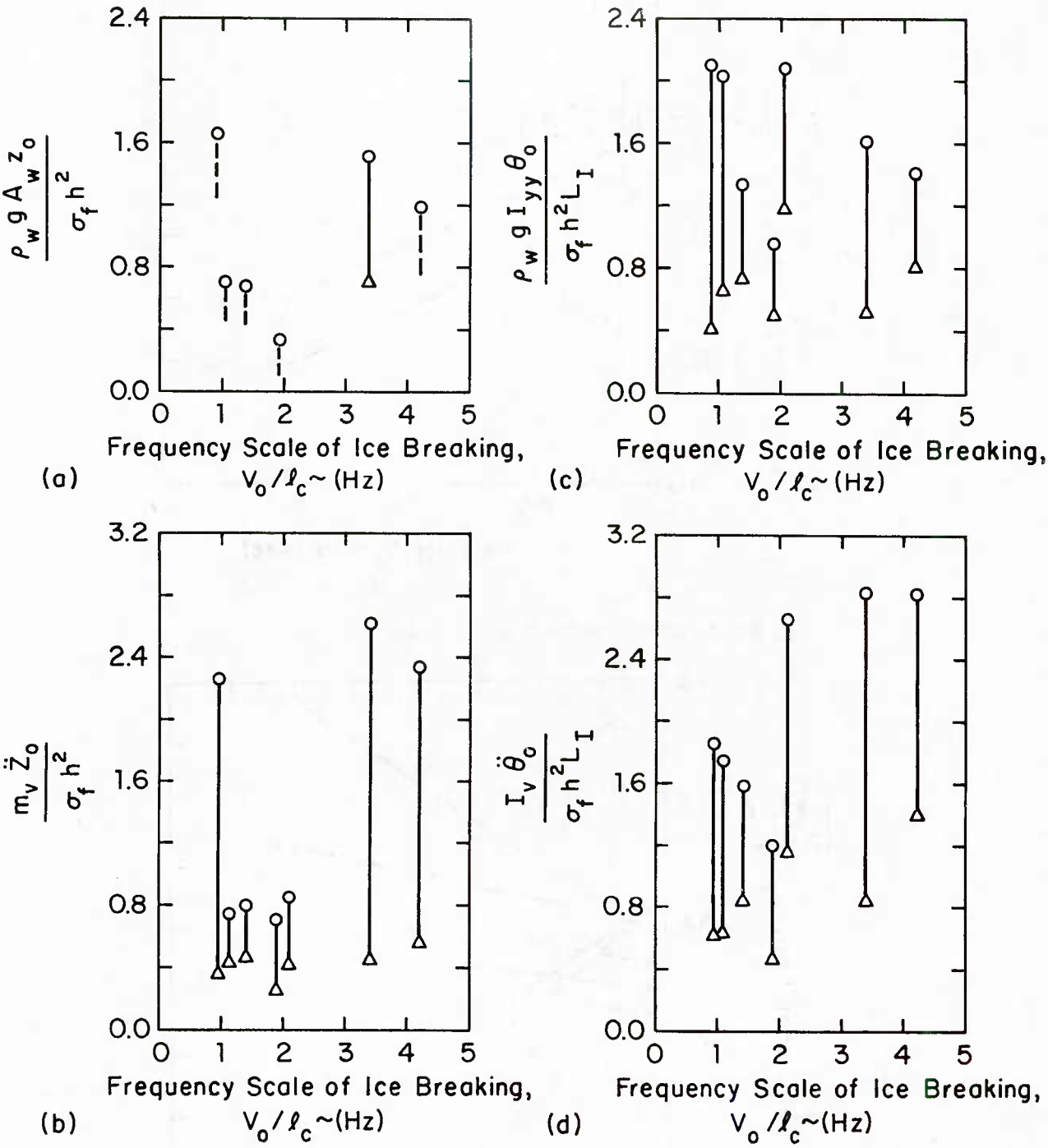

Figure 13. Typical maxima (0) and minima (Δ) of peak-to-peak values of vertical forces and moments plotted versus frequency scale of ice breaking, V_o/l_c.

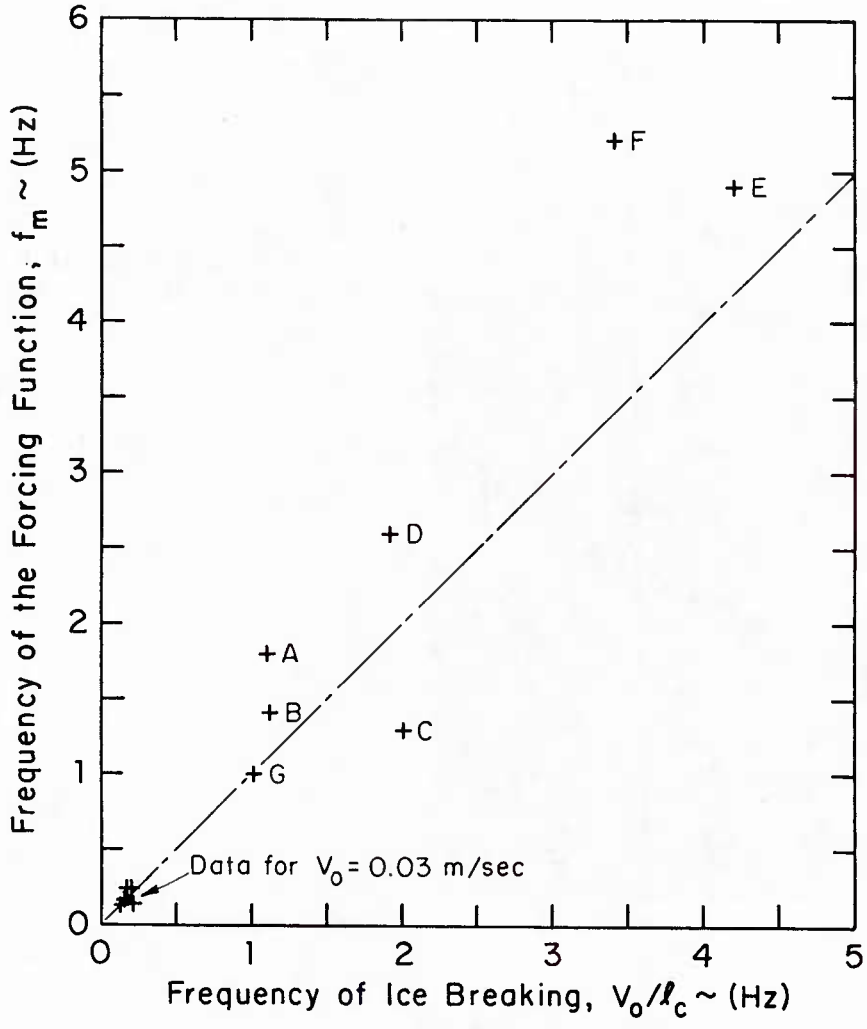

Figure 14. Correlation of frequency of forcing function, f_m, with frequency-scale of the breaking, V_o/l_c.

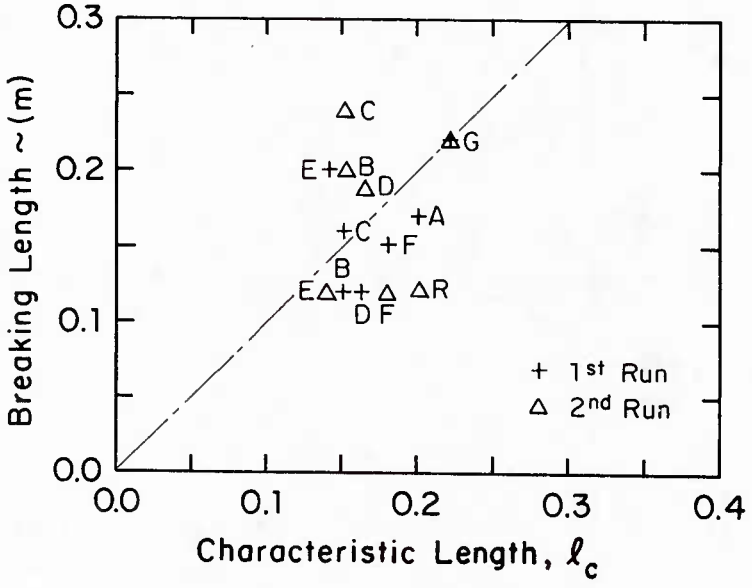

Figure 15. Correlation of ice-breaking length, Δx, with characteristic length of ice sheet, l_c.

(a) Hull moving at a relatively low velocity V_o = 0.03 m/s

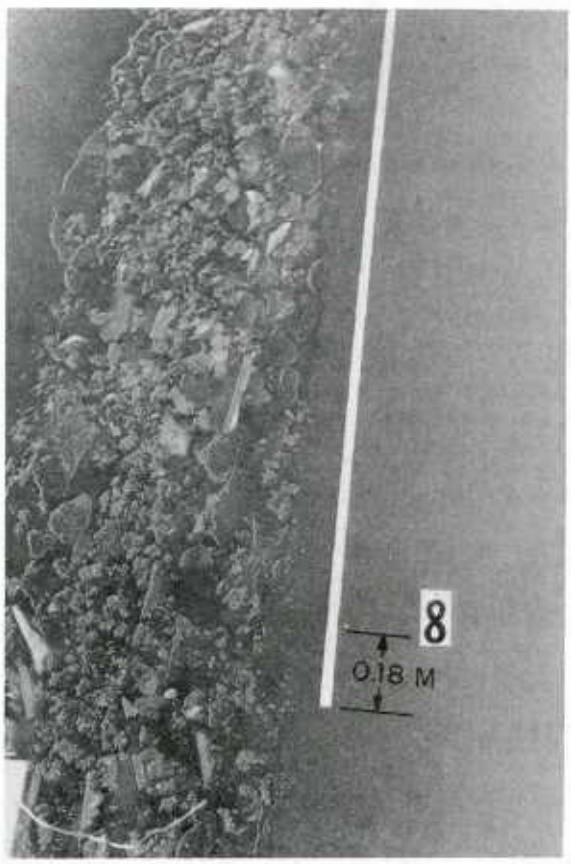

(b) Hull moving at a relatively high velocity V_o = 0.60 m/s

Figure 16. Typical sizes of ice rubble after the model hull has transmitted ice sheets.

Table 1. List of Physical Parameters of Ship Model

Overall length of hull	2.534 m
Length between perpendicular	2.235 m
Beam (maximum width)	0.530 m
Beam (design at waterline)	0.495 m
Draft (design)	0.178 m
Displacement	m = 102.6 kg
Virtual mass coefficient (heaving motion)	a = 1.38
Mass moment of inertia	$I = 33.3\ kgm^2$
Virtual mass moment of inertia coefficient	A = 0.55
Area of the waterplane of the hull	$A_w = 0.82\ m^2$
Area moment of inertia for pitch motion	$I_{yy} = 0.25\ m^4$
Wetted area of hull	$S = 1.32\ m^2$

Table 2. Measurement of Open-Water Resistance to Hull Motion

Hull Velocity V_o (m/sec)	Froude No. $\frac{V_o}{\sqrt{gL_s}}$	Reynolds No. $\frac{V_o L_s}{\nu}$	Resistance Force F_x (N)	Coefficient of Resistance C
0.03	0.0064	37×10^3	0.2	0.34
0.15	0.032	188×10^3	0.4	0.023
0.22	0.046	276×10^3	0.4	0.012
0.30	0.064	377×10^3	0.5	0.0084
0.59	0.128	741×10^3	1.5	0.0065

Table 3. List of the Bandwidths and the Sensitivities of the Instruments

	Bandwidth		Sensitivity
	Range (Hz)	Limited by	
Force F_x	0-3	digital filtering to remove resonant frequency and 6 Hz	33.5 N/Volt
Accelerometers	0-6	analog-filter before A/D conversion	0.42 m/sec^2/volt
$\ddot{z}(t)$	0.5-6	Rolling of hull	
Linear Potentiometers	0 - ∞		0.013 m/Volt
Velocity	0	Speed control of the carriage	0.137 m/sec/Volt

Table 4. List of Experimental Errors

Parameter	Error	Main Source of Error
F_x	± 1N	electrical drift
Draft z	< ±0.00065 m	static friction of
$\rho_w g A_w z$	± 5N	ball bushings
Pitch θ	± 0.0004 radius	electrical drift
$\rho_w g I_{yy} \theta$	+ 1Nm	
$\ddot{z}$	± 0.02 m/sec^2	Rolling of Ship
$m_v \ddot{z}$	± 5N	($\Delta \ddot{z}$ = 0.005 m/sec^2/degree
		error occuring at low frequencies)
$\ddot{\theta}$	± 0.01 sec^{-2}	electrical drift
$I_v \ddot{\theta}$	± 0.5 Nm	

Table 5. Physical Parameters of Ice Sheets and Test Runs

Sheet	Date	h (m)	σ_f (kPa)	E_f (MPa)	l_c (m)	$\sigma_f h^2$ (N)	Run No	V_o (m/sec)	$\frac{V_o}{l_c}$ (sec^{-1})	$\frac{V_o}{f_o l_c}$	T (sec)
A	10/15/82	0.25	23	11	0.20	14.4	02015	0.03	0.15	0.15	47.7
							03015	0.22	1.1	1.1	36.0
B	10/27/82	0.021	29	6.5	0.15	12.9	04027	0.03	0.20	0.20	48.9
							06027	0.22	1.5	1.4	19.2
C	10/18/82	0.023	10	4.2	0.15	5.3	02018	0.03	0.20	0.20	42.9
							03018	0.30	2.0	2.0	29.8
D	10/25/82	0.023	25	6.0	0.16	13.0	04025	0.03	0.19	0.19	44.1
							05025	0.30	1.9	1.9	30.0
E	10/20/82	0.022	19	3.8	0.14	9.3	04020	0.03	0.21	0.21	59.1
							05020	0.59	4.2	4.2	6.0
F	10/29/82	0.023	29	8.5	0.18	15.3	06029	0.03	0.17	0.17	49.1
							07029	0.60	3.4	3.4	12.0
G	10/22/82	0.032	18	8.3	0.22	18.1	04022	0.03	0.13	0.13	49.1
							05022	0.22	1.0	1.0	27.0

Table 6. List of Scaling Factors

Draft:	$\rho_w g A_w z = 7950\ z$ (N)
Vertical Acceleration:	$m_v \ddot{z} = 244\ \ddot{z}$ (N)
Pitch:	$\rho_w g I_{yy} \theta = 2450\ \theta$ (Nm)
Angular Acceleration:	$I_v \ddot{\theta} = 51.6\ \ddot{\theta}$ (Nm)

Table 7. Effect of the Depression of the Water Level at the Bow

Sheet	V_o (m/sec)	$\overline{F}_x$ (N)	$\overline{F}_z$ (N)	$\overline{M}_y$ (Nm)	α_1	L_I (m)	$\Delta B'_z$ (N)	Δz (m)	$\Delta M'_y$ (Nm)	L (m)	$\Delta B'_x$ (N)
E	0.59	18.6	8.74	13.72	0.47	1.56	19.2	0.024	6.7	0.35	1.5
F	0.60	26.5	19.9	20.8	0.75	1.04	19.9	0.025	8.2	0.41	1.5

APPENDIX A

Mean, Standard Deviations, Covariances and Correlation Coefficients of the Experimental Runs

Nomenclature:

Draft	$z(t)$
A_z	$\ddot{z}(t)$
Pitch	$\theta(t)$
Omega	$\ddot{\theta}(t)$

SHEET A VEL = 0.03 (RUN NO : 02015)

	Fx	Draft	Az	Pitch	Omega
	N	m	m/sec**2	radians	1/sec**2
MEAN	13.64	0.0026	-0.003	0.0043	-0.007
SIGMA	3.41	0.0002	0.003	0.0009	0.004
scaled as forces and moments					
	N	N	N	Nm	Nm
MEAN	13.64	20.59	-0.81	10.46	-0.38
SIGMA	3.41	1.27	0.71	2.31	0.21
Covariance of					
Fx with : (N*N) or (N*Nm)		-0.58	-0.83	4.35	-0.09
Draft with : (N*N) or (N*Nm)			-0.20	1.60	-0.07
Az with : (N*Nm)				-0.79	0.02
Pitch with : (Nm*Nm)					-0.17
Corr. Coefficient					
Fx with :		-0.13	-0.35	0.55	-0.13
Draft with :			-0.23	0.54	-0.26
Az with :				-0.48	0.15
Pitch with :					-0.35

SHEET A VEL = 0.22 (RUN NO : 03015)

	Fx	Draft	Az	Pitch	Omega
	N	m	m/sec**2	radians	1/sec**2
MEAN	13.59	0.0025	-0.012	0.0050	-0.008
SIGMA	3.76	0.0004	0.010	0.0017	0.050
scaled as forces and moments					
	N	N	N	Nm	Nm
MEAN	13.59	20.19	-2.92	12.27	-0.40
SIGMA	3.76	3.15	2.48	4.23	2.57
Covariance of					
Fx with : (N*N) or (N*Nm)		7.16	-0.86	9.19	-2.77
Draft with : (N*N) or (N*Nm)			0.08	8.48	-1.71
Az with : (N*Nm)				0.43	0.46
Pitch with : (Nm*Nm)					-7.87
Corr. Coefficient					
Fx with :		0.60	-0.09	0.58	-0.29
Draft with :			0.01	0.64	-0.21
Az with :				0.04	0.07
Pitch with :					-0.72

SHEET B VEL = 0.03 (RUN NO : 04027)

	Fx	Draft	Az	Pitch	Omega
	N	m	m/sec**2	radians	1/sec**2
MEAN	8.06	0.0017	0.004	0.0046	-0.004
SIGMA	1.65	0.0002	0.005	0.0008	0.011
scaled as forces and moments					
	N	N	N	Nm	Nm
MEAN	8.06	13.12	0.92	11.20	-0.23
SIGMA	1.65	1.32	1.24	2.03	0.58
Covariance of					
Fx with : (N*N) or (N*Nm)		0.52	-0.47	1.32	-0.05
Draft with : (N*N) or (N*Nm)			-1.14	1.80	-0.16
Az with : (N*Nm)				-1.30	0.06
Pitch with : (Nm*Nm)					-0.53
Corr. Coefficient					
Fx with :		0.24	-0.23	0.39	-0.05
Draft with :			-0.70	0.67	-0.21
Az with :				-0.52	0.08
Pitch with :					-0.45

SHEET B VEL = 0.22 (RUN NO : 06027)

	Fx	Draft	Az	Pitch	Omega
	N	m	m/sec**2	radians	1/sec**2
MEAN	15.12	0.0027	-0.001	0.0047	-0.001
SIGMA	3.60	0.0003	0.008	0.0014	0.059
scaled as forces and moments					
	N	N	N	Nm	Nm
MEAN	15.12	21.51	-0.26	11.64	-0.04
SIGMA	3.60	2.61	1.91	3.33	3.05
Covariance of					
Fx with : (N*N) or (N*Nm)		0.62	-2.43	5.17	-2.77
Draft with : (N*N) or (N*Nm)			-0.91	2.67	-1.66
Az with : (N*Nm)				-2.73	3.00
Pitch with : (Nm*Nm)					-7.39
Corr. Coefficient					
Fx with :		0.07	-0.35	0.43	-0.25
Draft with :			-0.18	0.31	-0.21
Az with :				-0.43	0.51
Pitch with :					-0.73

SHEET C VEL = 0.03 (RUN NO : 02018)

	Fx	Draft	Az	Pitch	Omega
	N	m	m/sec**2	radians	1/sec**2
MEAN	7.73	0.0014	0.004	0.0038	-0.002
SIGMA	2.01	0.0001	0.003	0.0006	0.004
scaled as forces and moments					
	N	N	N	Nm	Nm
MEAN	7.73	10.94	1.06	9.21	-0.12
SIGMA	2.01	0.66	0.68	1.35	0.23
Covariance of					
Fx with : (N*N) or (N*Nm)		-0.22	-0.10	1.77	-0.03
Draft with : (N*N) or (N*Nm)			0.07	0.12	-0.02
Az with : (N*Nm)				-0.06	-0.03
Pitch with : (Nm*Nm)					-0.10
Corr. Coefficient					
Fx with :		-0.16	-0.08	0.65	-0.06
Draft with :			0.16	0.13	-0.10
Az with :				-0.06	-0.20
Pitch with :					-0.31

SHEET C VEL = 0.30 (RUN NO : 03018)

	Fx	Draft	Az	Pitch	Omega
	N	m	m/sec**2	radians	1/sec**2
MEAN	11.73	0.0020	0.003	0.0032	-0.002
SIGMA	2.76	0.0003	0.005	0.0009	0.044
scaled as forces and moments					
	N	N	N	Nm	Nm
MEAN	11.73	16.01	0.73	7.93	-0.09
SIGMA	2.76	2.45	1.31	2.12	2.27
Covariance of					
Fx with : (N*N) or (N*Nm)		1.19	-1.30	2.96	-1.24
Draft with : (N*N) or (N*Nm)			-0.28	1.20	-0.79
Az with : (N*Nm)				-0.83	0.85
Pitch with : (Nm*Nm)					-3.57
Corr. Coefficient					
Fx with :		0.18	-0.36	0.51	-0.20
Draft with :			-0.09	0.23	-0.14
Az with :				-0.30	0.29
Pitch with :					-0.74

SHEET D VEL = 0.03 (RUN NO : 04025)

	Fx	Draft	Az	Pitch	Omega
	N	m	m/sec**2	radians	1/sec**2
MEAN	11.25	0.0027	-0.004	0.0052	0.003
SIGMA	3.70	0.0002	0.002	0.0015	0.014
scaled as forces and moments					
	N	N	N	Nm	Nm
MEAN	11.25	21.17	-1.00	12.65	0.16
SIGMA	3.70	1.24	0.47	3.62	0.74
Covariance of					
Fx with : (N*N) or (N*Nm)		1.08	-0.80	7.70	-0.21
Draft with : (N*N) or (N*Nm)			-0.20	2.68	-0.07
Az with : (N*Nm)				-0.95	0.04
Pitch with : (Nm*Nm)					-0.62
Corr. Coefficient					
Fx with :		0.23	-0.46	0.58	-0.08
Draft with :			-0.34	0.60	-0.08
Az with :				-0.56	0.11
Pitch with :					-0.23

SHEET D VEL = 0.30 (RUN NO : 05025)

	Fx	Draft	Az	Pitch	Omega
	N	m	m/sec**2	radians	1/sec**2
MEAN	15.16	0.0024	0.002	0.0052	-0.003
SIGMA	3.41	0.0004	0.009	0.0013	0.060
scaled as forces and moments					
	N	N	N	Nm	Nm
MEAN	15.16	19.11	0.48	12.80	-0.13
SIGMA	3.41	3.23	2.21	3.29	3.10
Covariance of					
Fx with : (N*N) or (N*Nm)		4.14	-1.77	5.59	-2.01
Draft with : (N*N) or (N*Nm)			-2.27	7.24	-2.52
Az with : (N*Nm)				-2.72	3.82
Pitch with : (Nm*Nm)					-6.68
Corr. Coefficient					
Fx with :		0.38	-0.23	0.50	-0.19
Draft with :			-0.32	0.68	-0.25
Az with :				-0.37	0.56
Pitch with :					-0.66

SHEET E VEL = 0.03 (RUN NO : 04020)

	Fx	Draft	Az	Pitch	Omega
	N	m	m/sec**2	radians	1/sec**2
MEAN	10.46	0.0015	0.000	0.0039	0.000
SIGMA	3.34	0.0001	0.001	0.0005	0.003
scaled as forces and moments					
	N	N	N	Nm	Nm
MEAN	10.46	12.09	0.01	9.60	0.01
SIGMA	3.34	0.68	0.36	1.26	0.18
Covariance of					
Fx with : (N*N) or (N*Nm)		-0.42	-0.39	1.65	0.00
Draft with : (N*N) or (N*Nm)			0.02	0.40	-0.01
Az with : (N*Nm)				0.02	0.01
Pitch with : (Nm*Nm)					-0.03
Corr. Coefficient					
Fx with :		-0.18	-0.32	0.39	0.00
Draft with :			0.07	0.47	-0.08
Az with :				0.05	0.11
Pitch with :					-0.15

SHEET E VEL = 0.59 (RUN NO : 05020)

	Fx	Draft	Az	Pitch	Omega
	N	m	m/sec**2	radians	1/sec**2
MEAN	18.63	0.0011	-0.001	0.0056	0.001
SIGMA	4.10	0.0002	0.013	0.0006	0.056
scaled as forces and moments					
	N	N	N	Nm	Nm
MEAN	18.63	8.96	-0.17	13.78	0.03
SIGMA	4.10	1.50	3.18	1.41	2.88
Covariance of					
Fx with : (N*N) or (N*Nm)		0.78	0.36	1.65	0.36
Draft with : (N*N) or (N*Nm)			-2.16	0.37	-1.24
Az with : (N*Nm)				-0.79	5.71
Pitch with : (Nm*Nm)					-2.30
Corr. Coefficient					
Fx with :		0.13	0.03	0.28	0.03
Draft with :			-0.45	0.18	-0.29
Az with :				-0.18	0.62
Pitch with :					-0.57

SHEET F VEL = 0.03 (RUN NO : 06029)

	Fx	Draft	Az	Pitch	Omega
	N	m	m/sec**2	radians	1/sec**2
MEAN	13.60	0.0024	-0.003	0.0058	-0.002
SIGMA	3.84	0.0001	0.010	0.0012	0.009
scaled as forces and moments					
	N	N	N	Nm	Nm
MEAN	13.60	18.91	-0.75	14.33	-0.11
SIGMA	3.84	0.99	2.56	2.98	0.46
Covariance of					
Fx with : (N*N) or (N*Nm)		0.26	-5.84	1.77	0.06
Draft with : (N*N) or (N*Nm)			0.29	0.58	-0.02
Az with : (N*Nm)				-2.93	0.01
Pitch with : (Nm*Nm)					-0.26
Corr. Coefficient					
Fx with :		0.07	-0.59	0.16	0.04
Draft with :			0.11	0.20	-0.04
Az with :				-0.39	0.01
Pitch with :					-0.19

SHEET F VEL = 0.60 (RUN NO : 07029)

	Fx	Draft	Az	Pitch	Omega
	N	m	m/sec**2	radians	1/sec**2
MEAN	26.54	0.0025	-0.010	0.0085	-0.002
SIGMA	7.25	0.0006	0.031	0.0015	0.085
scaled as forces and moments					
	N	N	N	Nm	Nm
MEAN	26.54	19.56	-2.33	20.73	-0.09
SIGMA	7.25	4.72	7.66	3.78	4.39
Covariance of					
Fx with : (N*N) or (N*Nm)		12.27	-20.78	10.39	-4.30
Draft with : (N*N) or (N*Nm)			-17.37	14.47	-8.48
Az with : (N*Nm)				-16.05	25.03
Pitch with : (Nm*Nm)					-9.84
Corr. Coefficient					
Fx with :		0.36	-0.37	0.38	-0.13
Draft with :			-0.48	0.81	-0.41
Az with :				-0.55	0.74
Pitch with :					-0.59

SHEET G VEL = 0.03 (RUN NO : 04022)

	Fx	Draft	Az	Pitch	Omega
	N	m	m/sec**2	radians	1/sec**2
MEAN	19.74	0.0037	0.002	0.0081	-0.004
SIGMA	5.50	0.0005	0.002	0.0018	0.009
scaled as forces and moments					
	N	N	N	Nm	Nm
MEAN	19.74	29.08	0.53	19.89	-0.23
SIGMA	5.50	4.10	0.53	4.39	0.45
Covariance of					
Fx with : (N*N) or (N*Nm)		13.31	-1.66	14.12	-0.17
Draft with : (N*N) or (N*Nm)			-0.70	4.65	-0.11
Az with : (N*Nm)				-1.57	0.04
Pitch with : (Nm*Nm)					-0.34
Corr. Coefficient					
Fx with :		0.59	-0.57	0.59	-0.07
Draft with :			-0.32	0.26	-0.06
Az with :				-0.67	0.15
Pitch with :					-0.17

SHEET G VEL = 0.22 (RUN NO : 05022)

	Fx	Draft	Az	Pitch	Omega
	N	m	m/sec**2	radians	1/sec**2
MEAN	36.65	0.0048	-0.042	0.0118	-0.001
SIGMA	11.43	0.0008	0.044	0.0027	0.097
scaled as forces and moments					
	N	N	N	Nm	Nm
MEAN	36.65	37.96	-10.24	28.83	-0.08
SIGMA	11.43	6.13	10.80	6.71	5.03
Covariance of					
Fx with : (N*N) or (N*Nm)		56.55	-91.17	59.71	-16.61
Draft with : (N*N) or (N*Nm)			-48.24	35.16	-14.07
Az with : (N*Nm)				-53.72	22.75
Pitch with : (Nm*Nm)					-22.72
Corr. Coefficient					
Fx with :		0.81	-0.74	0.78	-0.29
Draft with :			-0.73	0.85	-0.46
Az with :				-0.74	0.42
Pitch with :					-0.67

APPENDIX B

Time Series of the Measured Quantities

Top Figure	$F_x(t)$	———
	$\rho_w g A_w z(t)$	- - - - - - - -
	$m_v \ddot{z}(t)$	— — — —
Middle Figure	$\rho_w g I_{yy} \theta(t)$	- - - - - - - -
	$I_v \ddot{\theta}$	— — — —
Bottom Figure	$V_o(t)$	———

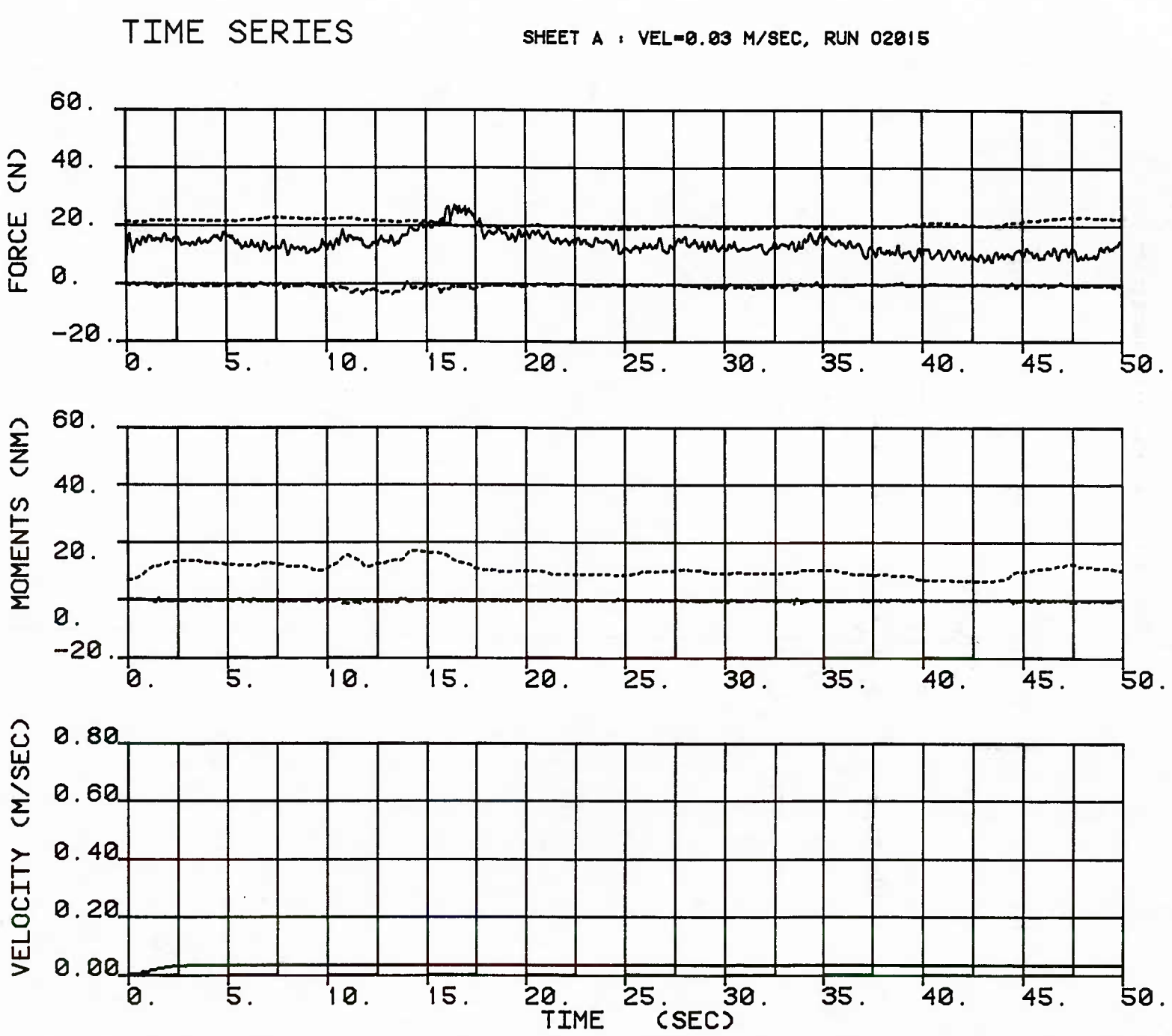
TIME SERIES
SHEET A : VEL=0.03 M/SEC, RUN 02015
FORCE (N)
60.
40.
20.
0.
-20.
0.
5.
10.
15.
20.
25.
30.
35.
40.
45.
50.
MOMENTS (NM)
60.
40.
20.
0.
-20.
0.
5.
10.
15.
20.
25.
30.
35.
40.
45.
50.
VELOCITY (M/SEC)
0.80
0.60
0.40
0.20
0.00
0.
5.
10.
15.
20.
25.
30.
35.
40.
45.
50.
TIME (SEC)

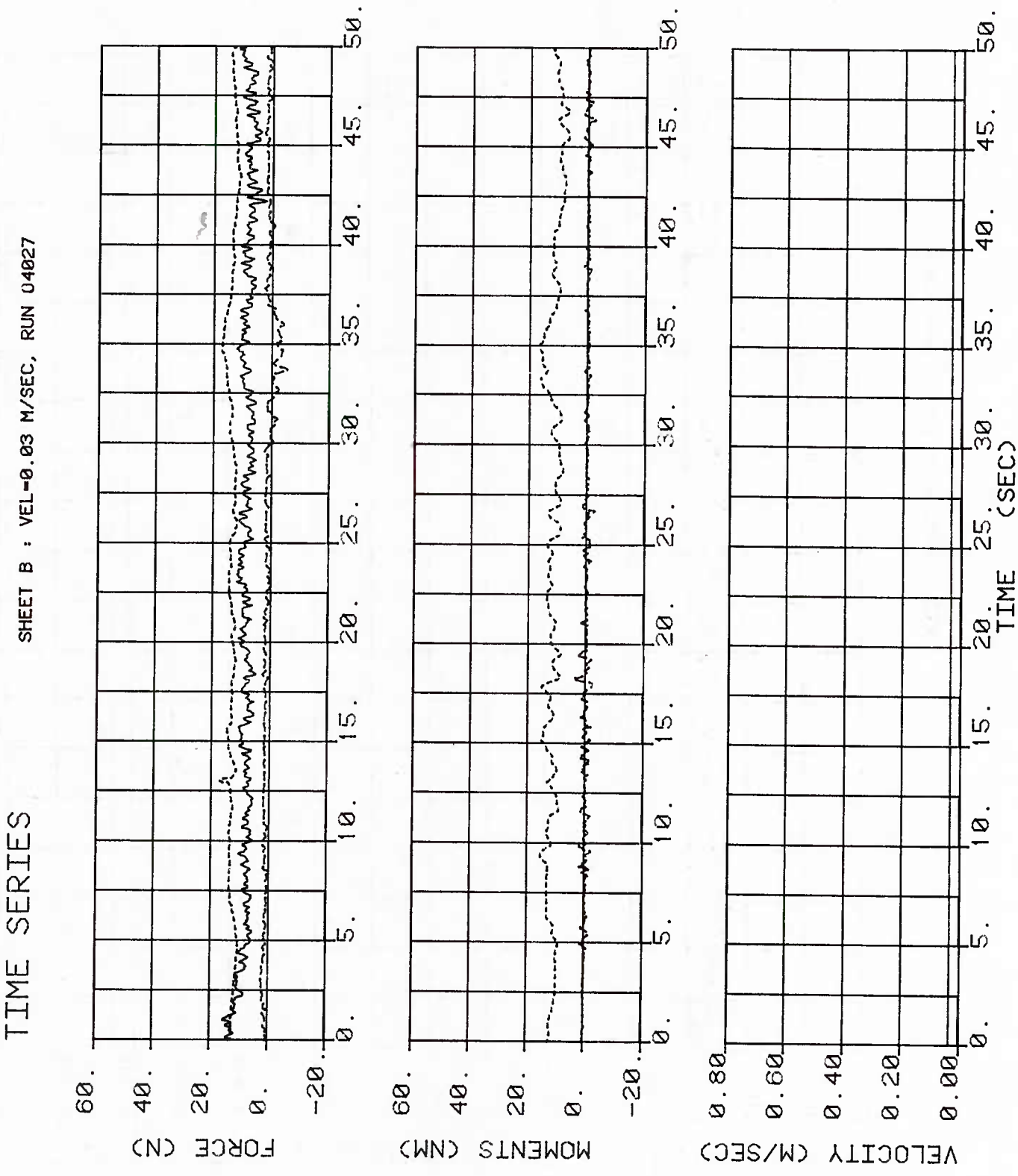
TIME SERIES
SHEET B : VEL=0.03 M/SEC, RUN 04027
FORCE (N)
60.
40.
20.
0.
-20.
MOMENTS (NM)
60.
40.
20.
0.
-20.
VELOCITY (CM/SEC)
0.80
0.60
0.40
0.20
0.00
0. 5. 10. 15. 20. 25. 30. 35. 40. 45. 50.
TIME (SEC)

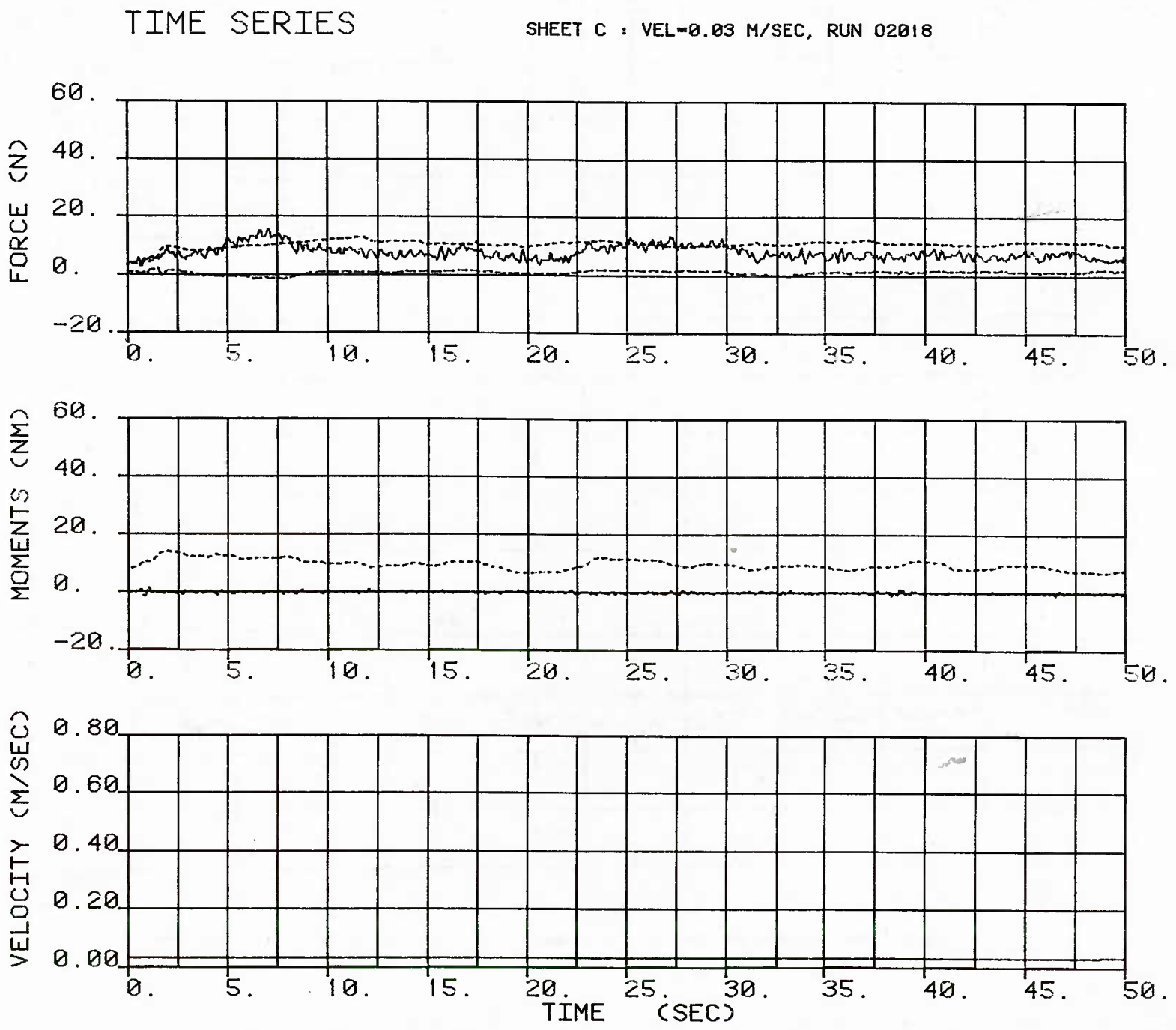
TIME SERIES
SHEET C : VEL=0.03 M/SEC, RUN 02018
FORCE (N)
60.
40.
20.
0.
-20.
0. 5. 10. 15. 20. 25. 30. 35. 40. 45. 50.
MOMENTS (NM)
60.
40.
20.
0.
-20.
0. 5. 10. 15. 20. 25. 30. 35. 40. 45. 50.
VELOCITY (M/SEC)
0.80
0.60
0.40
0.20
0.00
0. 5. 10. 15. 20. 25. 30. 35. 40. 45. 50.
TIME (SEC)

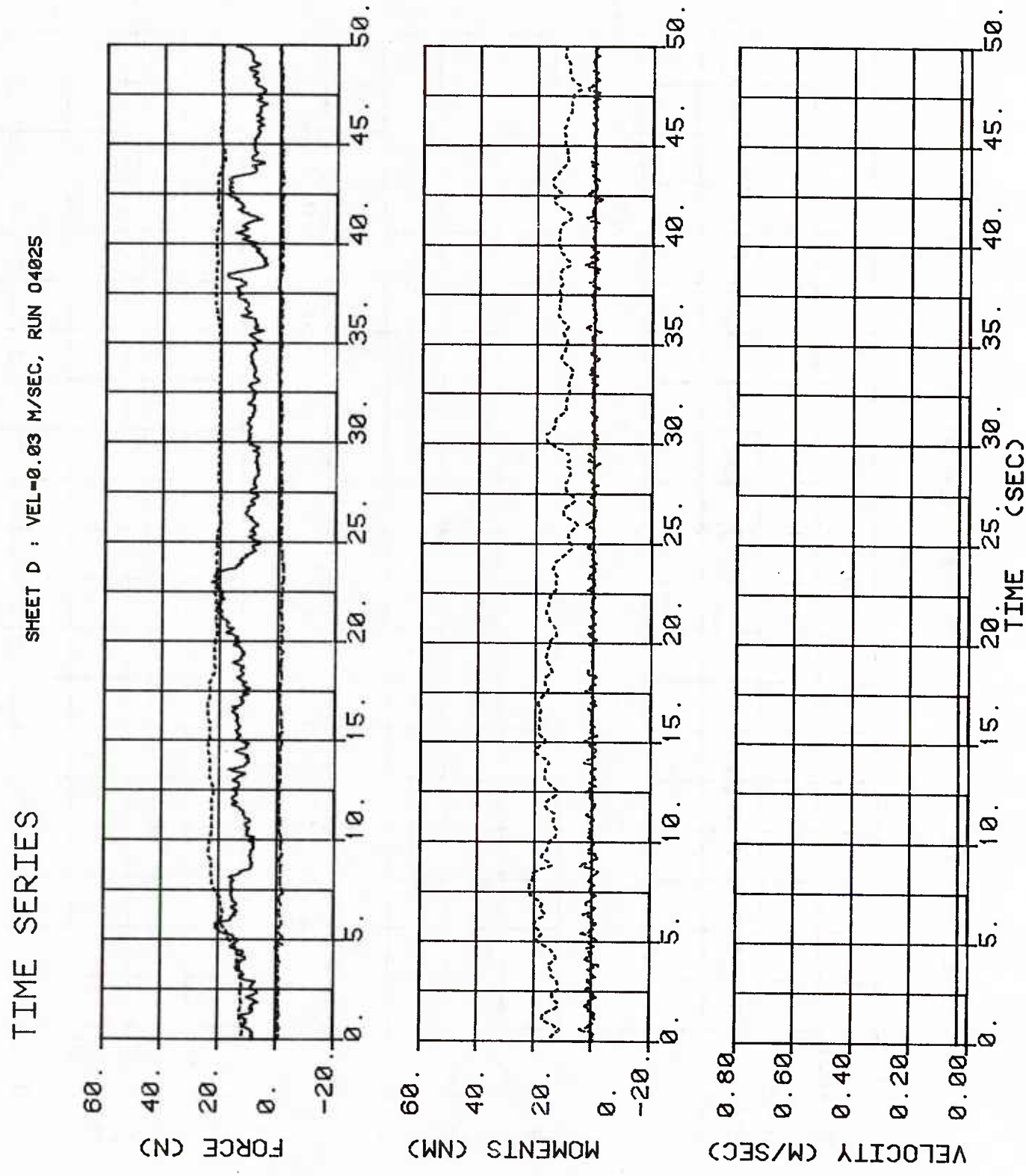
TIME SERIES
SHEET D : VEL=0.03 M/SEC, RUN 0402S
FORCE (N)
60.
40.
20.
0.
-20.
MOMENTS (NM)
60.
40.
20.
0.
-20.
VELOCITY (M/SEC)
0.80
0.60
0.40
0.20
0.00
0.
5.
10.
15.
20.
25.
30.
35.
40.
45.
50.
TIME (SEC)

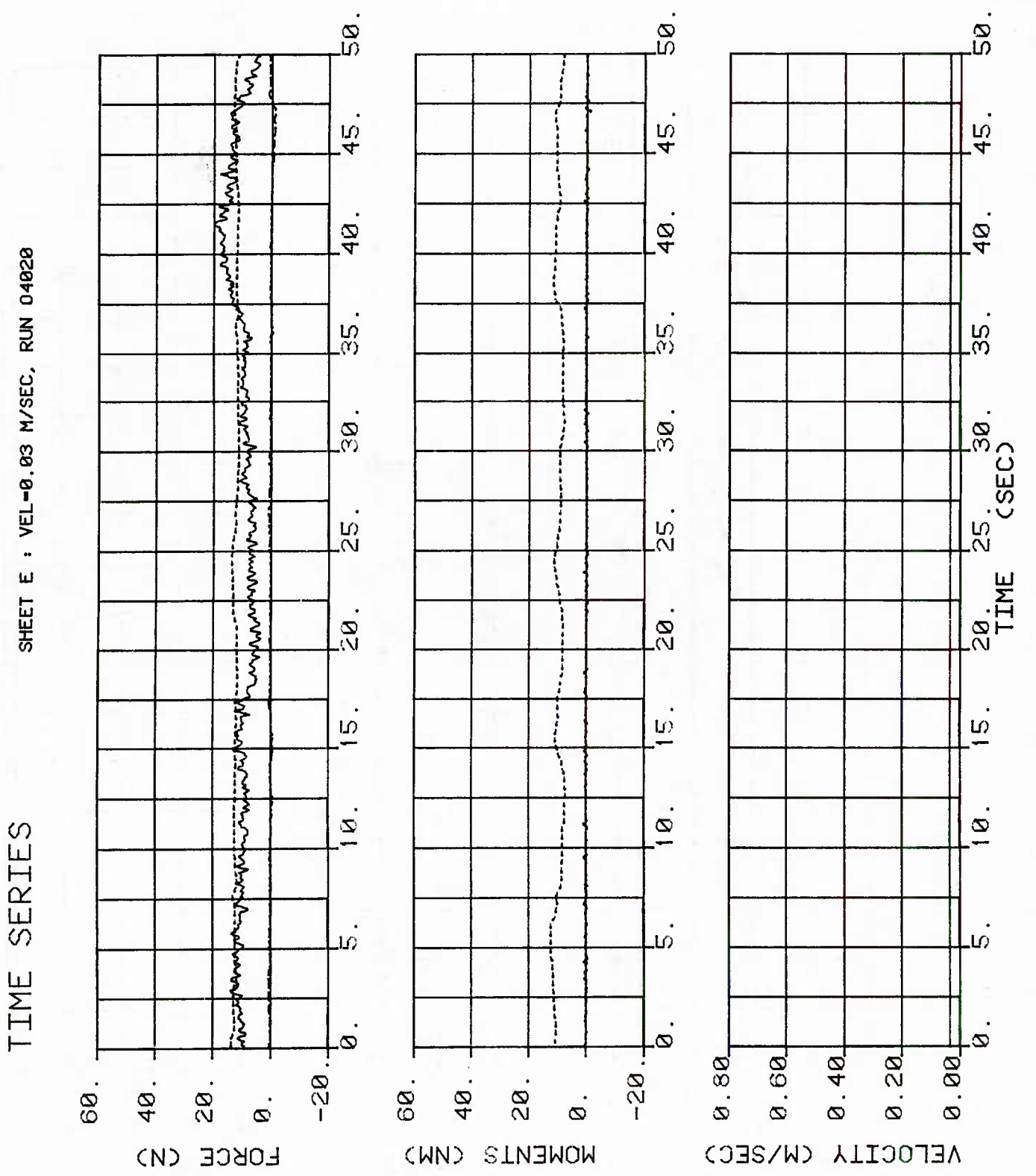
TIME SERIES
SHEET E : VEL=0.03 M/SEC, RUN 04020
FORCE (N)
60.
40.
20.
0.
-20.
MOMENTS (NM)
60.
40.
20.
0.
-20.
VELOCITY (M/SEC)
0.80
0.60
0.40
0.20
0.00
0.
5.
10.
15.
20.
25.
30.
35.
40.
45.
50.
TIME (SEC)

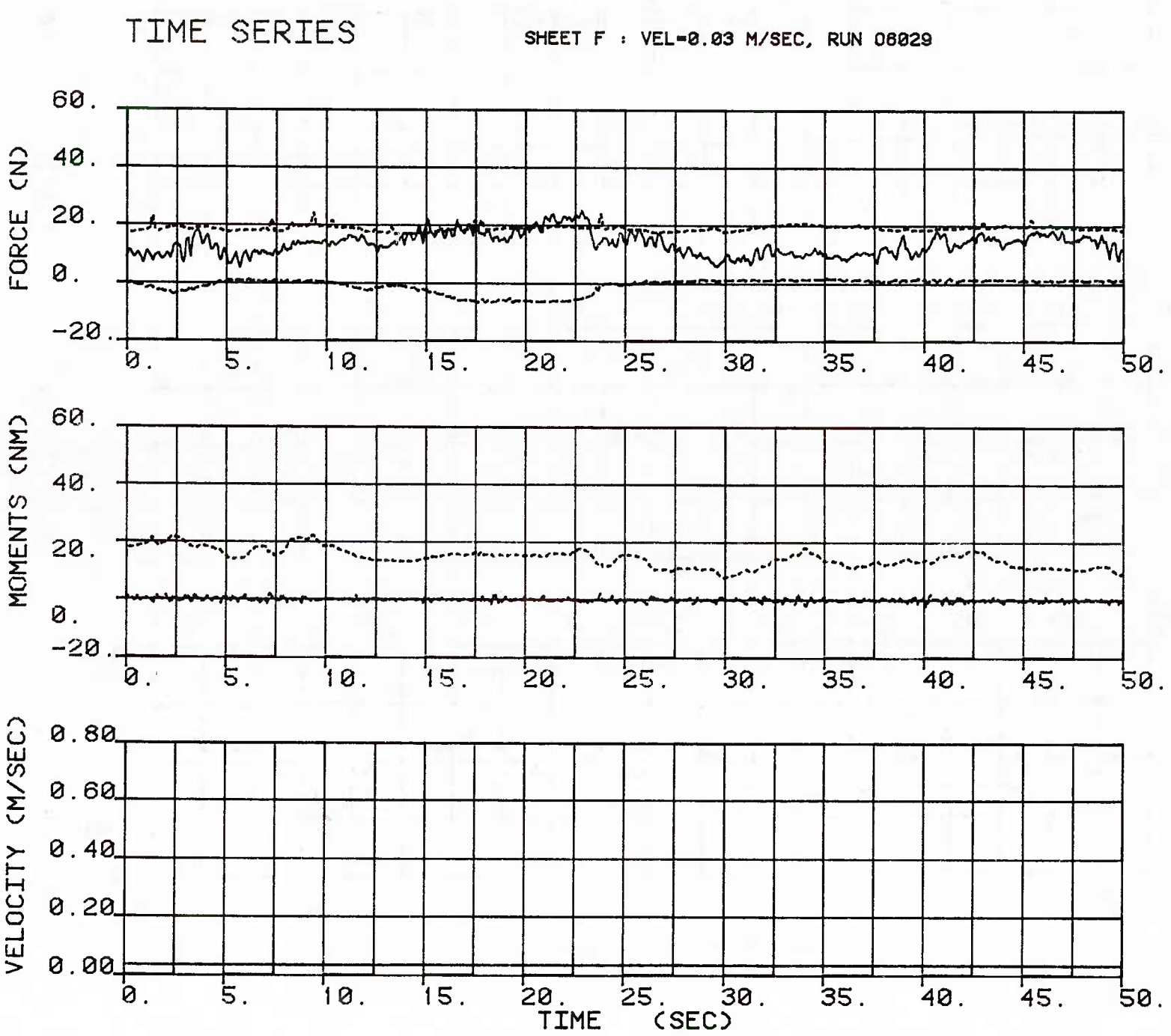
TIME SERIES
SHEET F : VEL=0.03 M/SEC, RUN 06029
FORCE (N)
60.
40.
20.
0.
-20.
MOMENTS (NM)
VELOCITY (M/SEC)
0.80
0.60
0.40
0.20
0.00
0. 5. 10. 15. 20. 25. 30. 35. 40. 45. 50.
TIME (SEC)

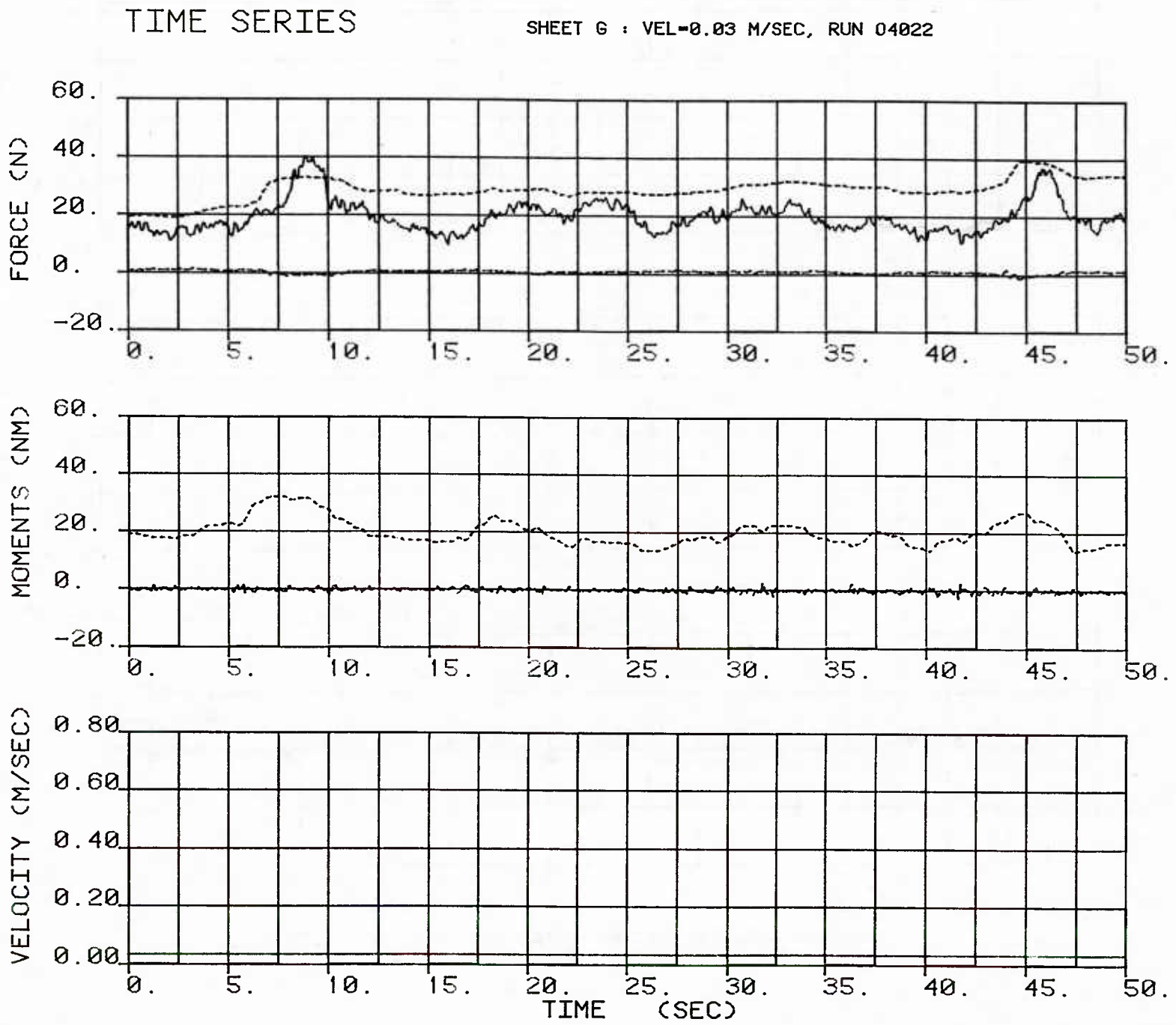
TIME SERIES
SHEET G : VEL=0.03 M/SEC, RUN 04022
FORCE (N)
60.
40.
20.
0.
-20.
MOMENTS (NM)
60.
40.
20.
0.
-20.
VELOCITY (M/SEC)
0.80
0.60
0.40
0.20
0.00
0. 5. 10. 15. 20. 25. 30. 35. 40. 45. 50.
TIME (SEC)

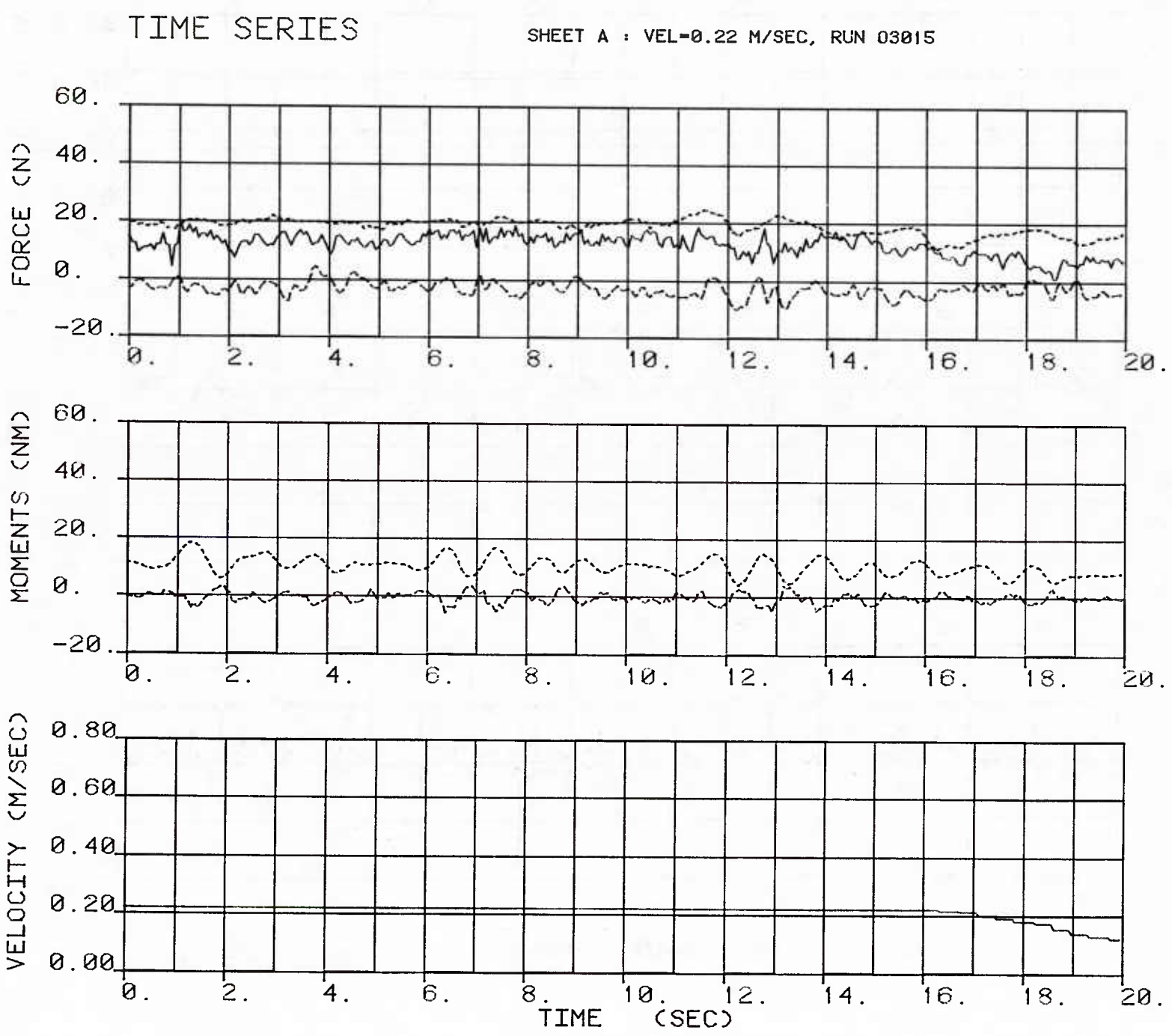
TIME SERIES
SHEET A : VEL=0.22 M/SEC, RUN 03015
FORCE (N)
60.
40.
20.
0.
-20.
0. 2. 4. 6. 8. 10. 12. 14. 16. 18. 20.
MOMENTS (NM)
60.
40.
20.
0.
-20.
0. 2. 4. 6. 8. 10. 12. 14. 16. 18. 20.
VELOCITY (M/SEC)
0.80
0.60
0.40
0.20
0.00
0. 2. 4. 6. 8. 10. 12. 14. 16. 18. 20.
TIME (SEC)

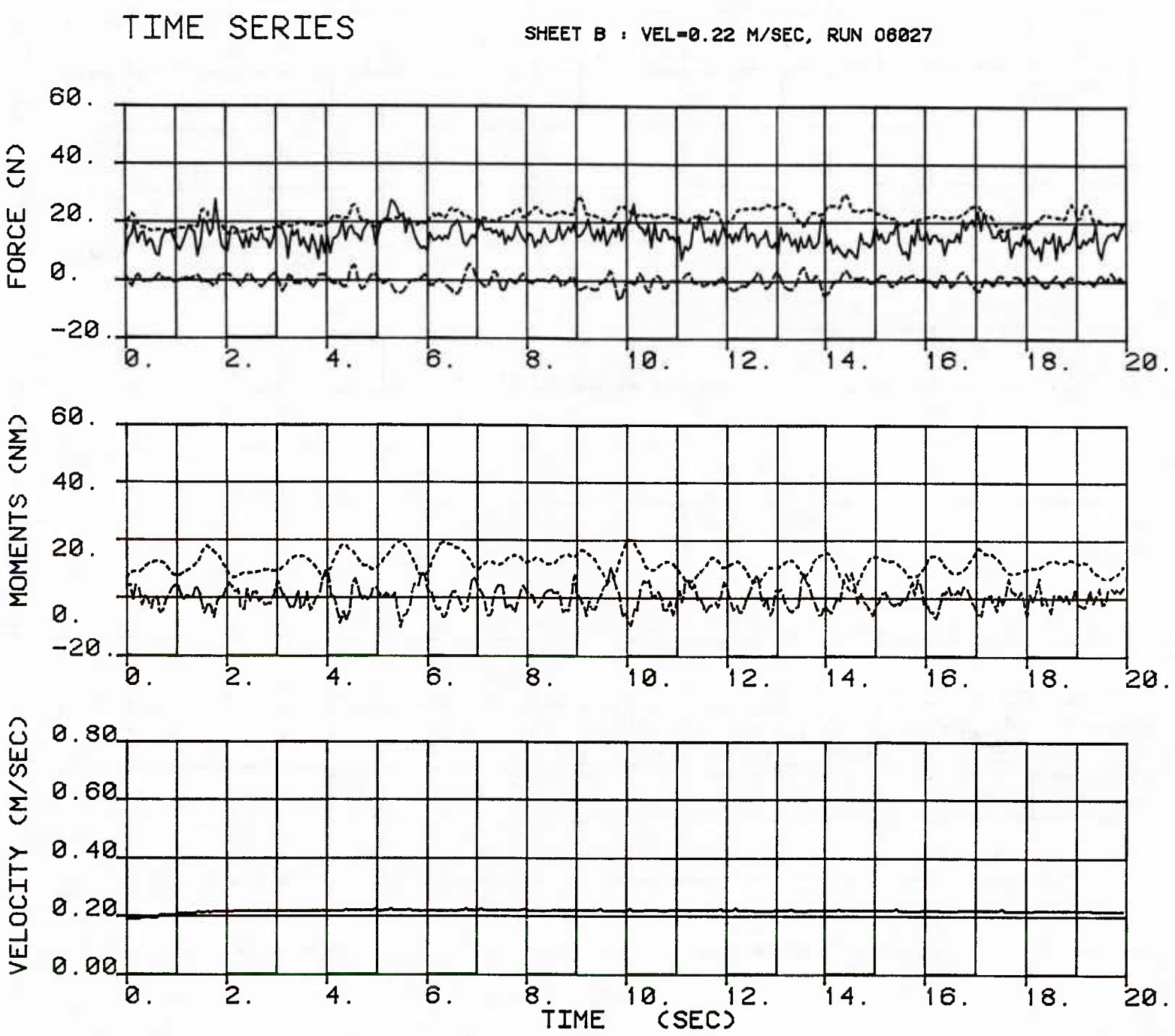
TIME SERIES
SHEET B : VEL=0.22 M/SEC, RUN 06027
FORCE (N)
60.
40.
20.
0.
-20.
0. 2. 4. 6. 8. 10. 12. 14. 16. 18. 20.
MOMENTS (NM)
60.
40.
20.
0.
-20.
0. 2. 4. 6. 8. 10. 12. 14. 16. 18. 20.
VELOCITY (M/SEC)
0.80
0.60
0.40
0.20
0.00
0. 2. 4. 6. 8. 10. 12. 14. 16. 18. 20.
TIME (SEC)

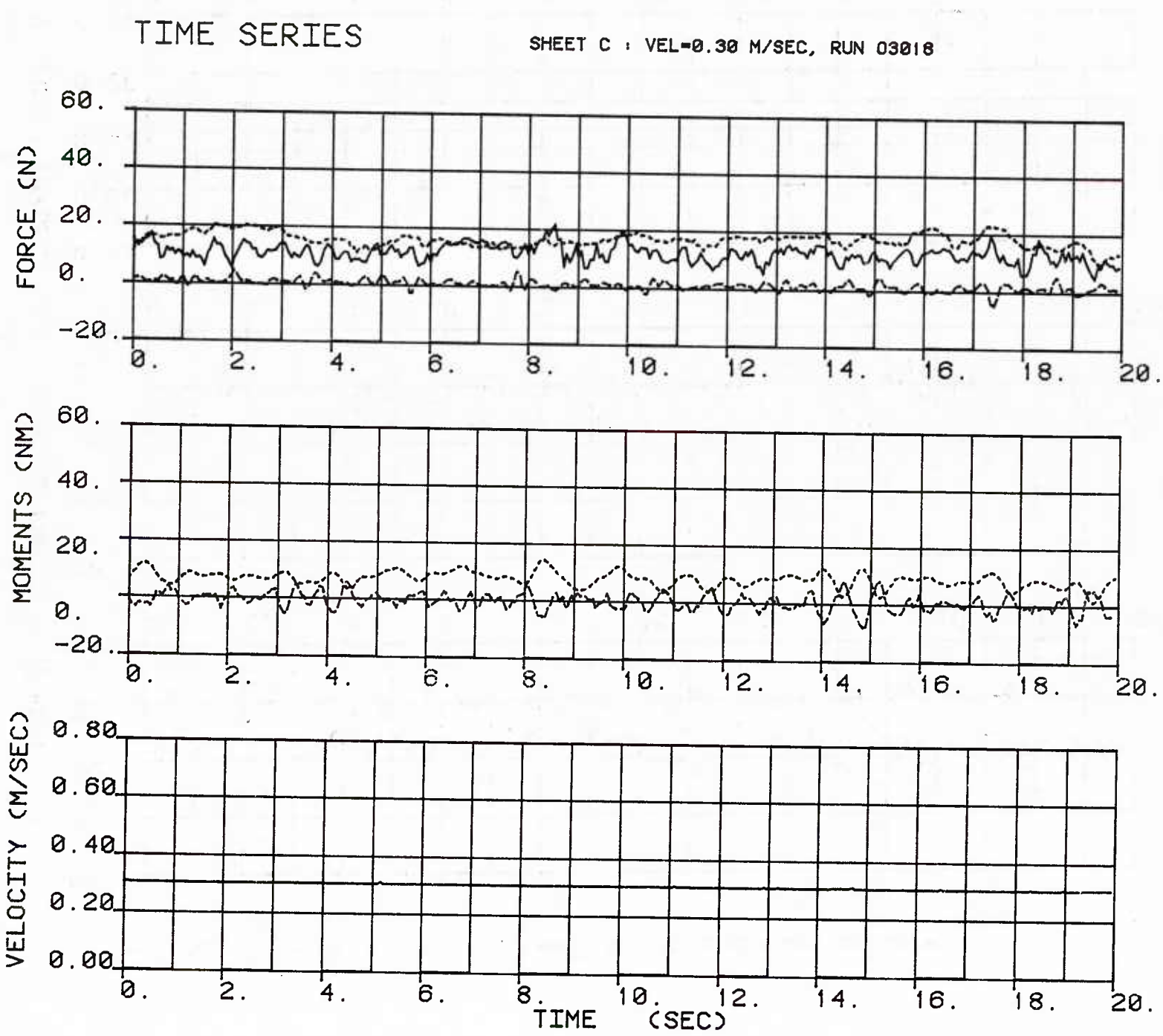
TIME SERIES
SHEET C : VEL=0.30 M/SEC, RUN 03018
FORCE (N)
60.
40.
20.
0.
-20.
0. 2. 4. 6. 8. 10. 12. 14. 16. 18. 20.
MOMENTS (NM)
60.
40.
20.
0.
-20.
0. 2. 4. 6. 8. 10. 12. 14. 16. 18. 20.
VELOCITY (M/SEC)
0.80
0.60
0.40
0.20
0.00
0. 2. 4. 6. 8. 10. 12. 14. 16. 18. 20.
TIME (SEC)

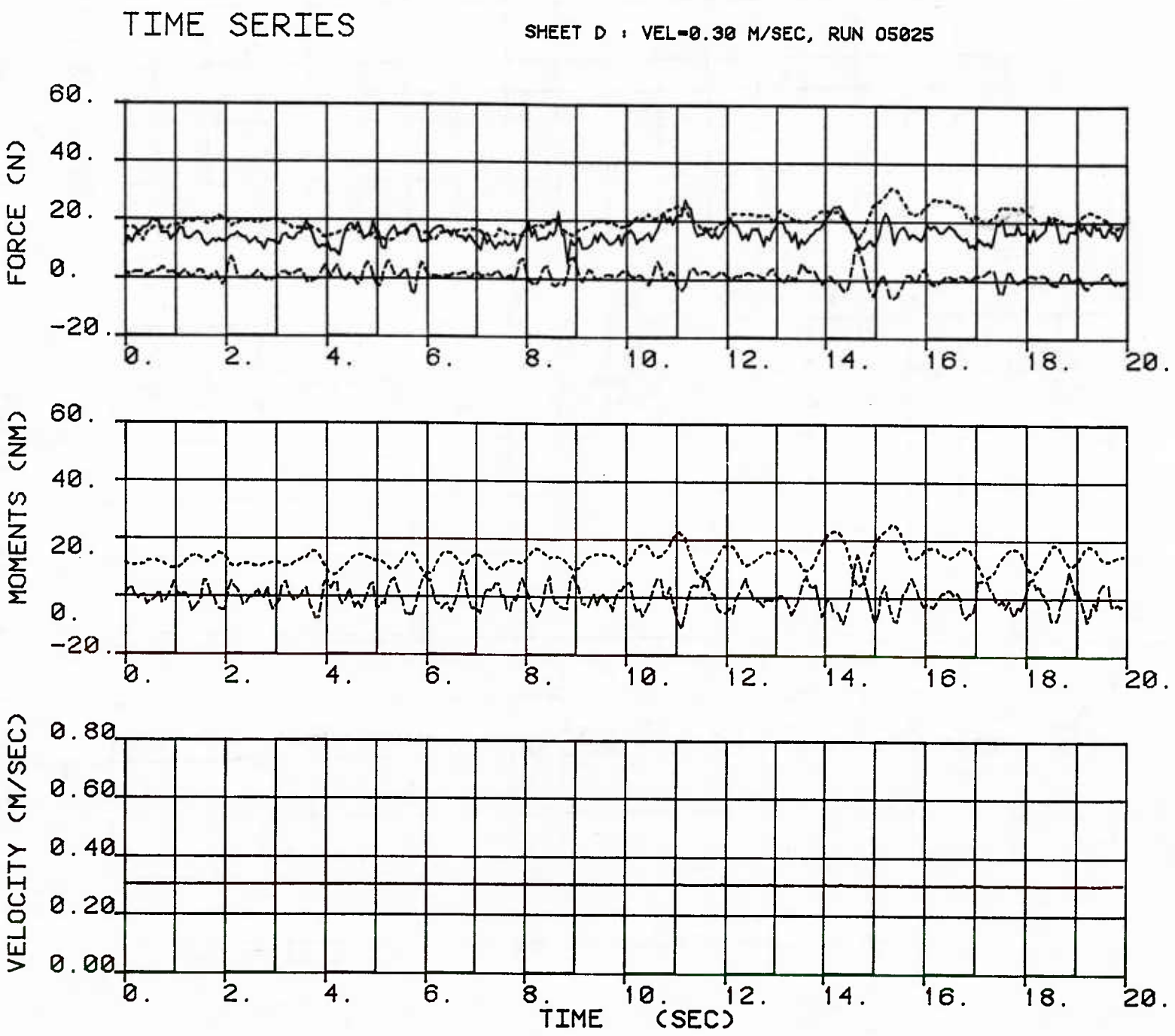
TIME SERIES
SHEET D : VEL=0.30 M/SEC, RUN 05025
FORCE (N)
60.
40.
20.
0.
-20.
0. 2. 4. 6. 8. 10. 12. 14. 16. 18. 20.
MOMENTS (NM)
60.
40.
20.
0.
-20.
0. 2. 4. 6. 8. 10. 12. 14. 16. 18. 20.
VELOCITY (M/SEC)
0.80
0.60
0.40
0.20
0.00
0. 2. 4. 6. 8. 10. 12. 14. 16. 18. 20.
TIME (SEC)

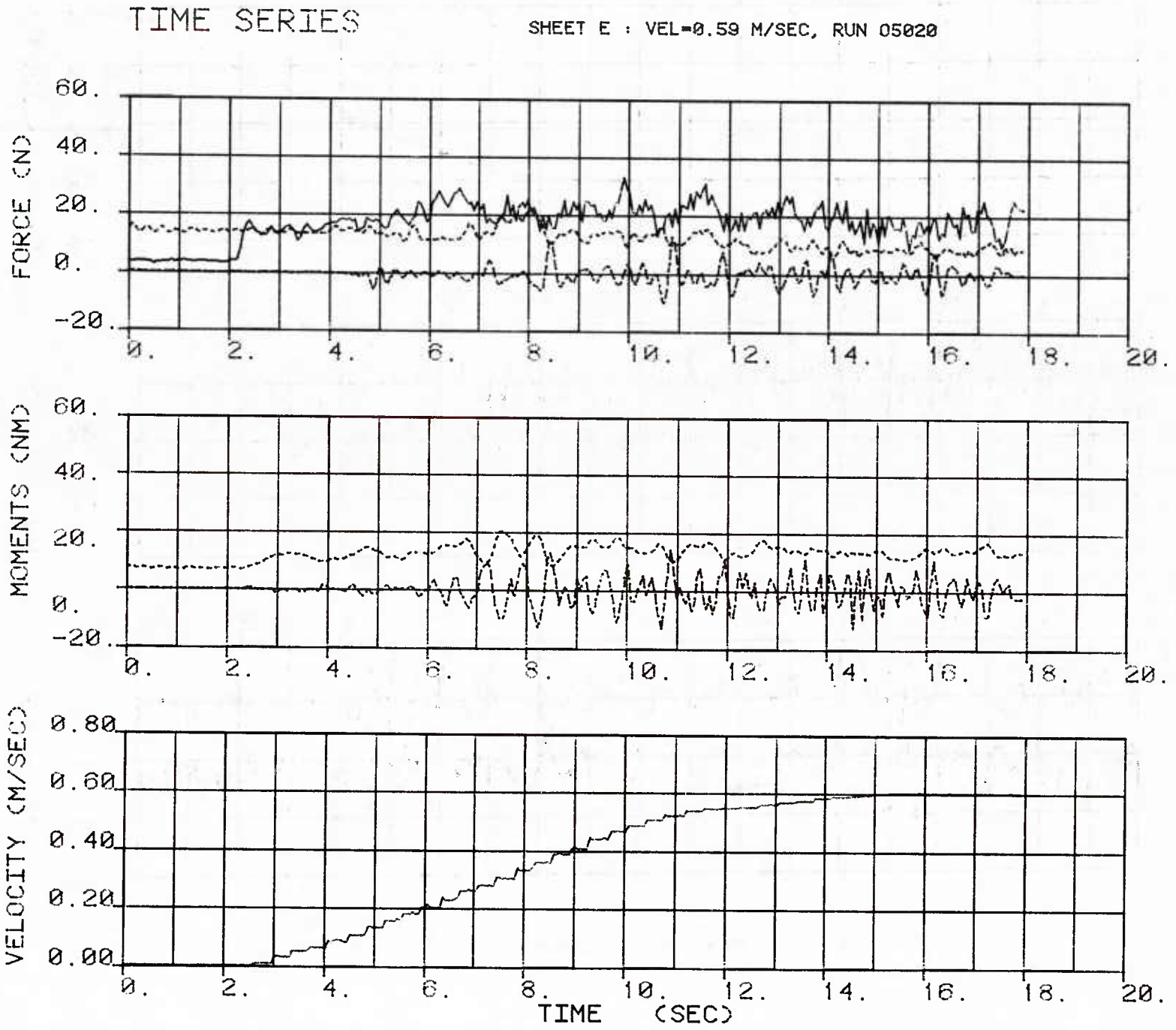
TIME SERIES
SHEET E : VEL=0.59 M/SEC, RUN 05020
FORCE (N)
60.
40.
20.
0.
-20.
0. 2. 4. 6. 8. 10. 12. 14. 16. 18. 20.
MOMENTS (NM)
60.
40.
20.
0.
-20.
0. 2. 4. 6. 8. 10. 12. 14. 16. 18. 20.
VELOCITY (M/SEC)
0.80
0.60
0.40
0.20
0.00
0. 2. 4. 6. 8. 10. 12. 14. 16. 18. 20.
TIME (SEC)

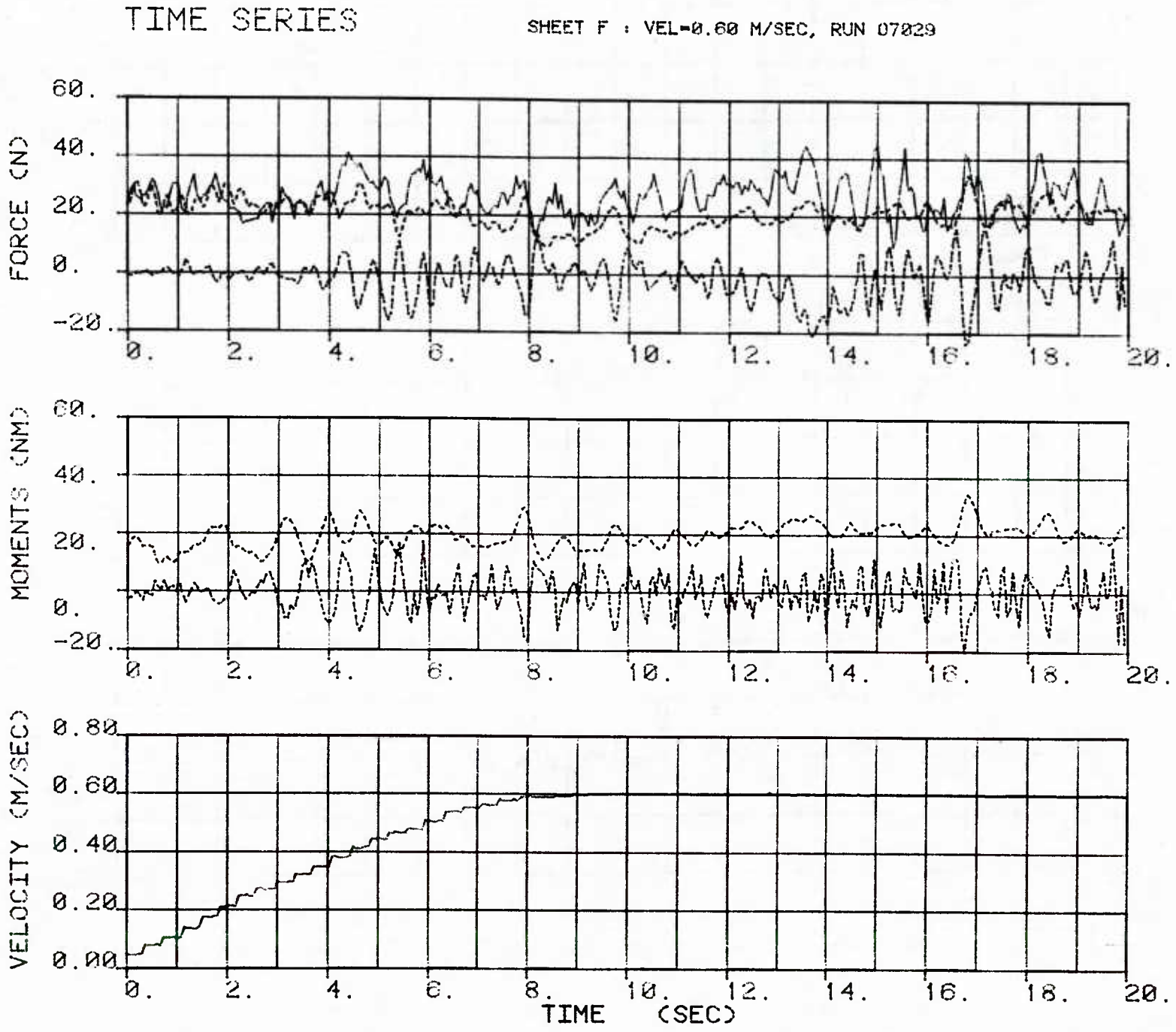
TIME SERIES
SHEET F : VEL=0.60 M/SEC, RUN 07029
FORCE (N)
60.
40.
20.
0.
-20.
0.
2.
4.
6.
8.
10.
12.
14.
16.
18.
20.
MOMENTS (NM)
60.
40.
20.
0.
-20.
0.
2.
4.
6.
8.
10.
12.
14.
16.
18.
20.
VELOCITY (M/SEC)
0.80
0.60
0.40
0.20
0.00
0.
2.
4.
6.
8.
10.
12.
14.
16.
18.
20.
TIME (SEC)

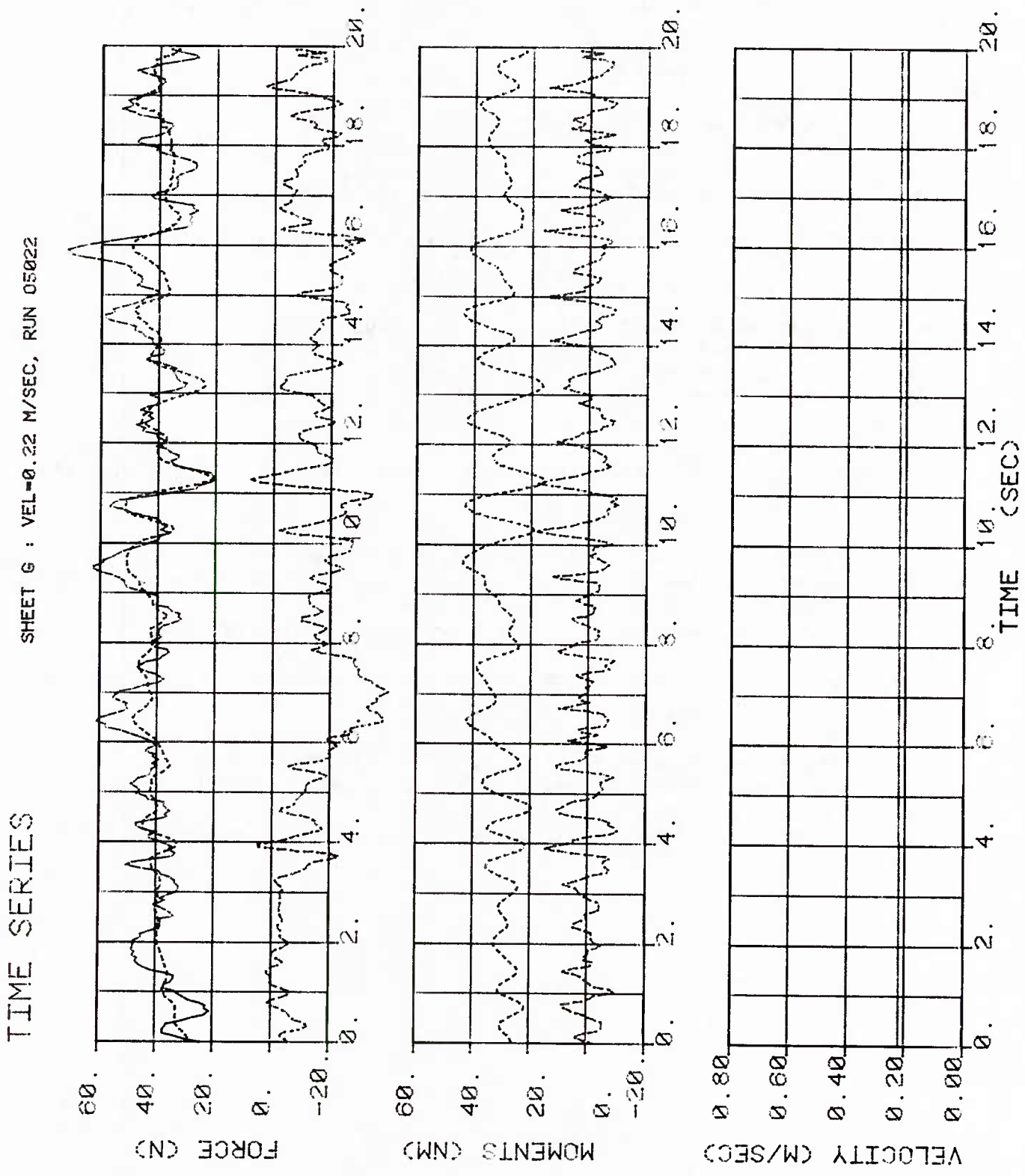
TIME SERIES
SHEET G : VEL=0.22 M/SEC, RUN 05022
FORCE (N)
60.
40.
20.
0.
-20.
MOMENTS (NM)
60.
40.
20.
0.
-20.
VELOCITY (M/SEC)
0.80
0.60
0.40
0.20
0.00
0.
2.
4.
6.
8.
10.
12.
14.
16.
18.
20.
TIME (SEC)

APPENDIX C

Power Spectra, Cross-Spectra and Coherance-Functions

Figure C1: Power Spectra

a) Examples of low velocity runs, V_o = .03 m/sec
b) Runs at medium velocity, V_o = 0.22 m/sec and V_o = 0.3 m/sec
c) Runs at high velocity, V_o = 0.6 m/sec
d) Runs with Sheet G, V_o = 0.03 m/sec, V_o = 0.22 m/sec

Figure C2: Cross Spectra and Coherance functions of $z(t)$ with $\ddot{z}(t)$, $\theta(t)$ and $\ddot{\theta}(t)$

a) Examples of low velocity runs, V_o = 0.03 m/sec
b) Runs at medium velocity, V_o = .22 m/sec and V_o = 0.3 m/sec
c) Runs at high velocity, V_o = 0.6 m/sec
d) Runs with sheet G, V_o = 0.03 m/sec V_o = 0.22 m/sec

Figure C3: Cross Spectra and Coherence Functions of $F_x(t)$ with $z(t)$, $F_x(t)$ with $\ddot{z}(t)$

a) Examples of low velocity runs, V_o = 0.03 m/sec
b) Runs at medium velocity, V_o = 0.22 m/sec and V_o = 0.3 m/sec
c) Runs at high velocity, V_o = 0.6 m/sec
d) Runs with sheet G, V_o = 0.03 m/sec and V_o = 0.22 m/sec

Figure C4: Cross-Spectra and Coherence Functions of $F_x(t)$ with $\theta(t)$ and $F_x(t)$ with $\ddot{\theta}(t)$

a) Examples of low velocity runs, V_o = 0.03 m/sec
b) Runs at medium velocity, V_o = 0.22 m/sec and V_o = 0.3 m/sec
c) Runs at high velocity, V_o = 0.6 m/sec
d) Runs with sheet G, V_o = 0.03 m/sec and V_o = 0.22 m/sec

Figure C1: Power Spectra

POWER-SPECTRUM

VEL = .03 M/SEC : SHEET A ⊡ , SHEET D ×
SHEET F ⧖

HORIZONTAL FORCE

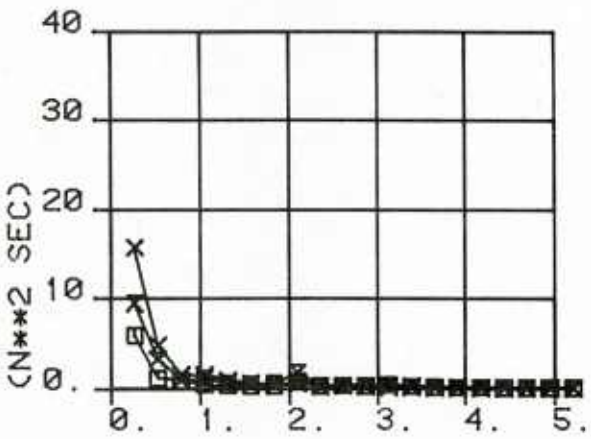

DRAFT

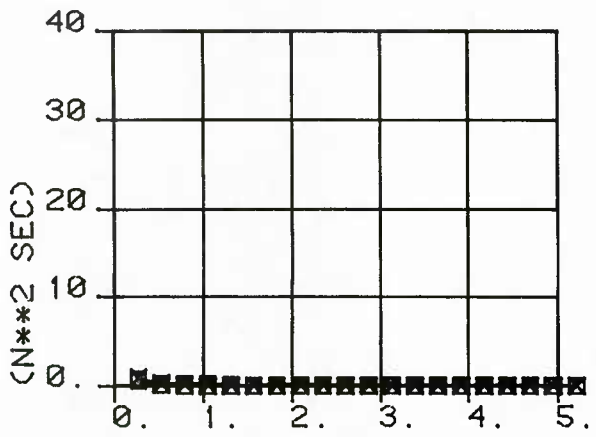

PITCH

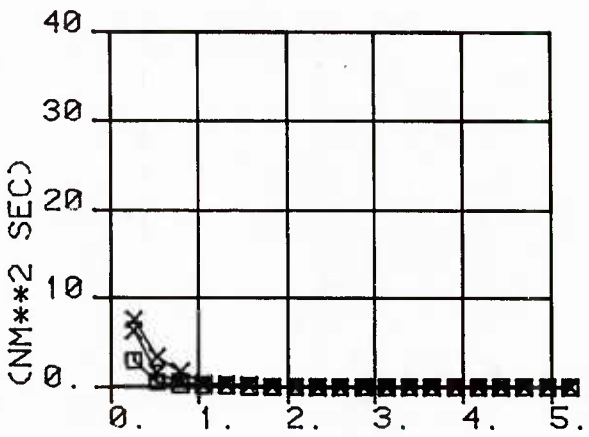

VERT.ACCELERATION

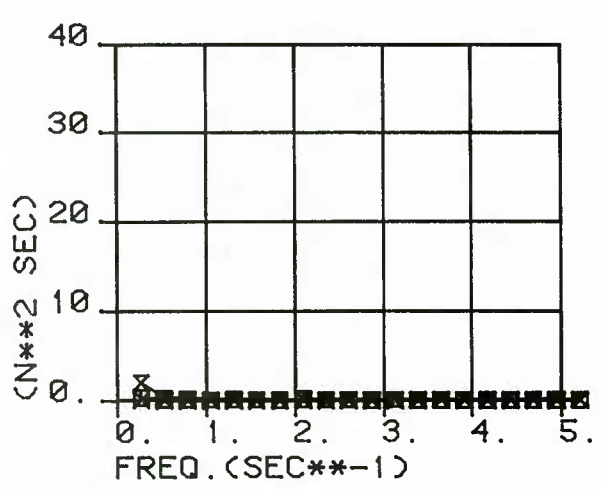

ANG.ACCELERATION

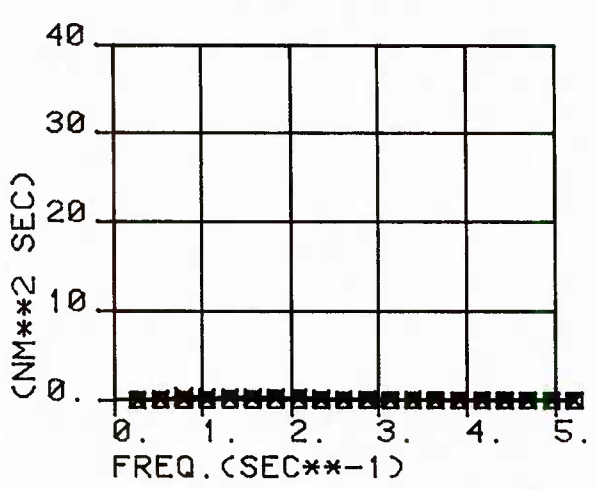

POWER-SPECTRUM

VEL = .22 M/SEC : SHEET A ⊡ ,SHEET B ⊙
VEL = .30 M/SEC : SHEET C + ,SHEET D ×

HORIZONTAL FORCE

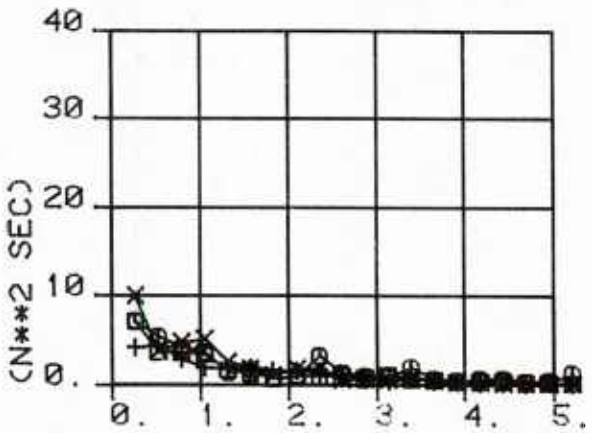

DRAFT

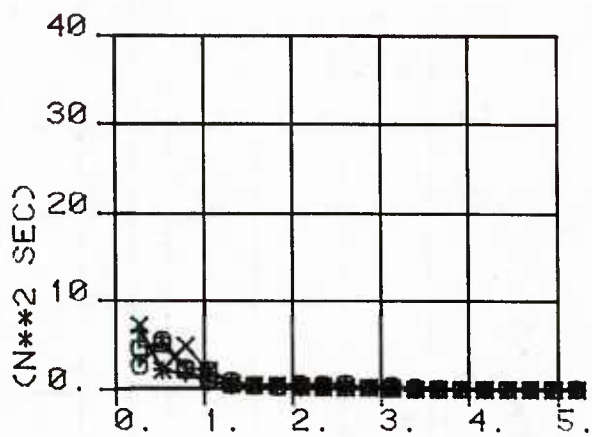

PITCH

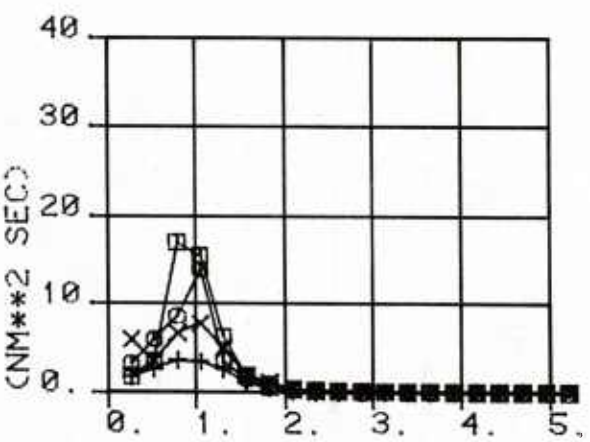

VERT.ACCELERATION

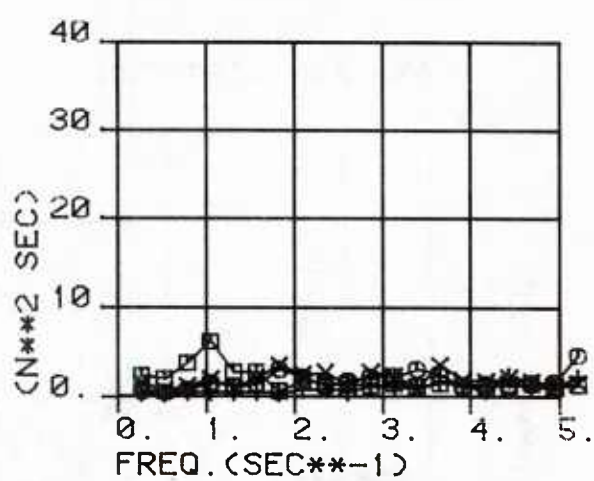

ANG.ACCELERATION

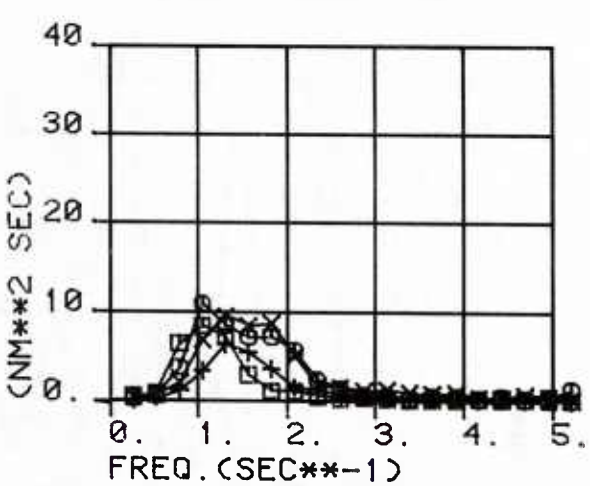

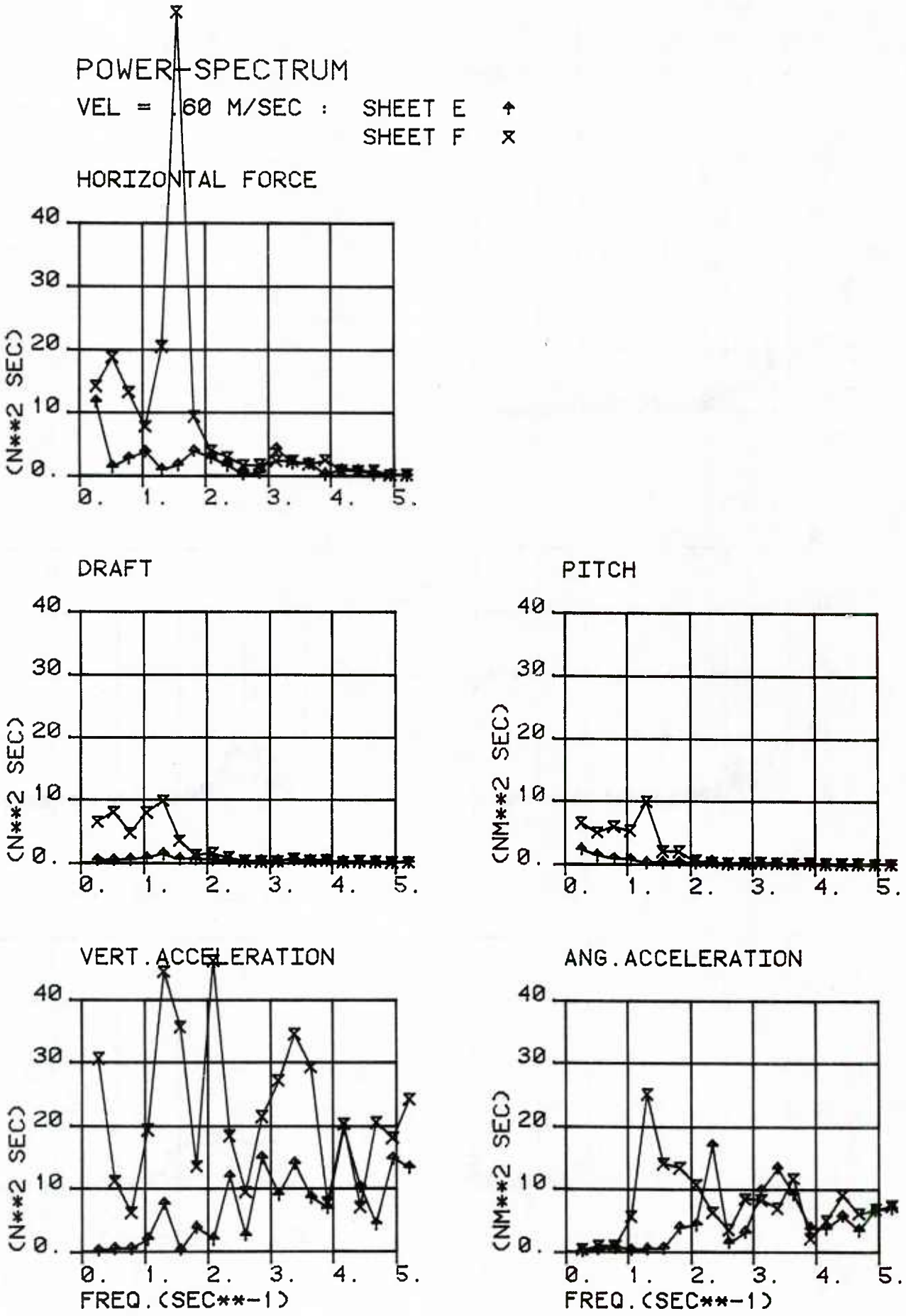
POWER-SPECTRUM
VEL = .60 M/SEC : SHEET E
SHEET F
HORIZONTAL FORCE
(N**2 SEC)
DRAFT
(N**2 SEC)
PITCH
(NM**2 SEC)
VERT. ACCELERATION
(N**2 SEC)
ANG. ACCELERATION
(NM**2 SEC)
0. 10 20 30 40
0. 1. 2. 3. 4. 5.
FREQ. (SEC**-1)

POWER-SPECTRUM

VEL = .03 M/SEC : SHEET G Z
VEL = .22 M/SEC : SHEET G Y

HORIZONTAL FORCE

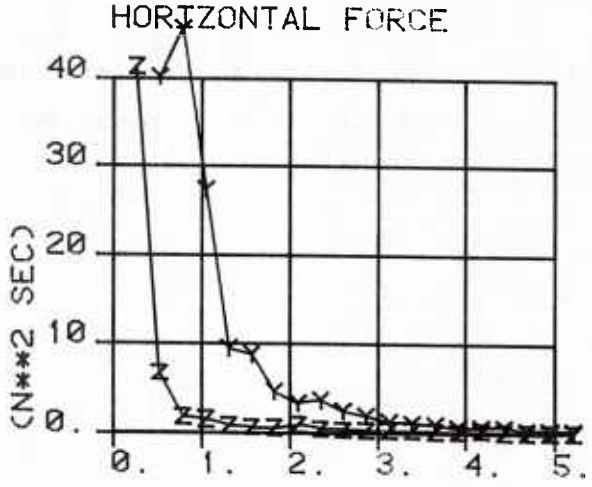

DRAFT

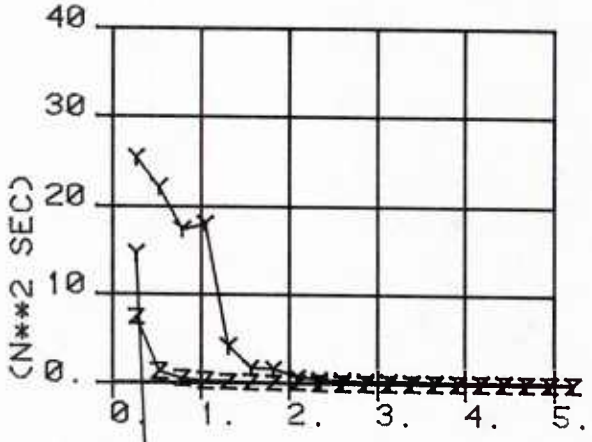

PITCH

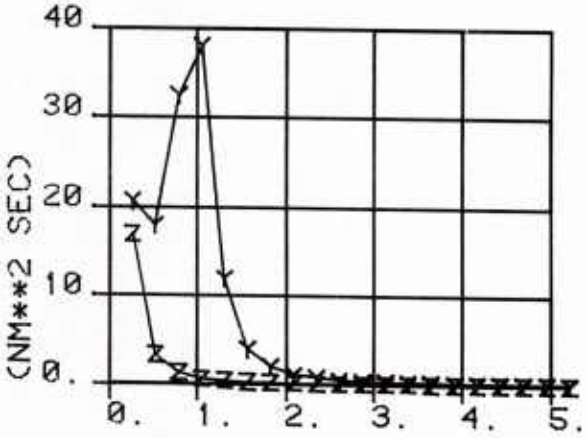

VERT.ACCELERATION

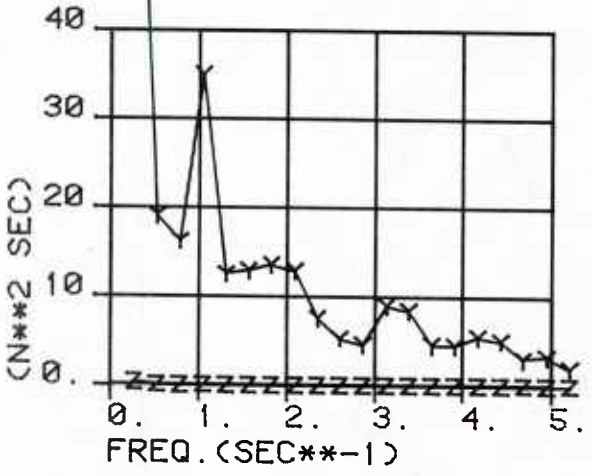

ANG.ACCELERATION

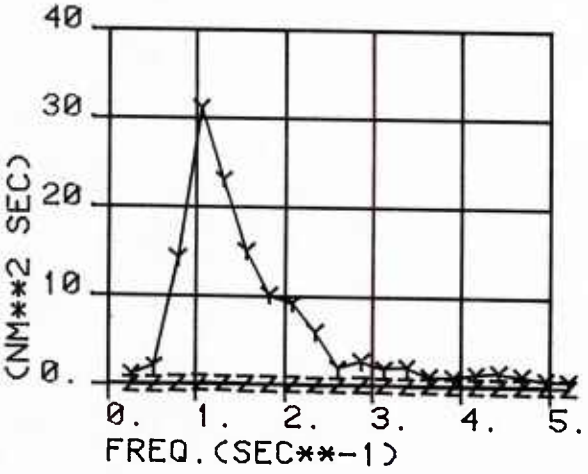

Figure C2: Cross-Spectra and Coherance Functions of Draft $z(t)$ with Vertical Acceleration $\ddot{z}(t)$, and Pitch $\theta(t)$ with Angular Acceleration $\ddot{\theta}(t)$

CROSS-SPECTRUM AND COHERENCE-FUNCTION

VEL = .03 M/SEC : SHEET A ⊡ , SHEET D ×
SHEET F ×

DRAFT WITH VERT.ACC

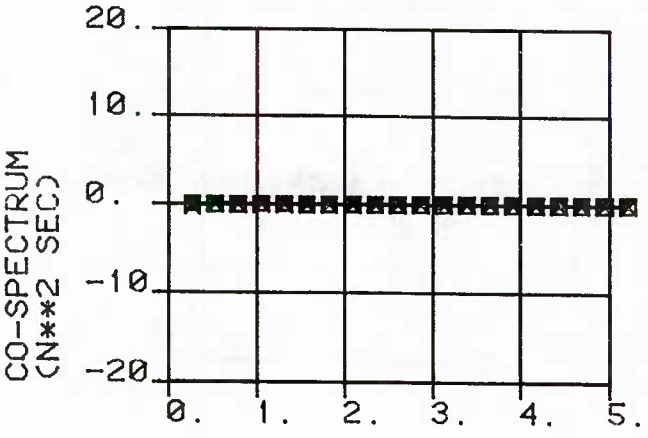

PITCH WITH ANG.ACC

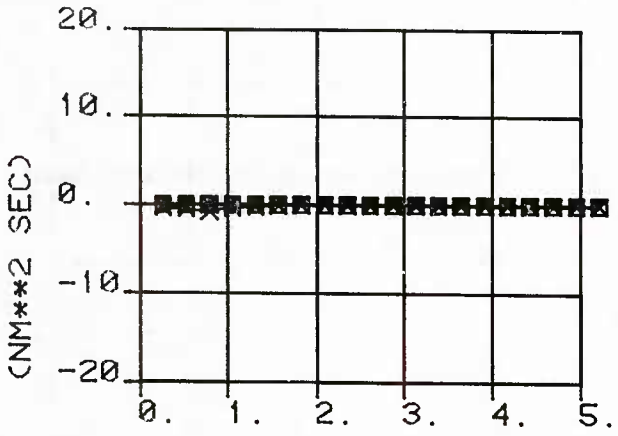

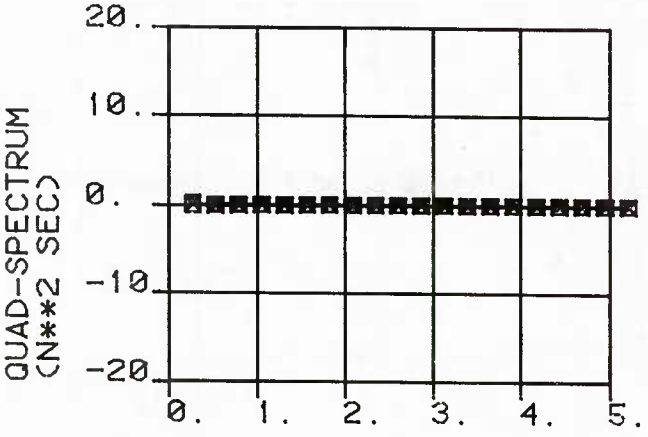

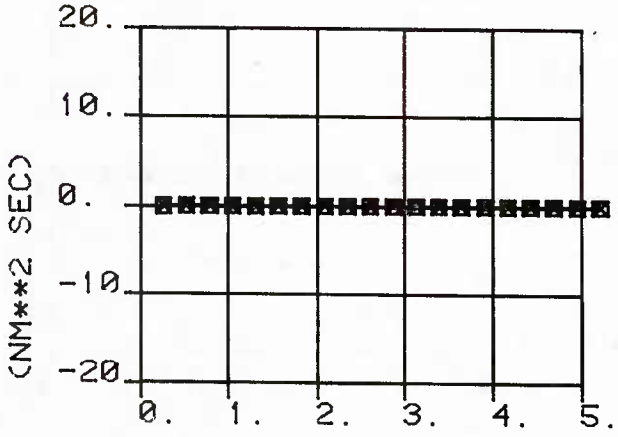

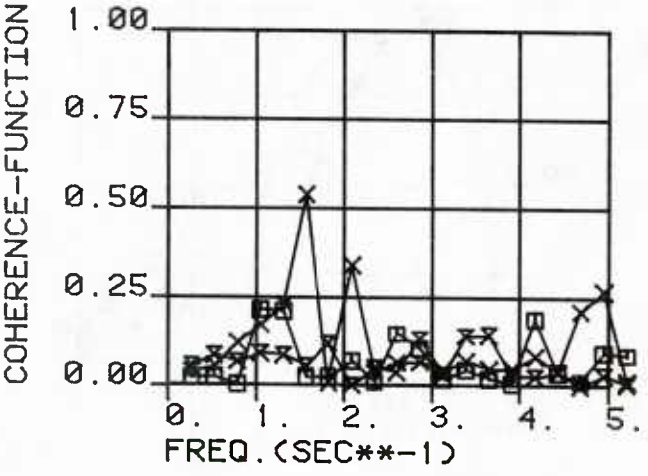

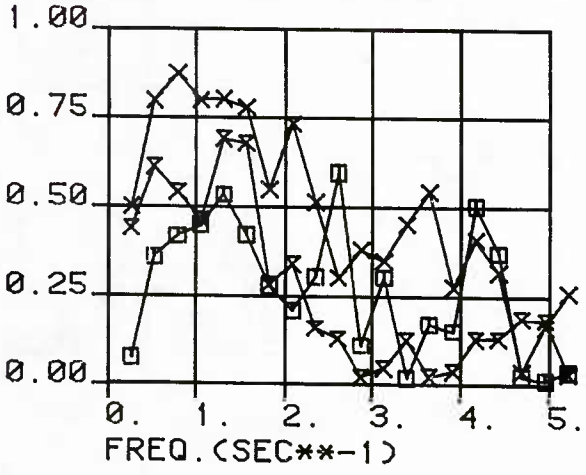

CROSS-SPECTRUM AND COHERENCE-FUNCTION

VEL = .22 M/SEC : SHEET A ⊡ ,SHEET B ⊙
VEL = .30 M/SEC : SHEET C + ,SHEET D ×

DRAFT WITH VERT.ACC

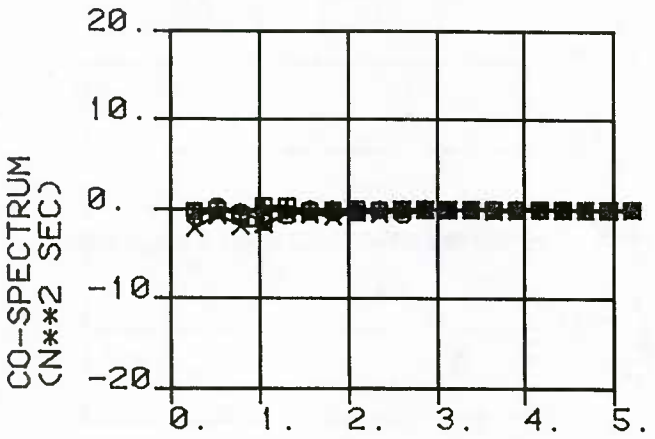

PITCH WITH ANG.ACC

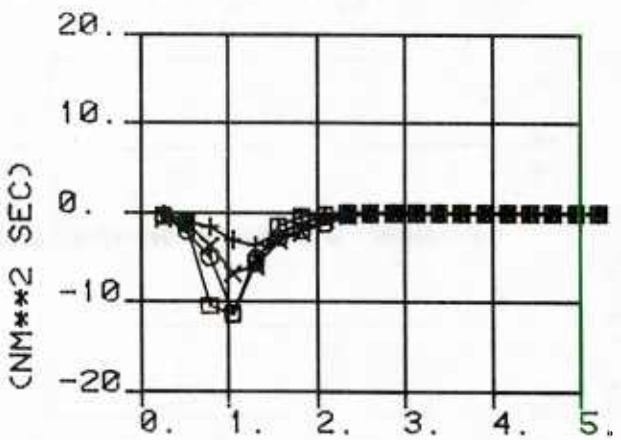

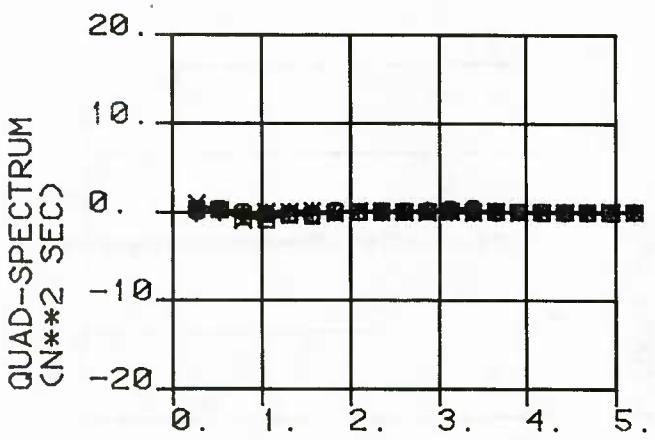

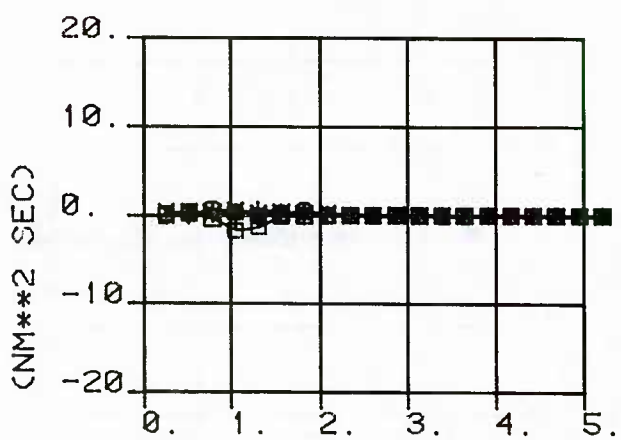

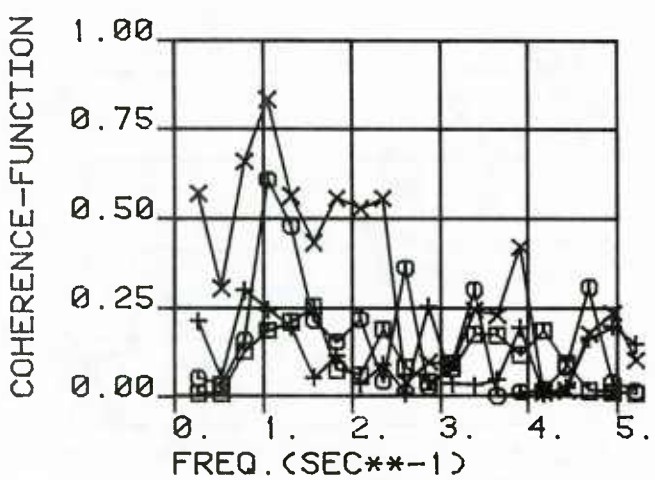

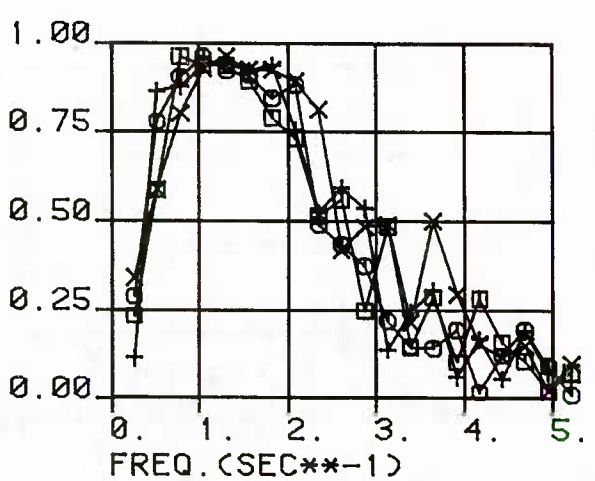

CROSS-SPECTRUM AND COHERENCE-FUNCTION

VEL = .60 M/SEC : SHEET E ✦
SHEET F ✕

DRAFT WITH VERT.ACC

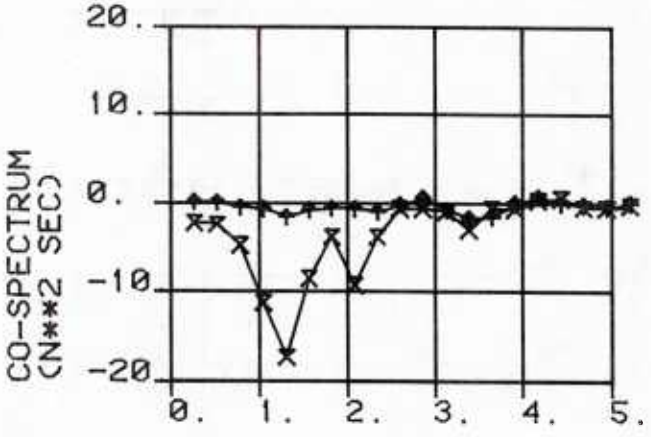

PITCH WITH ANG.ACC

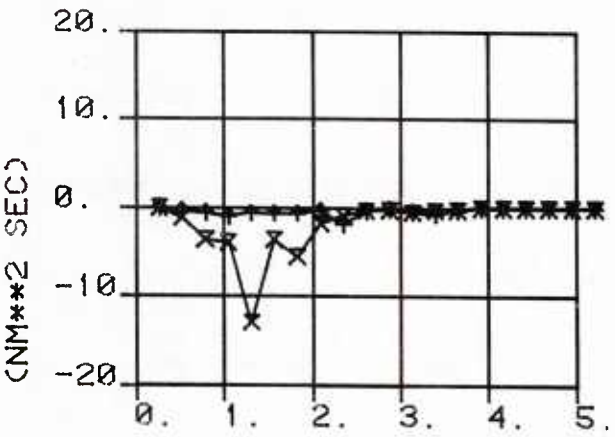

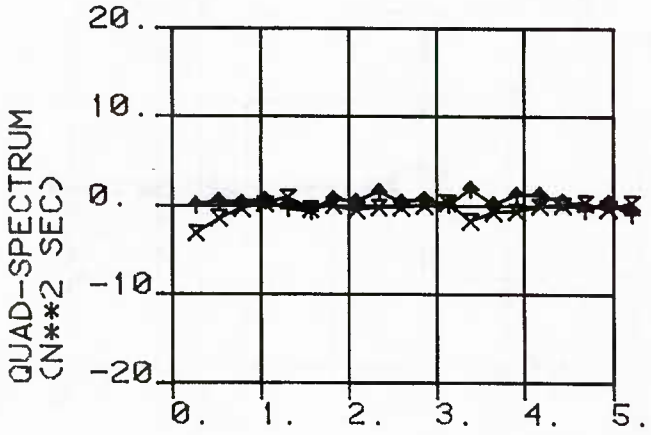

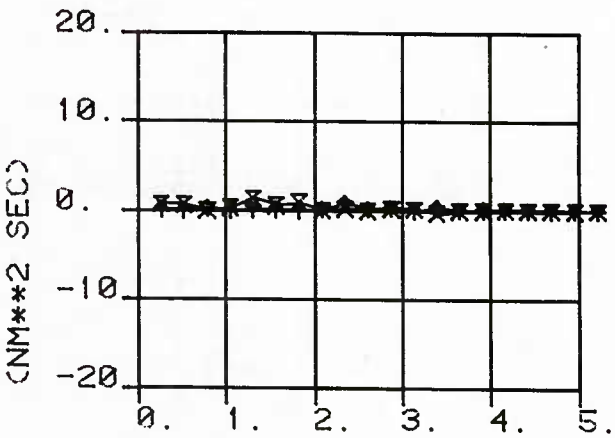

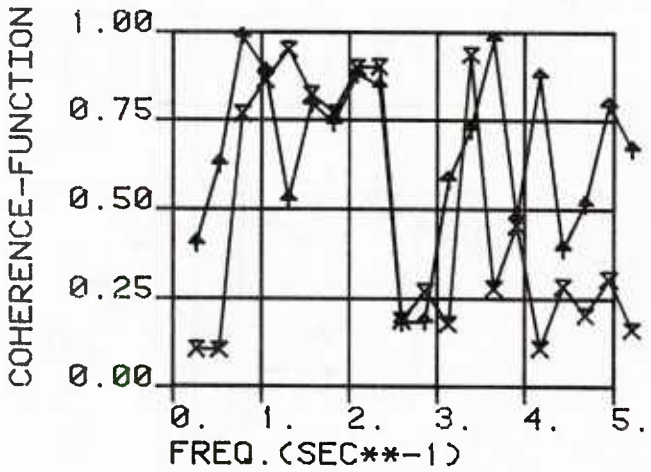

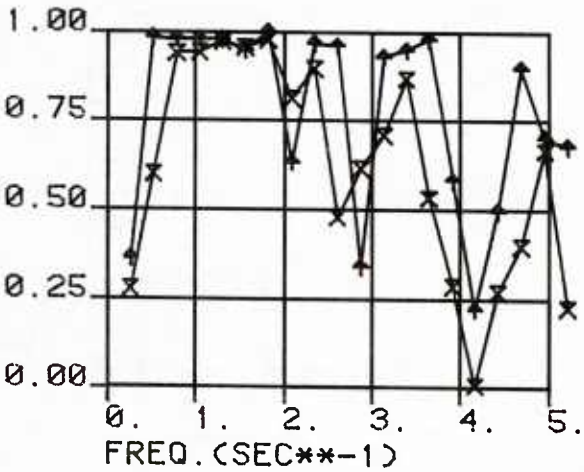

CROSS-SPECTRUM AND COHERENCE-FUNCTION

VEL = .03 M/SEC : SHEET G Z
VEL = .22 M/SEC : SHEET G Y

DRAFT WITH VERT.ACC

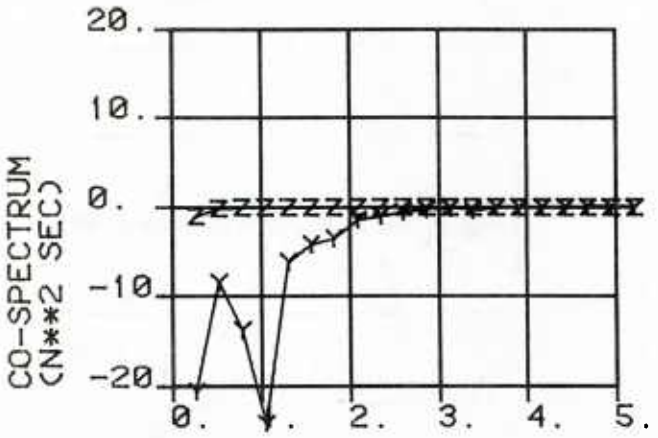

PITCH WITH ANG.ACC

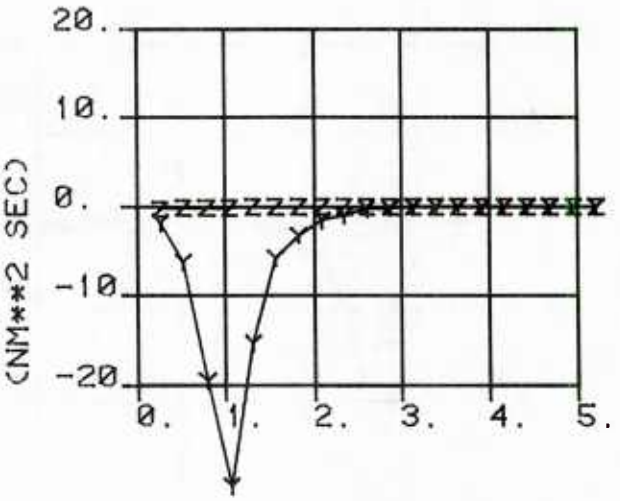

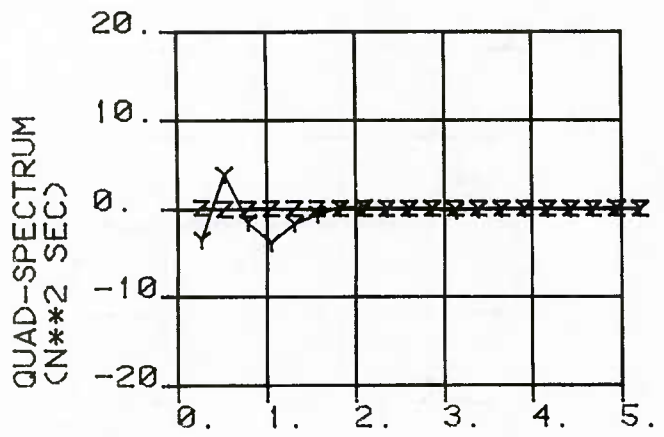

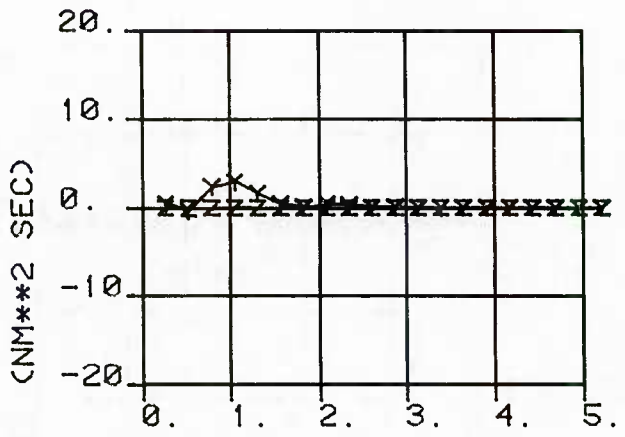

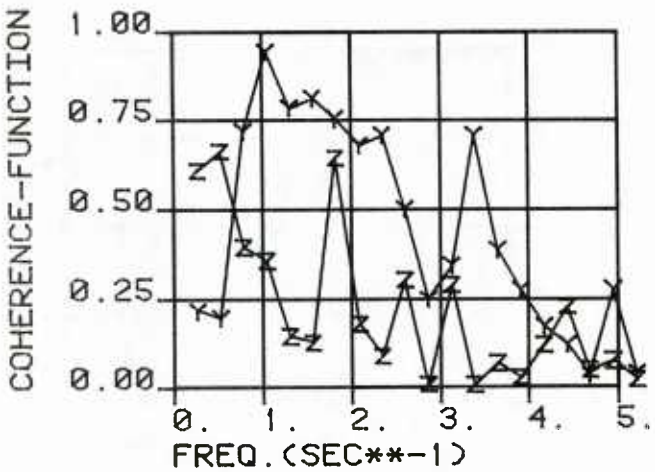

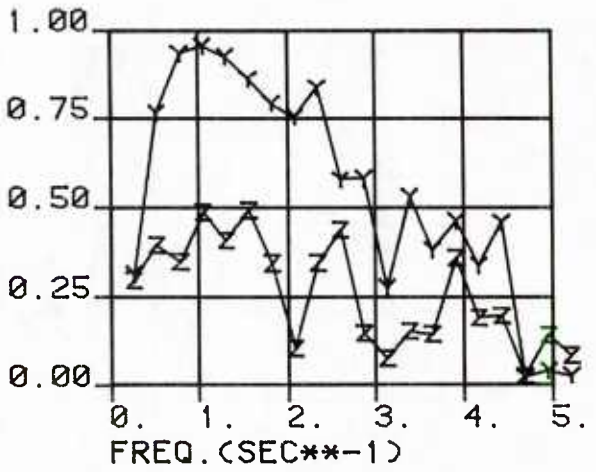

Figure C3: Cross-Spectra and Coherance Functions of $F_x(t)$ with draft $z(t)$, and $F_x(t)$ with Vertical Acceleration $\ddot{z}(t)$

CROSS-SPECTRUM AND COHERENCE-FUNCTION

VEL = .03 M/SEC : SHEET A ⊡ , SHEET D ×
SHEET F ⊠

FX WITH DRAFT

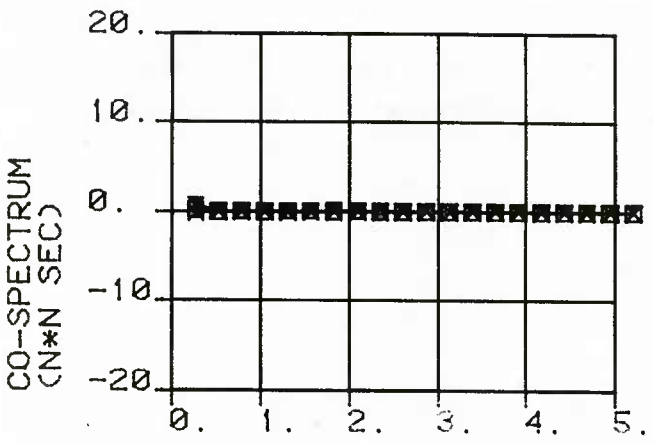

FX WITH VERT.ACC

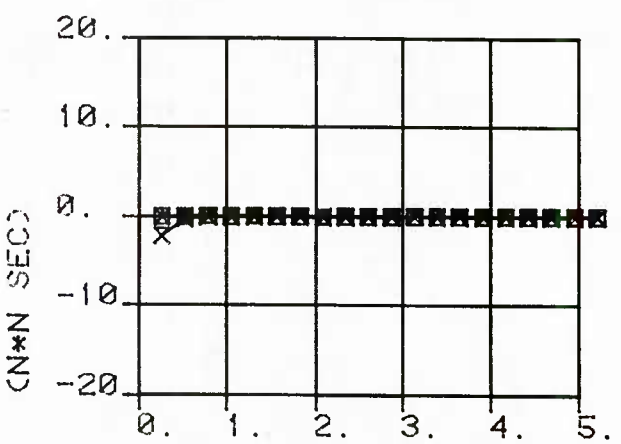

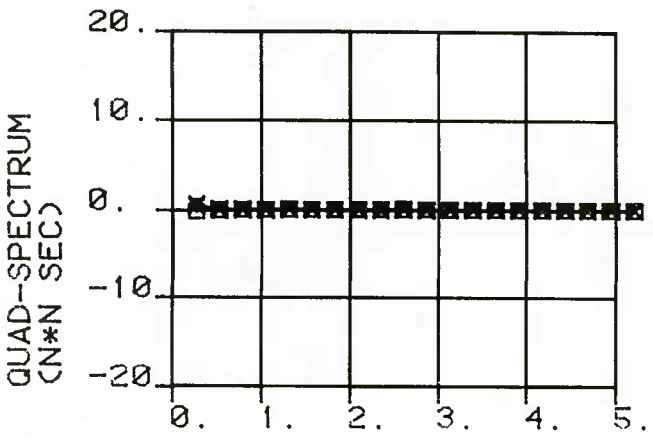

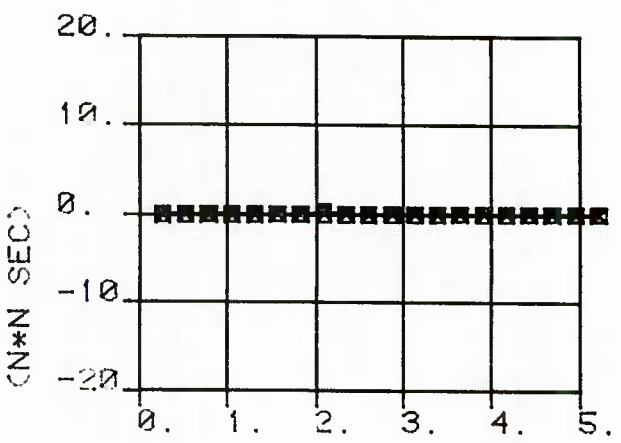

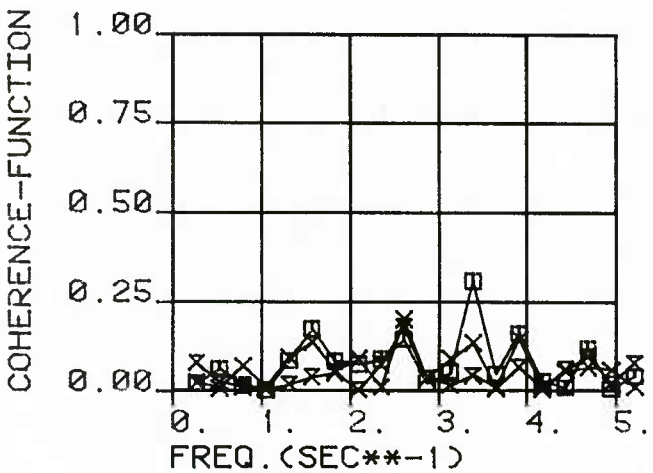

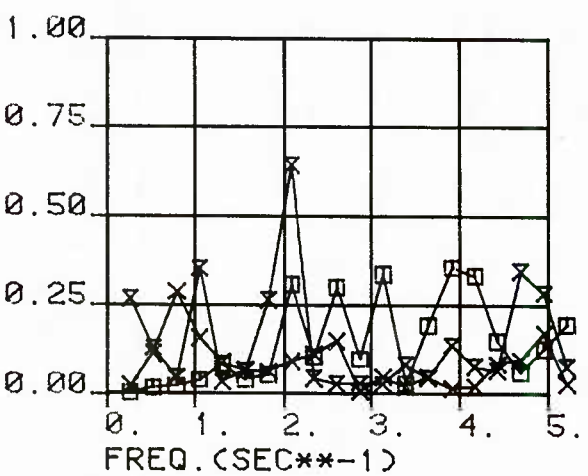

CROSS-SPECTRUM AND COHERENCE-FUNCTION

VEL = .22 M/SEC : SHEET A ⊡ ,SHEET B ⊙
VEL = .30 M/SEC : SHEET C + ,SHEET D ×

FX WITH DRAFT

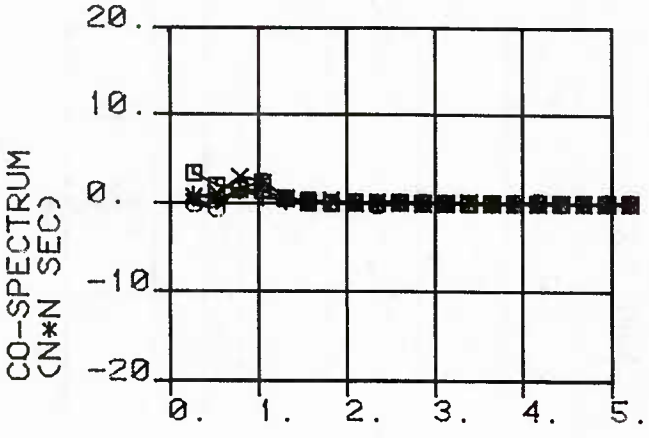

FX WITH VERT.ACC

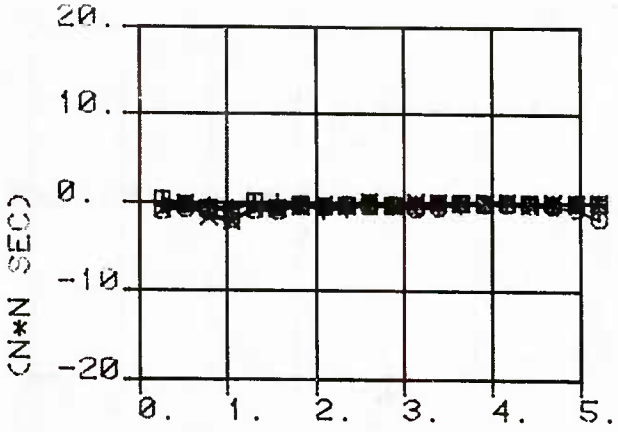

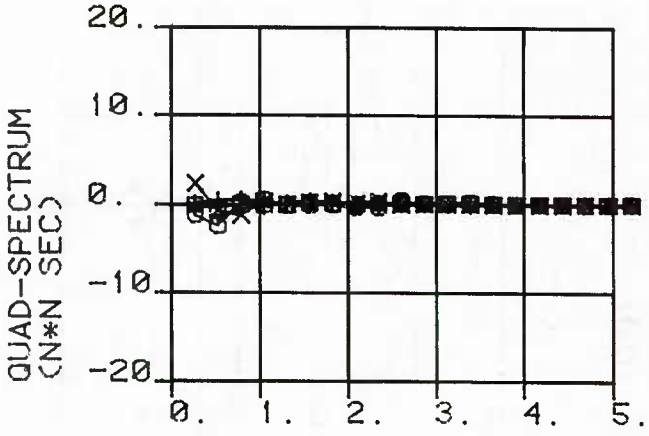

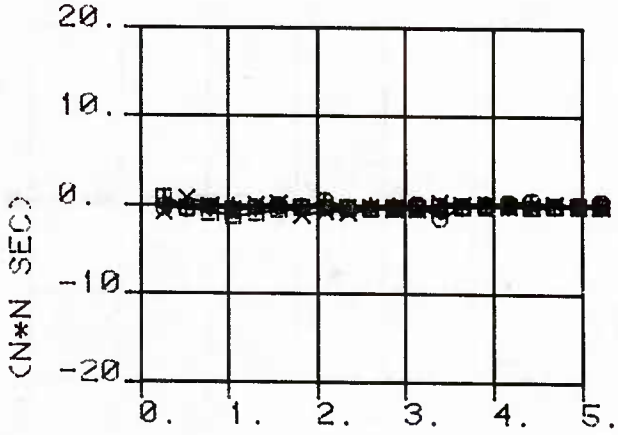

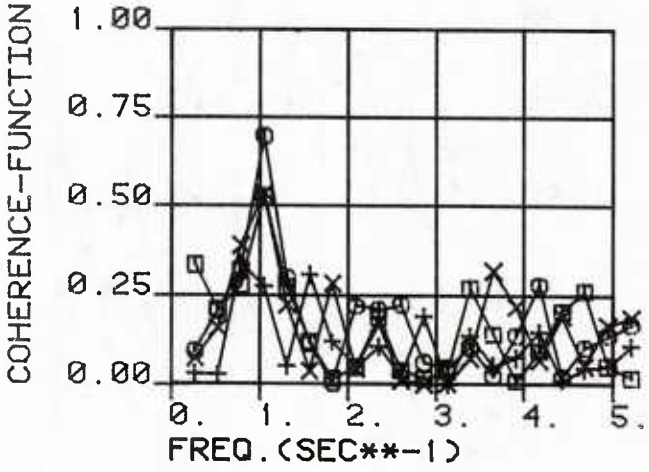

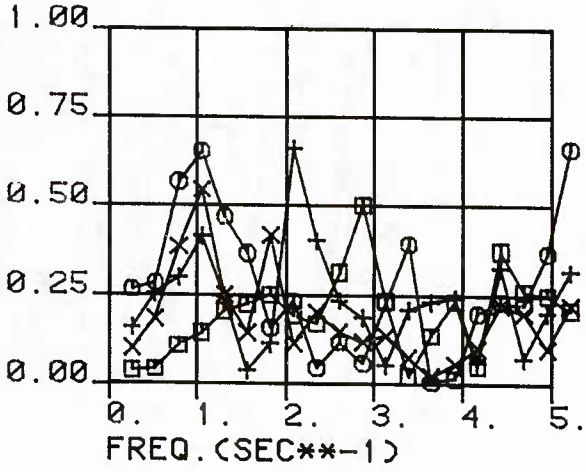

CROSS-SPECTRUM AND COHERENCE-FUNCTION

VEL = .60 M/SEC : SHEET E ↑
SHEET F ⧖

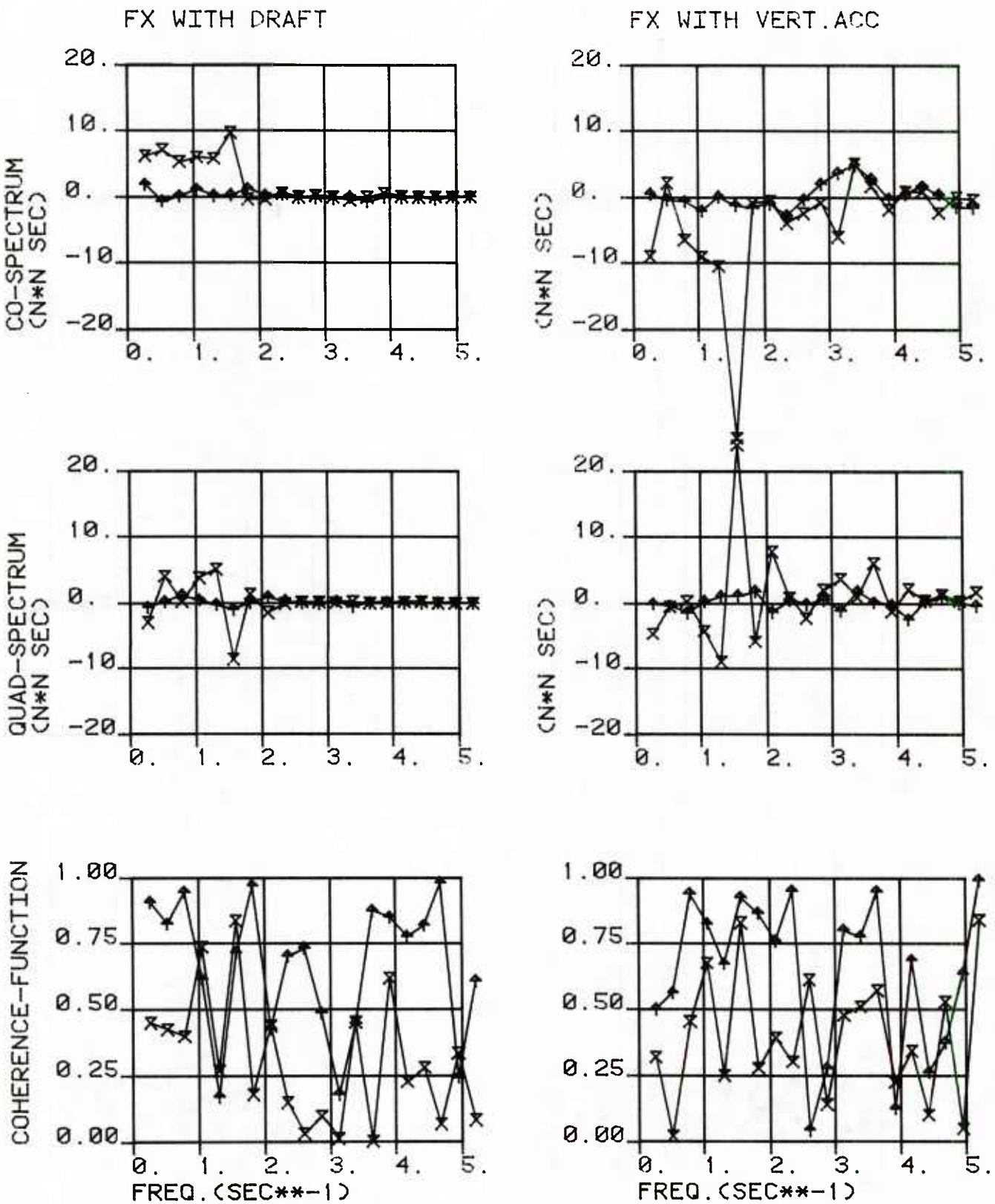

CROSS-SPECTRUM AND COHERENCE-FUNCTION

VEL = .03 M/SEC : SHEET G Z
VEL = .22 M/SEC : SHEET G Y

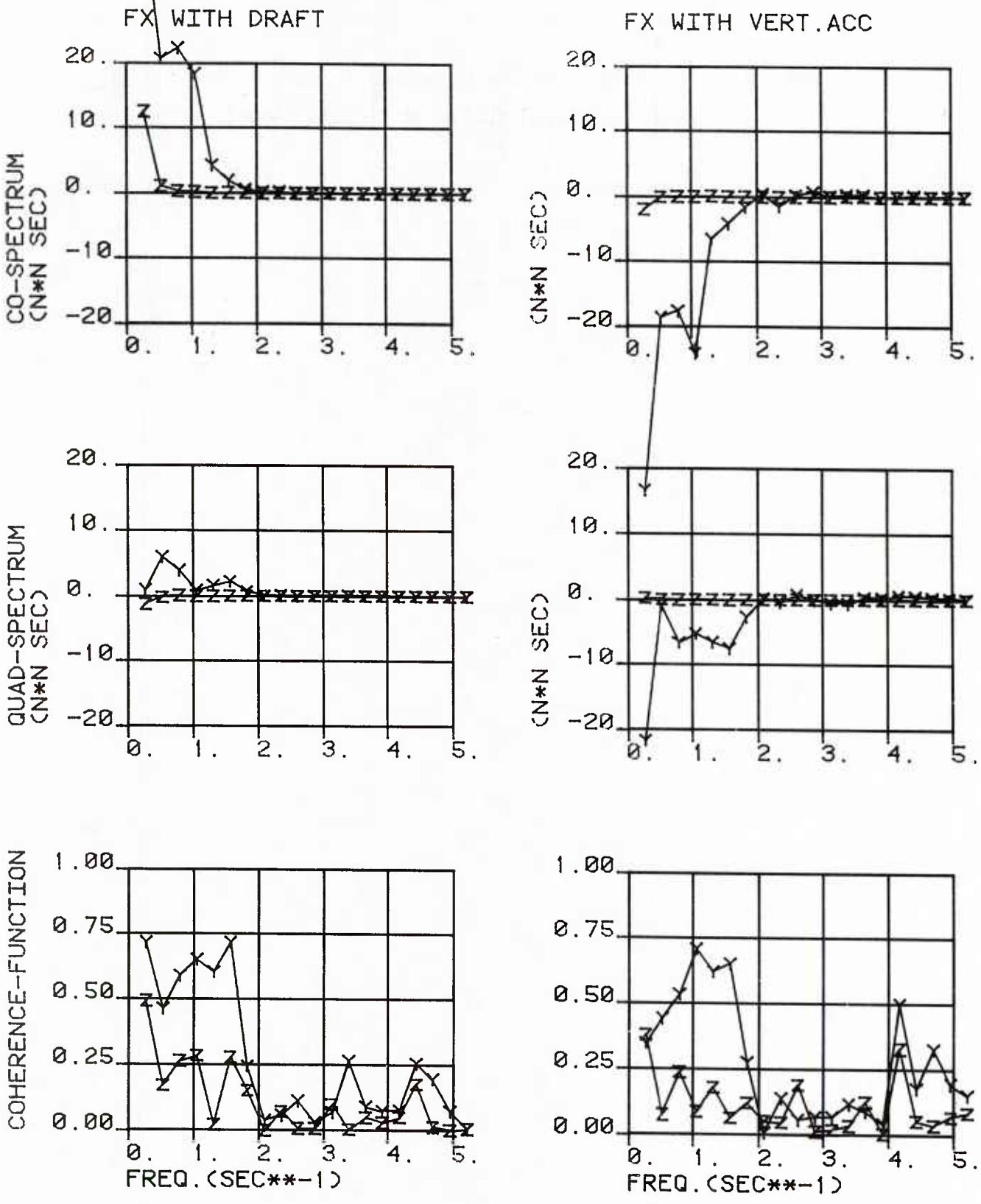

Figure C4: Cross-Spectra and Coherance Functions of $F_x(t)$ with Pitch $\theta(t)$ and $F_x(t)$ with Angular Acceleration, $\ddot{\theta}(t)$

CROSS-SPECTRUM AND COHERENCE-FUNCTION

VEL = .03 M/SEC : SHEET A ⊡ ,SHEET D ×
SHEET F ⧖

FX WITH PITCH

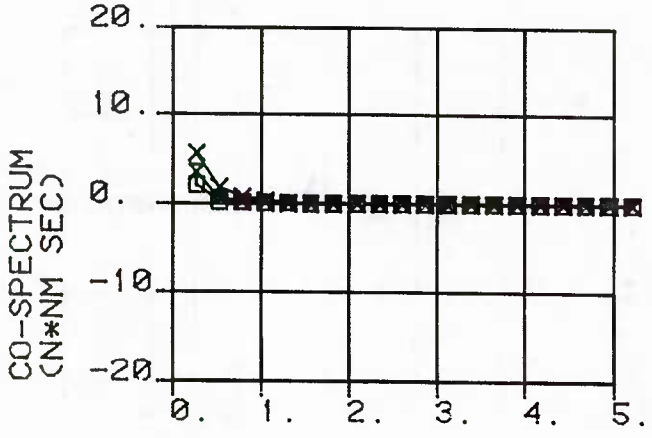

FX WITH ANG.ACC

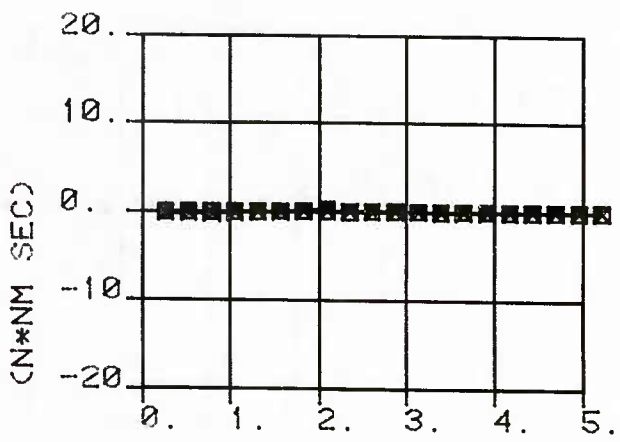

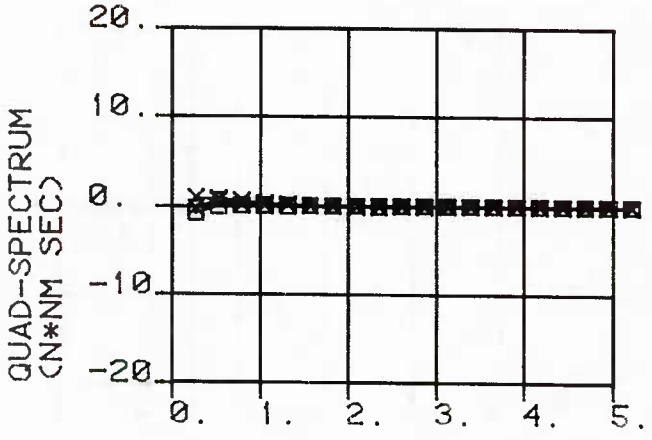

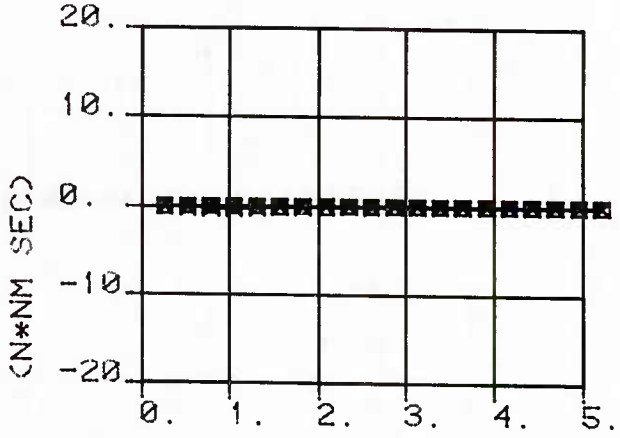

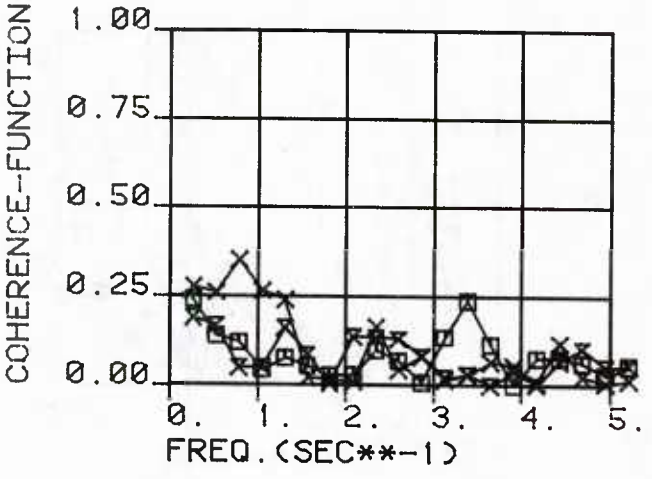

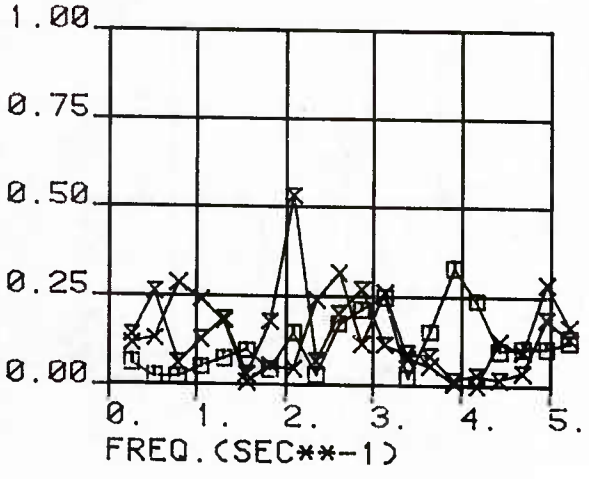

CROSS-SPECTRUM AND COHERENCE-FUNCTION

VEL = .22 M/SEC : SHEET A ⊡ , SHEET B ⊙
VEL = .30 M/SEC : SHEET C + , SHEET D ×

FX WITH PITCH

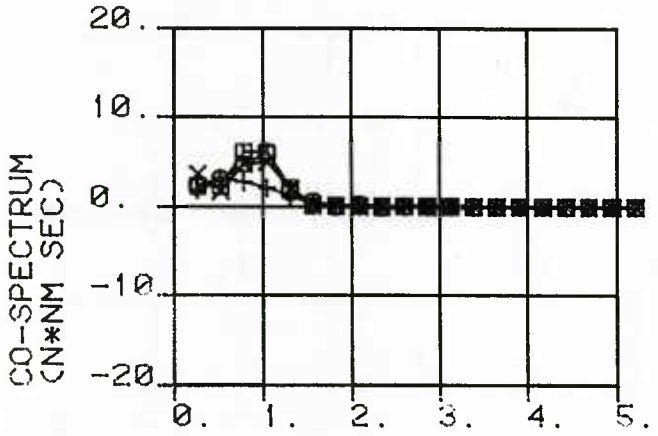

FX WITH ANG.ACC

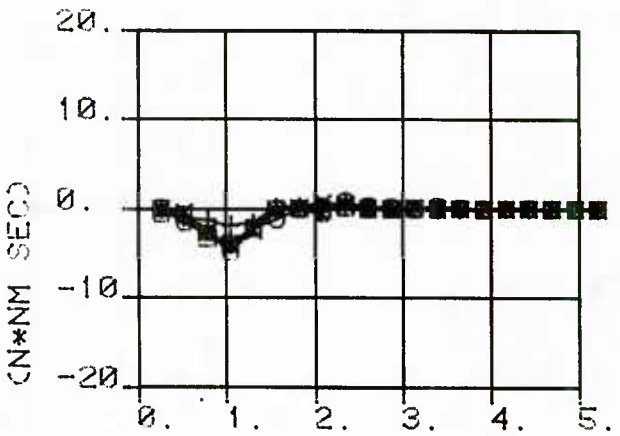

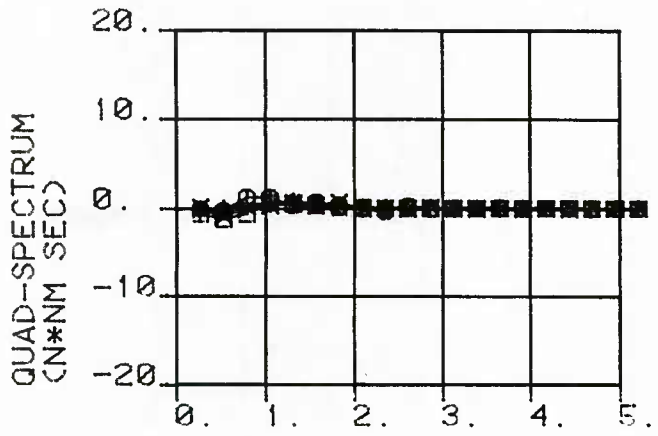

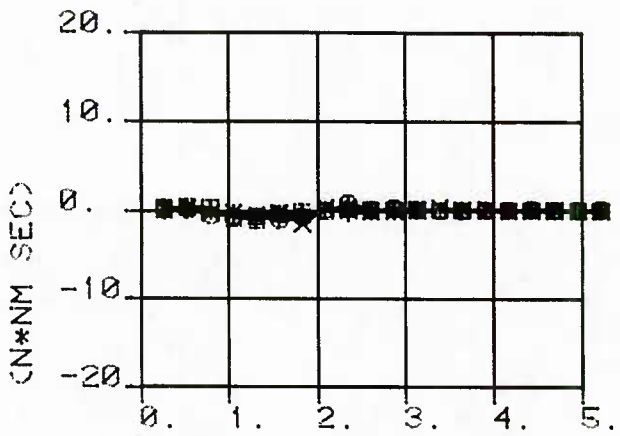

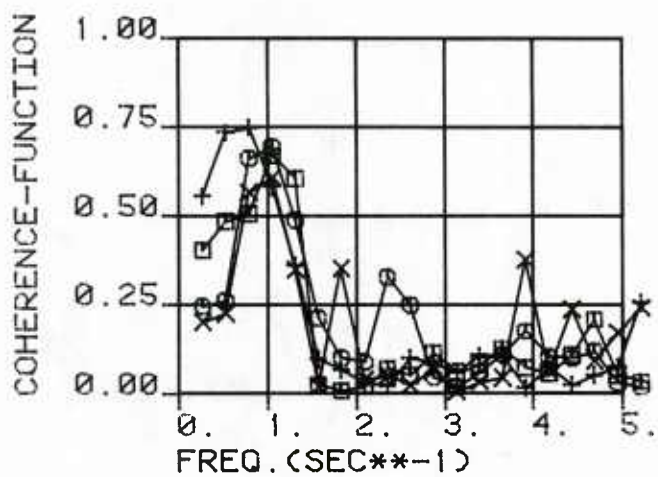

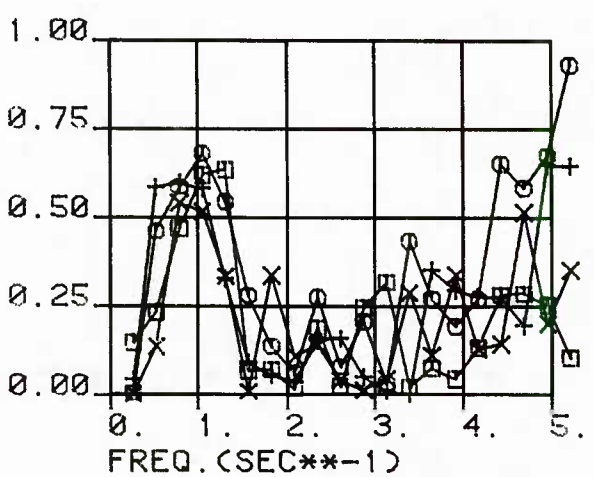

CROSS-SPECTRUM AND COHERENCE-FUNCTION

VEL = .60 M/SEC : SHEET E ✦
SHEET F ✕

FX WITH PITCH

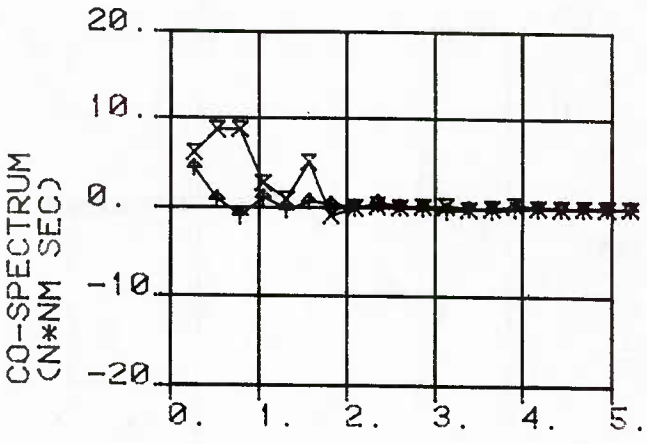

FX WITH ANG.ACC

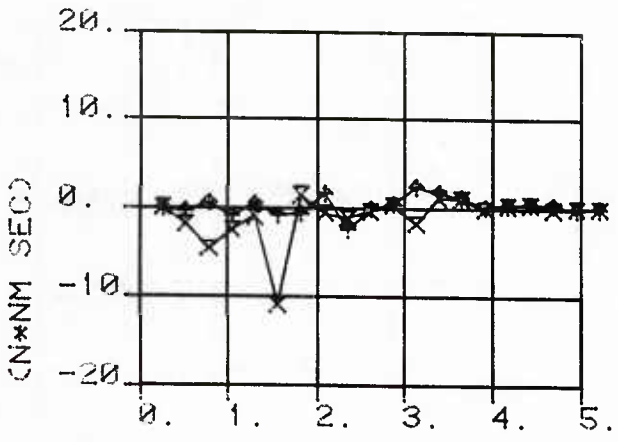

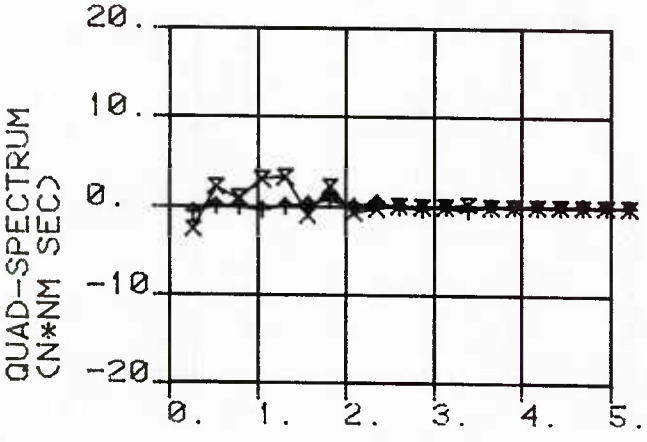

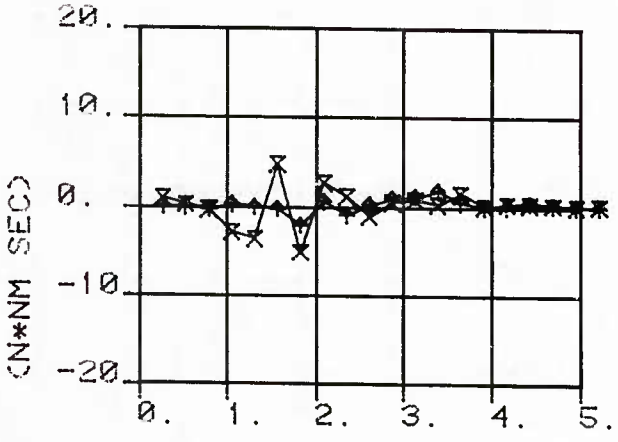

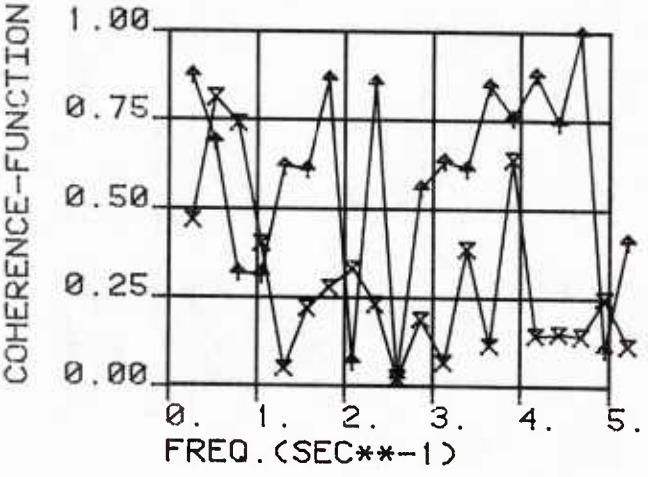

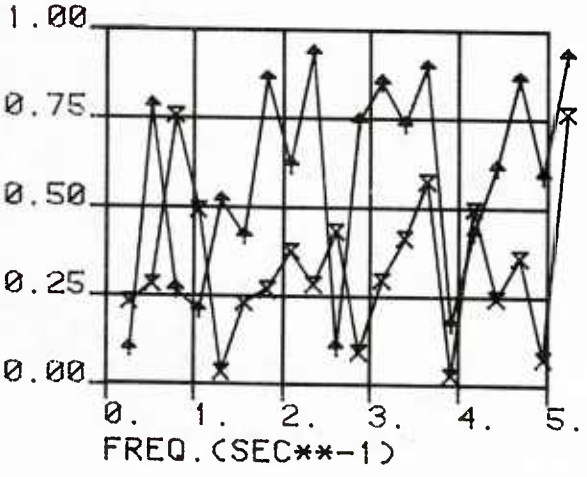

CROSS-SPECTRUM AND COHERENCE-FUNCTION

VEL = .03 M/SEC : SHEET G Z
VEL = .22 M/SEC : SHEET G Y

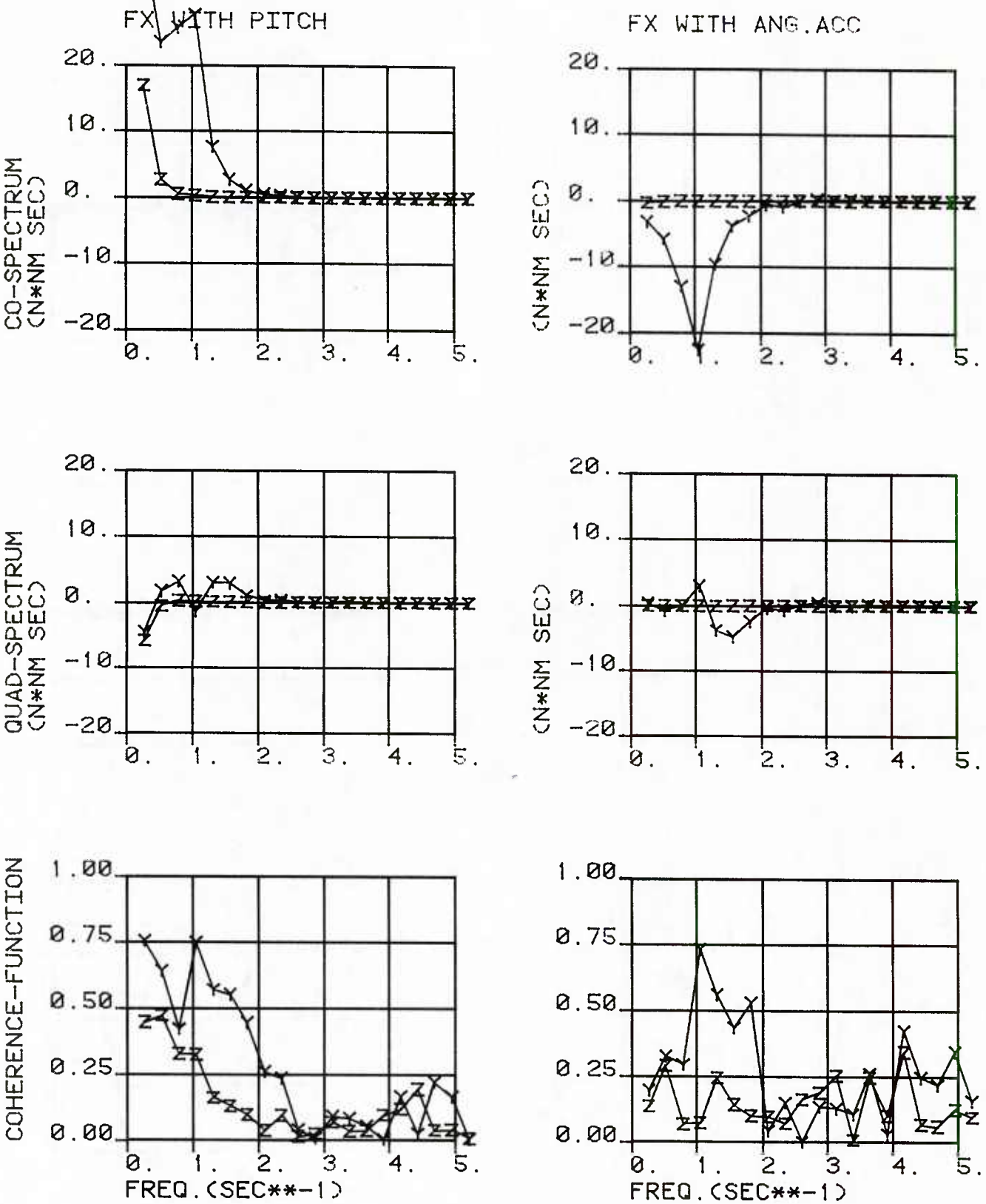

NORTH AMERICAN DISTRIBUTION LIST

Commander
David W. Taylor Naval Ship
R & D Center (ATTN: Code 1505)
Bldg. 19, Room 129B
Bethesda, Maryland 20084
15 Copies

Commander
Naval Sea Systems Command
Washington, D.C. 20362
ATTN: 05R22 (J. Sejd)

Commander
Naval Sea Systems Command
Washington, D.C. 20362
ATTN:55W (R. Keane, Jr.)

Commander
Naval Sea Systems Command
Washington, D.C. 20362
ATTN: 55W3 (W. Sandberg)

Commander
Naval Sea Systems Command
Washington, D.C. 20362
ATTN: 50151 (C. Kennell)

Commander
Naval Sea Systems Command
Washington, D.C. 20362
ATTN: 56X1 (F. Welling)

Commander
Naval Sea Systems Command
Washington, D.C. 20362
ATTN: 63R31 (T. Pierce)

Commander
Naval Sea Systems Command
Washington, D.C. 20362
ATTN: 55X42 (A. Paladino)

Commander
Naval Sea Systems Command
Washington, D.C. 20362
ATTN: 99612 (Library)

Director
Defense Documentation Center
5010 Duke Street
Alexandria, Va 22314
12 Copies

Library of Congress
Science & Technology Division
Washington, D.C. 20540

Naval Ship Engineering Center
Norfolk Division
Combatant Craft Engr Dept
Attn: D. Blount (6660)
Norfolk, VA 23511

Naval Underwater Weapons Research
& Engineering Station (Library)
Newport, R.I. 02840

Office of Naval Research
800 N. Quincy Street
Arlington, Virginia 22217
ATTN: Dr. C.M. Lee, Code 432

Commanding Officer (L31)
Naval Civil Engineering Laboratory
Port Hueneme, CA 93043

Commander
Naval Ocean Systems Center
San Diego, CA 92152
Attn: Library

Library
Naval Underwater Systems Center
Newport, RI 02840

Research Center Library
Waterways Experiment Station
Corps of Engineers
P.O. Box 631
Vicksburg, Mississippi 39180

Charleston Naval Shipyard
Technical Library
Naval Base
Charleston, S.C. 29408

Norfolk Naval Shipyard
Technical Library
Portsmoth, VA 23709

Puget Sound Naval Shipyard
Engineering Library
Bremerton, WA 98314

Long Beach Naval Shipyard
Technical Library (246L)
Long Beach, CA 90801

Mare Island Naval Shipyard
Shipyard Technical Library (202.3)
Vallejo, CA 94592

Assistant Chief Design Engineer
for Naval Architecture (Code 250)
Mare Island Naval Shipyward
Vallejo, CA 94592

U.S. Naval Academy
Annapolis, Md 21402
Attn: Technical Library

Naval Postgraduate School
Monterey, CA 93940
Attn: Library (2124)

Study Center
National Maritime Research Center
U.S. Merchant Marine Academy
Kings Point, LI, New York 11024

The Pennsylvania State University
Applied Research Laboratory (Library)
P.O. Box 30
State College, PA 16801

Dr. B. Parkin, Director
Garfield Thomas Water Tunnel
Appliled Research Laboratory
P.O. Box 30
State College, PA

Bolt, Beranek & Newman (Library)
50 Moulton Street
Cambridge, MA 02138

Cambridge Acoustical Associates, Inc.
54 Rindge Ave Extension
Cambridge, MA 02140

R & D Manager
Electric Boat Division
General Dynamics Corporation
Groton, Conn 06340

Gibbs & Cox, Inc. (Tech Info Control)
21 West Street
New York, New York 10006

Hydronautics, Inc. (Library)
Pindell School Rd.
Laurel, MD 20810

Newport News Shipbuilding and Dry
Dock Company (Tech. Library)
4101 Washington Ave.
Newport News, VA 23607

Mr. S. Spangler
Nielsen Engineering & Research, Inc.
510 Clyde Ave.
Mountain View, CA 94043

Society of Naval Architects and
Marine Engineers (Tech Library)
One World Trade Center, Suite 1369
New York, NY 10048

Sun Shipbuilding & Dry Dock Co.
Attn: Chief Naval A rchitect
Chester, PA 19000

Sperry Systems Management Division
Sperry Rand Corporation (Library)
Great Neck, N.Y. 10020

Stanford Research Institute
Attn: Library
Menlo Park, CA 94025

Southwest Research Institute
P.O. Drawer 28510
San Antonio, TX 78284
Attn: Applied Mech. Review
Dr. H. Abramson
2 copies

Tracor, Inc.
6500 Tracor Lane
Austin, Texas 78721

Mr. Robert Taggart
9411 Lee Highway, Suite P
Fairfax, VA 22031

Ocean Engr Department
Woods Hole Oceanographic Inc.
Woods Hole, Mass. 02543

Worcester Polytechnic Inst.
Alden Research Lab (Tech Library)
Worcester, MA 01609

Applied Physics Laboratory
University of Washington (Tech Library)
1013 N. E. 40th Street
Seattle, Washington 98105

University of California
Naval Architecture Department
Berkeley, CA 94720
4 Copies - ATTN: Profs. Webster, Paulling, Wehausen & Library

California Institute of Technology
ATTN: Library
Pasadena, CA 91109

Engineering Research Center
Reading Room
Colorado State University
Foothills Campus
Fort Collins, Colorado 80521

Florida Atlantic University
Ocean Engineering Department
Boca Raton, Florida 33432
Attn: Technical Library

Gordon McKay Library
Harvard University
Pierce Hall
Cambridge, MA 02138

Department of Ocean Engineering
University of Hawaii (Library)
2565 The Mall
Honolulu, Hawaii 96822

Institute of Hydraulic Research
The University of Iowa
Iowa City, Iowa 52242
ATTN: Library, Landweber, Patel

Prof. O. Phillips
Mechanics Department
The John Hopkins University
Baltimore, Maryland 21218

Kansas State University
Engineering Experiment Station
Seaton Hall
Manhattan, Kansas 66502
Attn: Prof. D. Nesmith

University of Kansas
Chm Civil Engr Department Library
Lawrence, Kansas 60644

Fritz Engr Laboratory Library
Department of Civil Engr
Lehigh University
Bethelehem, PA 18015

Department of Ocean Engineering
Massachusetts Institute of Technology
Cambridge, MA 02139
2 Copies: Attn: Profs. Leehey & Kerwin

Engineering Technical Reports
Room 10-500
Massachusetts Institute of Technology
Cambridge, MA 02139

St. Anthony Falls Hydraulic Laboratory
University of Minnesota
Mississippi River at 3rd Ave., S.E.
Minneapolis, Minnesota 55414
2 Copies: Attn: Dr. Arndt & Library

Department of Naval Architecture
and Marine Engineering - North Campus
ATTN: Library
University of Michigan
Ann Arbor, Michigan 48109

Davidson Laboratory
Stevens Institute of Technology
711 Hudson Street
Hoboken, New Jersey 07030
Attn: Library

Applied Research Laboratory
University of Texas
P.O. Box 8029
Austin, Texas 78712

Stanford University
Stanford, California 94305
2 Copies:
Attn: Engineering Library, Dr. Street

Webb Institute of Naval Archtecture
Attn: Library
Crescent Beach Road
Glen Cove, L.I., New York 11542

National Science Foundation
Engineering Division Library
1800 G Street N.W.
Washington, D.C. 20550

Mr. John L. Hess
4338 Vista Street
Long Beach, CA 90803

Dr. Tuncer Cebeci
Mechanical Engineering Dept.
California State University
Long Beach, CA 90840

Science Applications, Inc.
134 Holiday Court, Suite 318
Annapolis, MD 21401

U.S. Army Cold Regions Research
and Engineering Laboratory
Lyme Road
Hanover, New Hampshire 03755

LCDR David Humphreys, Chief
Icebreaker Technology Section
United States Coast Guard
Office of Engineering
Naval Engineering Section
Commandant (G-ENE-5I)
2100 Second Street S.W.
Washington, D.C. 20593